Eksenel Kompresör Aerodinamik Tasarımı

İbrahim ERYILMAZ

Yüksek Lisans Tezi

Sivil Havacılık Ana Bilim Dalı

Eylül 2013

ANADOLU ÜNİVERSİTESİ

JÜRİ VE ENSTİTÜ ONAYI

İbrahim ERYILMAZ'ın "Eksenel Kompresör Aerodinamik Tasarımı" başlıklı **Sivil Havacılık** Anabilim Dalındaki, Yüksek Lisans Tezi 17.09.2013 tarihinde, aşağıdaki jüri tarafından Anadolu Üniversitesi Lisansüstü Eğitim-Öğretim ve Sınav Yönetmeliğinin ilgili maddeleri uyarınca değerlendirilerek kabul edilmiştir.

		Adı Soyadı	**İmza**
Üye (Tez Danışmanı) :		**Prof. Dr. MEHMET ŞERİF KAVSAOĞLU**	**……..**
Üye	**:**	**Doç. Dr. NECATİ MAHİR**	**……..**
Üye	**:**	**Yard. Doç. Dr. ENİS TURHAN TURGUT**	**……..**

Anadolu Üniversitesi Fen Bilimleri Enstitüsü Yönetim Kurulu'nun …….. tarih ve …….. sayılı kararıyla onaylanmıştır.

Enstitü Müdürü

ÖZET

Yüksek Lisans Tezi

EKSENEL KOMPRESÖR AERODİNAMİK TASARIMI

İbrahim ERYILMAZ

Anadolu Üniversitesi
Fen Bilimleri Enstitüsü
Sivil Havacılık Anabilim Dalı

Danışman: Prof. Dr. Mehmet Şerif KAVSAOĞLU

2013, 110 Sayfa

Bu çalışmada tasarım, analiz ve optimizasyon araçları kullanılarak gaz türbinlerinde kullanılan eksenel kompresörlerde hava akışı incelenmiştir. Meridyonel tasarım ve analiz faaliyetleri radyal denge denklemi temel alınarak gerçekleştirilmiştir. Bu faaliyetlerde akış aksisimetrik ve adyabatik olarak değerlendirilmiştir. Radyal denge denkleminde radyal yöndeki entropi değişimleri göz önünde bulundurulmuş, radyal yöndeki hız değişimleri ihmal edilmiştir. Tasarımı yapılan kompresörün 3 Boyutlu Hesaplamalı Akışkan Dinamiği çözümleri gerçekleştirilmiş ve elde edilen akış parametreleri meridyonel analiz verileri ile karşılaştırılmıştır. Meridyonel analizde kayıp katsayılarının doğru olarak hesaplandığı durumlarda meridyonel analiz ve 3 Boyutlu Hesaplamalı Akışkan Dinamiği çözümleri uyum göstermektedir. Optimizasyon kısmında Yapay Sinir Ağı ile desteklenen Genetik Algotritma ile mevcut bir eksenel kompresör kademesinin rotor ve stator kanatları maksimum verim elde etmek amacıyla iyileştirilmiştir.

Anahtar Kelimeler: Eksenel Kompresör, Meridyonel Analiz, Radyal Denge, Optimizasyon, Yapay Sinir Ağı, Genetik Algoritma

ABSTRACT

Master of Science Thesis

AXIAL COMPRESSOR AERODYNAMIC DESIGN

İbrahim ERYILMAZ

Anadolu University
Graduate School of Sciences
Department of Civil Aviation

Supervisor: Prof. Dr. Mehmet Şerif KAVSAOĞLU
2013, 110 pages

In this study, air flow is investigated in gas turbine axial compressors by design, analysis and optimization tools. Meridional design and analysis are based on radial equilibrium equation. In these studies flow is considered as axisymmetric and adiabatic. In radial equilibrium equation radial variation of entropy is taken into account while radial component of air flow is ignored. 3 Dimensional Computational Fluid Dynamics analysis and meridional analysis results of designed axial compressor stage are done and results are compared. 3 Dimensional Computational Fluid Dynamics analysis and meridional analysis results are in agreement if loss coefficients in meridional design are predicted appropriately. Rotor and stator blades of an axial compressor stage are optimized for maximum efficiency with Artificial Neural Network assisted Genetic Algorithm.

Keywords: Axial Compressor, Meridional Analysis, Radial Equilibrium, Optimization, Artificial Neural Network, Genetic Algorithm

ACKNOWLEDGEMENTS

I would like to express appreciation to Prof. Dr. Mehmet Ş. KAVSAOĞLU for his guidance and support. I would like to express appreciation to Tusas Engine Industries Inc. for support and encouragement at both my professional carreer and this thesis work.

I would like to thank my teachers and friends who contribued to my academic life and I would like to thank my family who raised me.

Finally I would like to thank my wife Esen ERYILMAZ for her endless support and motivation.

İbrahim ERYILMAZ

September 2013

Dedicated to my wife Esen and my son Kubilay

CONTENTS

LIST OF FIGURES

LIST OF TABLES

LIST OF SYMBOLS

a : Factor in Tangential Velocity Distribution

b : Design Deviation Angle Exponent b, Factor in Tangential Velocity Distribution

c : Chord, Choking Condition, Critical Condition

e : Design Angle of Attack e factor

h : Static Enthalpy (kJ/kg.K), Hub

i : Incidence Angle

k : Factor, Ratio of Specific Heats

m : Mass, Mean, Design Deviation Angle m Factor, Minimum Condition Designation, Meridional Component

n : Design Incidence Angle n Factor, Factor in Tangential Velocity Distribution

p : Zero Camber Incidence p Factor

r : Radius, Radial Component

s : Streamline, Stall Condition, Pitch, Entropy

t : Tip, Tangential Component

o : Total Condition

w : Loss Coefficient, Weight in Neural Net

z : Axial Direction

A : Incoming Flow

B : Blockage, Shock Location

D : Diffusion Factor

H : Boundary Layer Shape Factor

K : Blade Metal Angle

M : Mach

N : Rotational Speed (rad/s)

P : Static Pressure (Pa)

R : Universal Gas Constant, Profile Loss Working Range

T : Static Temperature (Kelvin)

U : Rotational Speed (m/s)

W	: Flow Velocity in Relative Frame (m/s), Power (Watt)
V	: Flow Velocity in Absolute Frame
α	: Flow Angle in Absolute Frame, Angle of Attack
β	: Flow Angle in Relative Frame
δ	: Deviation Angle, Boundary Layer Displacement Thickness
ζ	: Stagger Angle
θ	: Camber Angle, Boundary Layer Momentum Thickness, Angle
λ	: Work Done Factor
μ	: Learning Rate
ρ	: Density (kg/m^3)
σ	: Solidity
τ	: Prandtl Meyer Expansion Angle, Supersonic Turning
ν	: Prandtl Meyer Function
Λ	: Degree of Reaction
C_p	: Heat Capacity of Fluid (J/kg.K)
K_{sh}	: Blade Shape Parameter
K_{ti}	: Blade Thickness Correction Parameter
$K_{t\delta}$	: Design Deviation Angle Thickness Correction Factor
BS	: Before Shock
NSW	: Normal Shock Wave
ANN	: Artificial Neural Network
DCA	: Double Circular Arc
USL	: Upper Specification Limit
LSL	: Lower Specification Limit
C_{pk}	: Process Capability Index
P_{pk}	: Process Performance Index
eq	: Equivalent Condition
max	: Maximum Conditiom
min	: Minimum Condition
le	: Leading Edge

te	: Trailing Edge
*	: Design Condition Designation
1	: Station 1
10	: Zero Camber Designation

1. INTRODUCTION

1.1.Overview

In a gas turbine usually air is utilized. In closed cycle gas turbines other gases like carbon dioxide and helium may also be utilized [1]. Fundamental analysis will be applicable to any of gases but in thesis work air is the working fluid.

In a turbojet gas turbine cycle air is compressed in the compressor. Energy is added to the compressed fluid in the combustion chamber. High pressure and high temperature air is expanded in the turbine. Some of the energy extracted by the expansion is used to drive compressor and the remaining amount is used to get thrust by accelerating flow in nozzle. In Figure 1.1 a picture of Rolls Royce Olympus Turbojet Engine is given [1]. In Figure 1.2 core engine components for a gas turbine are given [8].

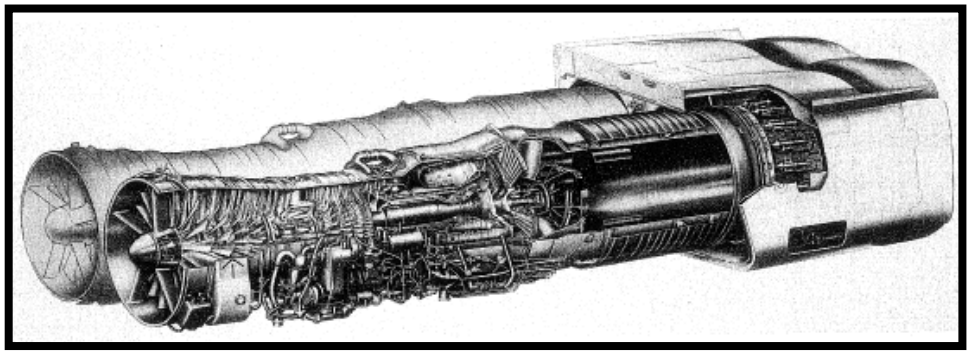

Figure 1.1. Rolls Royce Olympus turbojet engine [1]

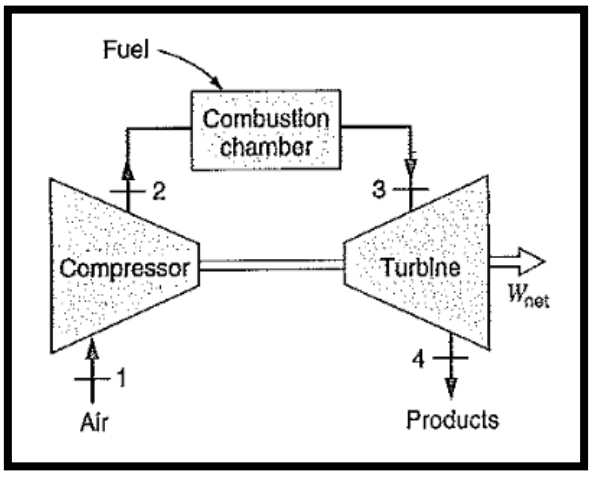

Figure 1.2. Core engine components for a gas turbine [8]

Ideal cycle for the gas turbine is the Brayton Cycle [1]. Energy transfer in gas turbine cycle is given in temperature-entropy (T-s) diagram in Figure 1.3 [8]. Many types of compressors are utilized in industry. In Figure 1.4 compressor types in general are given [9].

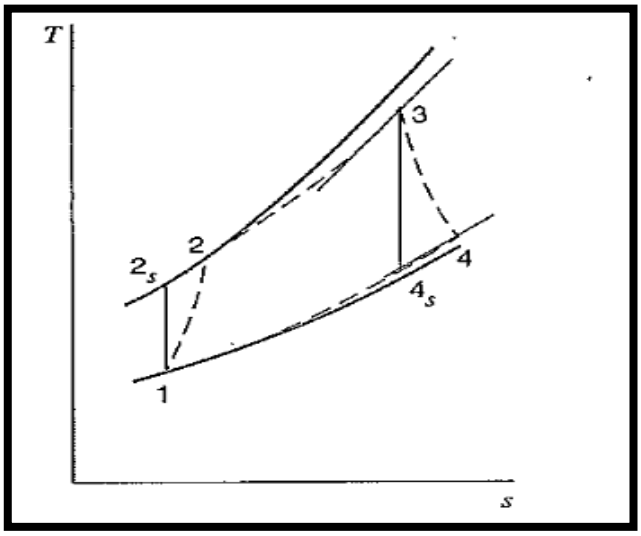

Figure 1.3. Brayton cycle T-s diagram [1]

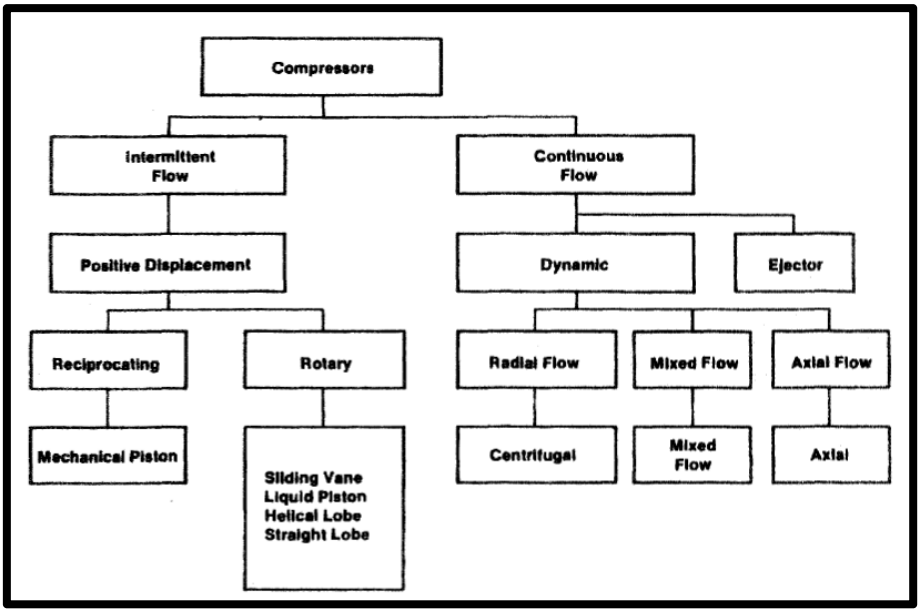

Figure 1.4. Compressor types in general [9]

Compressors are selected according to their duties. Pressure ratio, flow rate, mass, dimensions, reliability etc. affect the type of compressor that will be selected for a specific duty. In Figure 1.5 compressors are classified according to pressure ratio and flow rate requirements [9].

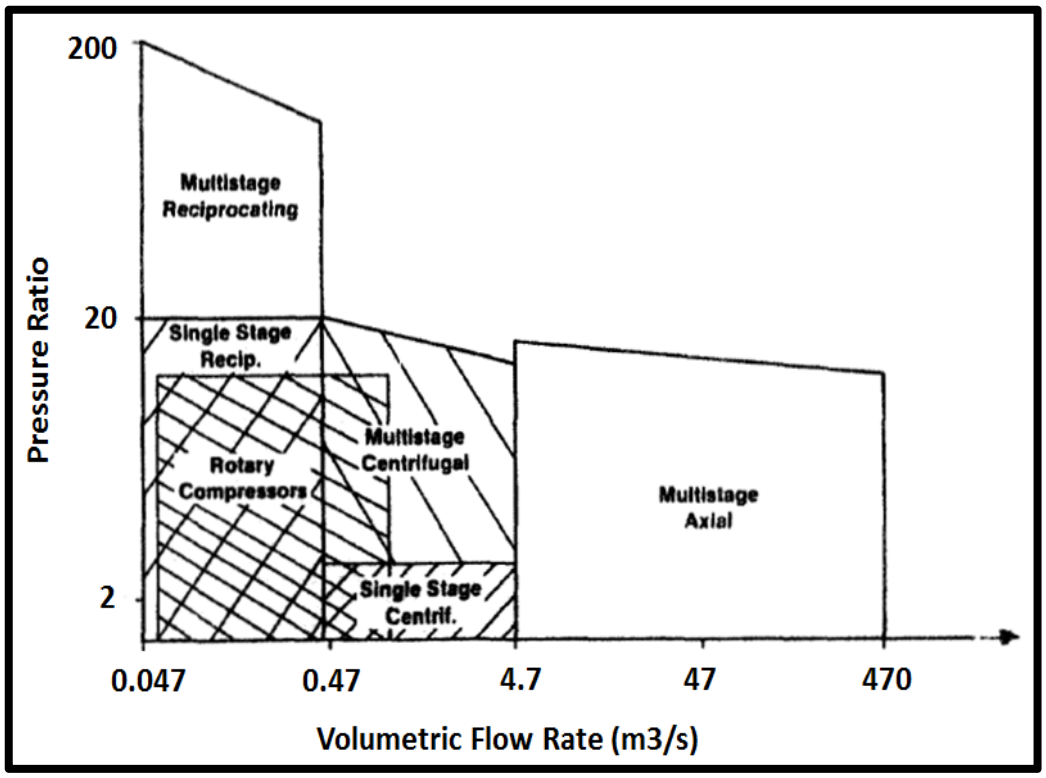

Figure 1.5. Compressor types for different applications [9]

For gas turbine engines axial and centrifugal compressors are used. In Figure 1.6 and Figure 1.7 axial [10] and centrifugal [11] compressors for different applications are given.

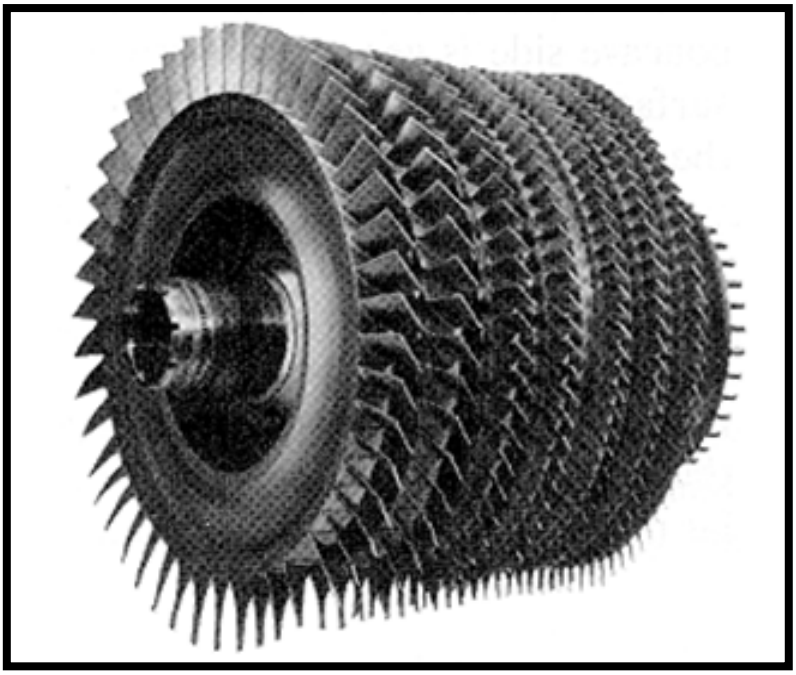

Figure 1.6. Axial compressor, GE F404 engine [10]

Figure 1.7. Centrifugal compressor, DLR test rig [11]

Generally multistage axial flow compressors have properties of high mass flow rate per area, high pressure ratio, high efficiency. Centrifugal compressors have properties of low mass flow rate per area, high pressure ratio per stage, lower cost. With the improved design technology overall compressor pressure ratio, efficiency, life, overhauls time for compressors will be increased; length, weight as well as cost will be decreased. Figure 1.8 shows yearly improvement of compressor pressure ratio for aircraft and industrial applications [12].

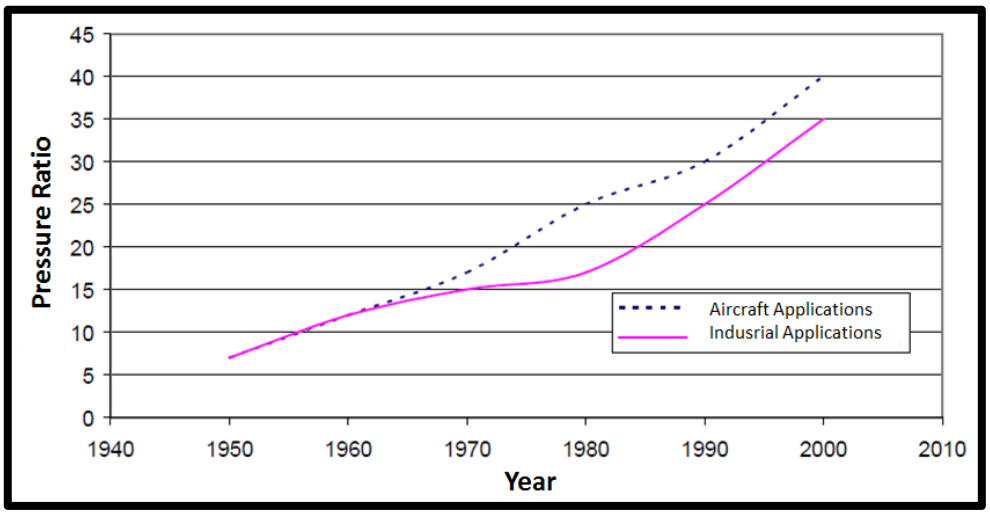

Figure 1.8. Yearly improvement of compressor pressure ratio [12]

Improved design technology gives the chance to cope with higher rotor inlet relative Mach numbers which drives the higher pressure ratio for a stage. Table 1.1 gives information about pressure ratio, inlet Mach number and efficiency values for different axial flow compressor applications [12].

Table 1.1. Properties of axial flow compressors for different applications [12]

Type of Application	Flow Type	Rotor Inlet Relative Mach Number	Pressure Ratio per Stage	Efficiency per Stage
Industrial	Subsonic	0.4 - 0.8	1.05 - 1.2	88% - 92%
Aerospace	Transonic	0.7 – 1.1	1.15 - 1.6	80% - 85%
Research	Supersonic	1.05 - 2.5	1.8 – 2.2	75% - 85%

Complete design of an axial compressor is a multidisciplinary process. Classical approach for compressor design is based on a sequential strategy. Compressor is optimized in individual disciplines and differences in interactions between these disciplines are covered one by one. With the introduction of modern products design strategy is evolved to a simultaneous process from sequential process. Each individual work such as aerodynamics, heat transfer, structure, materials, manufacturing, testing, validation etc. play a simultaneous role in design process. Additionally to the compressor design team, a whole engine team exists which provides interface with other design groups of gas turbine engine [13]. Figure 1.9 is a schematic view of integrated multi-disciplinary design of high pressure multistage compressor system.

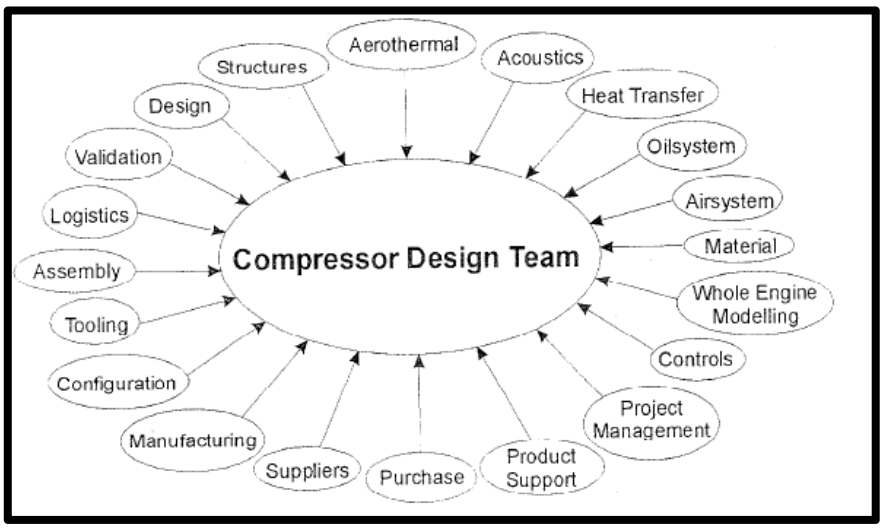

Figure 1.9. Simultaneous engineering team for compressor design [13]

2. LITERATURE SURVEY

Flow field analysis and generation of performance maps of compressors depend on various techniques. These techniques are:

-Direct testing of the compressor in a rig test or engine test,
-One dimensional techniques that are based on experimental data and empirical correlations.
-Two dimensional techniques that are based on experimental data and empirical correlations,
-Three dimensional techniques that are based on solution of Navier - Stokes equations.

Wide range of optimization techniques exist in the literature. Optimization can be done either single objective or multiobjective. Multiobjective optimization can be done either in a single discipline or in a multidisciplinary environment.

2.1.Testing of Compressors

Direct testing of compressors in a rig test or engine test gives the most accurate flow field data of the compressor. Effect of three dimensional and unsteady nature of compressor is completely investigated with the complexity of instrumentation in experimental work. This technique is also the most expensive one since building testing facilities and gathering testing hardware is required.

2.2.One Dimensional Techniques

Three dimensional nature of the compressor is modeled in a one dimensional technique. Average stage by stage characteristics are obtained with this method. A one dimensional method is presented by Attia and Schobeiri [14]. The method presented is based on geometry and design point data for the prediction of compressor performance maps. In this one dimensional row by row analysis a modified diffusion factor is used for off design efficiency. With the loss and deviation correlations accurate predictions obtained for stall regimes.

2.3.Two Dimensional Techniques

Two dimensional techniques are also based on experimental data and empirical correlations similar to one dimensional technique. Two dimensional

techniques are commonly called throughflow methods. Throughflow calculation corresponds to an axisymmetric computation of the flow field across flow path. Axisymmetric means no velocity component or fluid property varies in circumferential direction for a given set of axial and radial coordinate in the flow path. Flow is circumferentially averaged. Flow is modeled by a series of concentric stream surfaces in which no mass and momentum is transferred across each other [16].

Additionally to the axisymmetric flow assumption in through-flow methods for turbomachines, except for some cases associated with cooled turbines, the flow is assumed to be adiabatic so that no heat is transferred between fluid elements or across stream surfaces [16].

2.3.1. Simple radial equilibrium method

In this throughflow technique flow field analysis is based on solution of radial equilibrium, continuity and energy equations. In simple radial equilibrium equation, radial variation of velocity is ignored. Simple radial equilibrium method will be implemented in isentropic (ISRE) and non-isentropic (NISRE) modes. In non-isentropic radial equilibrium mode spanwise variation of total enthalpy and entropy is taken into account. The flow distribution at compressor outlet is determined from individual blade section of elements. Flow field is divided into two parts. First part includes blade to blade surfaces in several spanwise positions.

These blade to blade surfaces are surface of revolutions and are not stream surfaces in general [7]. Surface of revolutions are conical but if the radius is same at inlet and outlet these surface of revolutions are cylindrical. Second part includes hub to casing surfaces in several meridional positions.

Lieblien [15] used a blade element concept depending on axial flow compressor blades evolving from radial stacking of individual airfoil shapes called blade elements. The blade elements are assumed to be located along surfaces of revolution obtained by rotating a streamline about the compressor axis [3]. Figure 2.1 shows compressor blade elements along surface of revolution about compressor axis [3].

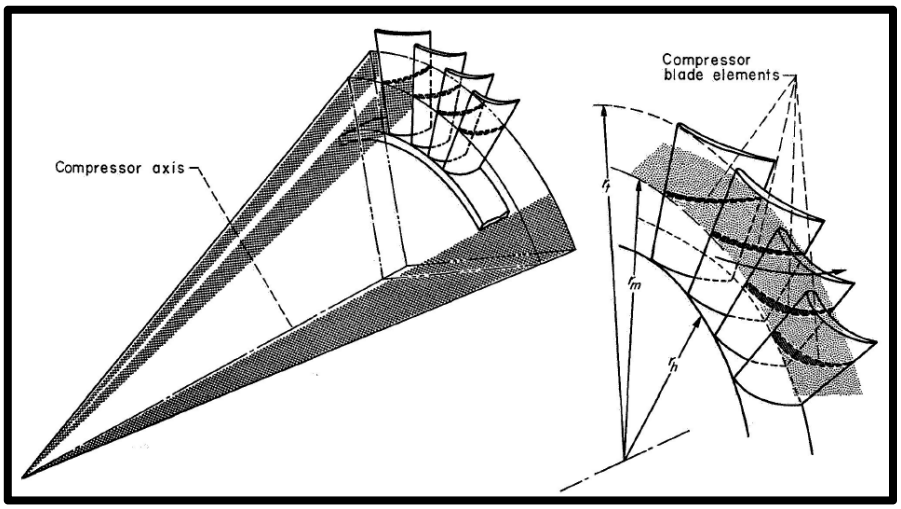

Figure 2.1. Compressor blade elements along surface of revolution [3]

Since surface of revolutions are not stream-surfaces in general an extra level of approximation is introduced when compared with streamline curvature methods [7]. When the compressor geometry has strong curvatures in meridional and blade to blade surfaces, radial variation of velocity gets important and this technique will fail to predict the flow field data. Figure 2.2 shows the meridional streamline pattern for actual flow and model flow by simple radial equilibrium. Dashed lines are the flow patterns approximated by simple radial equilibrium where full lines are the meridional streamline pattern for actual flow.

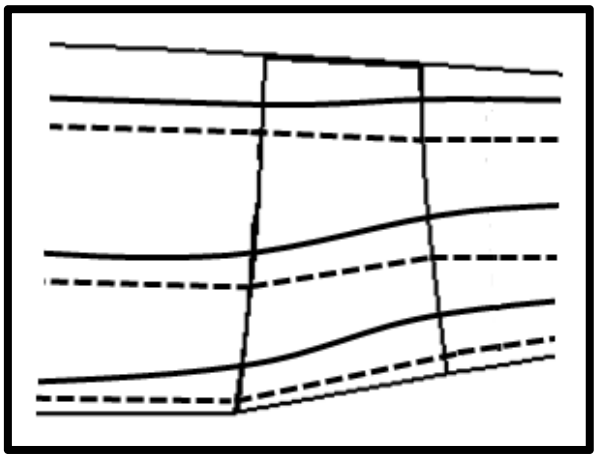

Figure 2.2. Meridional streamline pattern for actual flow and model flow

2.3.2. Streamline curvature method

In this throughflow technique flow field analysis is based on solution of radial equilibrium, continuity and energy equations. Streamline curvature method

is also called as full radial equilibrium method [34]. In the radial equilibrium equation streamline curvature effects, effects of radial forces due to flow along streamline and acceleration along streamline are included. Method is supported by empirical data to handle viscous effects. Flow field is divided into two parts.

First part includes blade to blade surfaces in several spanwise positions. These blade to blade surfaces are stream surfaces. Streamsurfaces twist and warp as they pass through blade row [7]. Second part includes hub to casing surfaces in several meridional positions. Wu [17] introduced a method based on streamline curvature. In this work streamurfaces are considered as S1 and S2. S1 is the blade to blade streamsurface; S2 is the hub to casing streamsurface.

Streamsurfaces start at the inlet as surface of revolution then they twist and warp along blade row. Forms of these streamsurfaces are iteratively changed until flow field solution convergence. Since streamsurfaces twist and warp three dimensional inviscid flow can be analyzed by two interesting surfaces [7]. This method is a successful tool for flow field analysis for turbomachines as well as axial compressors. S1 blade to blade steamsurface [17] and S2 hub to casing streamsurface [17] are given in Figure 2.3 and Figure 2.4.

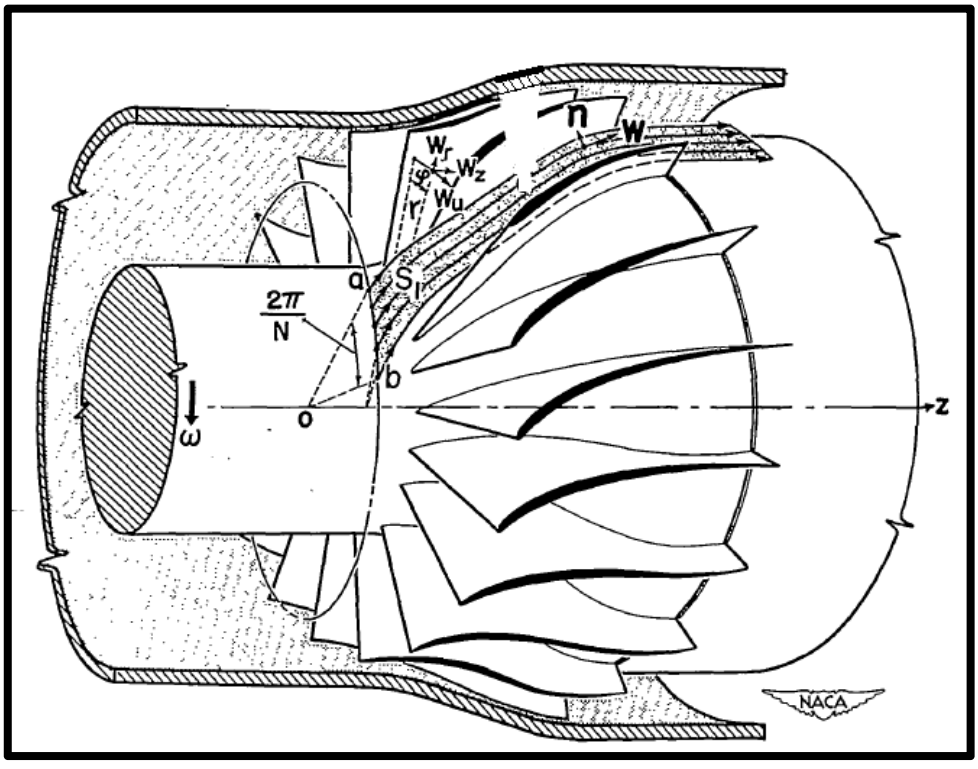

Figure 2.3. S1 blade to blade streamsurface [17]

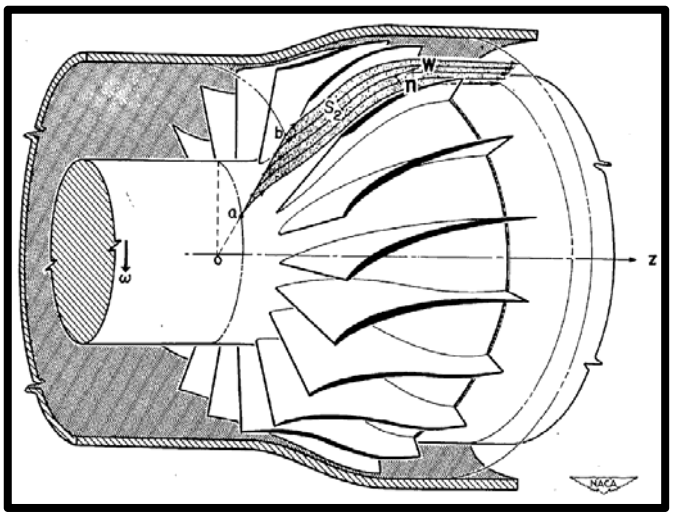

Figure 2.4. S2 hub to casing streamsurface [17]

2.3.3. Finite difference method

Flow field is investigated by a system of grid points or nodes throughout the flowpath [16]. Adiabatic inviscid flow calculation is combined with empirical correlations to handle viscous effects.

2.3.4. Finite element method

Flow field is investigated by a system of network lines and elements [16]. Adiabatic inviscid flow calculation is combined with empirical correlations to handle viscous effects. In Figure 2.5 two stage fan geometry with element boundaries and calculated streamlines are given [16].

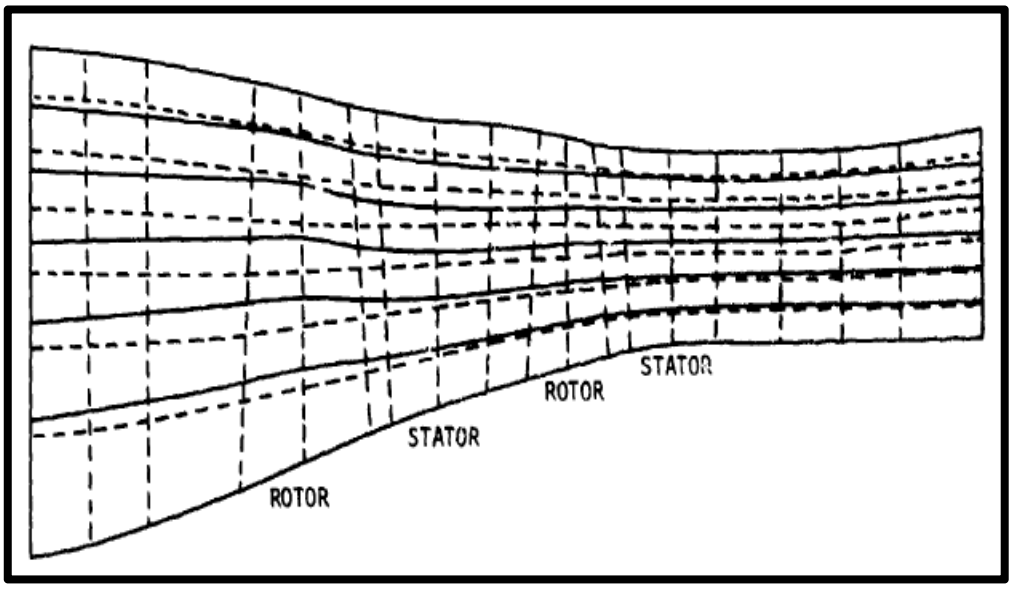

Figure 2.5. Fan geometry element boundaries and calculated streamlines [16]

2.3.5. Finite volume method

Flow field is investigated by system of small volume elements [16]. Adiabatic inviscid flow calculation is combined with empirical correlations to handle viscous effects. Equations are solved by a time marching process iteratively. This method can be extended to become an effective three dimensional flow analysis system.

2.3.6. Three dimensional techniques

Three dimensional techniques for turbomachinery flow analysis are mostly named under a general topic computational fluid dynamics (CFD).

These methods generally depend on solutions of Euler and Navier-Stokes equations with finite volume method. Reynolds Averaged Navier-Stokes and Large Eddy Methods use mathematical models for turbulence modeling. Direct Numerical Simulation depends on exact solutions of Navier-Stokes equations and do not require mathematical modeling for turbulence. With the increasing capacity in computational techniques based on software and hardware, resolution in flow field analysis in turbomachinery is increasing day by day. In Figure 2.6 a typical structure of an axial turbomachinery design system is given [16].

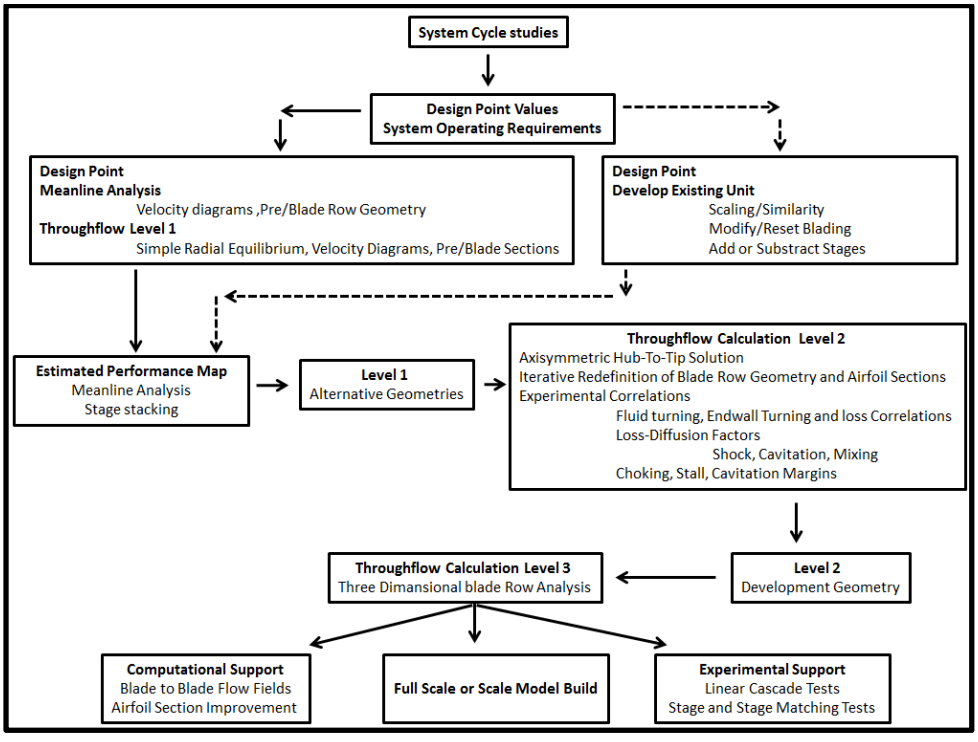

Figure 2.6. Structure of an axial turbomachinery design system [16]

2.4.Optimization Techniques

According to order of derivatives of the objective function, optimization techniques can be classified as second order, first order and zero order methods [19].

Thevenin and Janige [19] made inverse design of a 2-D duct by a second order optimization method, which is based on computation of Hessian Matrix [18]. A first order method is used by Papadimitriou et al. [19] for minimizing total pressure losses of a compressor cascade where the method is based on first order gradients. Entropy generation of NASA Rotor 67 is minimized by Oyama et al. [20] by a zero order method using an evoluationary algorithm . Zero order methods are also considered as derivative free methods [18].

Evoluationary algorithms may be assisted by metamodels. Metamodel [18] or Surrogate Model [19] is the representative of the case which is being optimized. This representative model generates outputs of the case for given inputs. Polynomial Response Surfaces, Artificial Neural Networks and Kriging are some types of metamodels [18].

Song et al [22] optimized a cryogenic liquid turbine by genetic algorithm and adaptive approximate model. This work used Kriging approximation model to approximate the time-costly objective function. Lian and Liu [23] presented multidisciplinary optimization of NASA Rotor 67 by Genetic Algorithm used with response surface approach. Optimization of a centrifugal impeller using evolution strategies is done by Meier et al. [24]. In the work an existing impeller is optimized to increase impeller isentropic efficiency. After the optimization Artificial Neural Network is just trained and used to predict isentropic efficiency values. Since Artificial Neural Network has showed success in predictions, this prediction technique is proposed to be integrated to the optimization process in order to speed up the optimization.

2.5.Present Study

Objectives of the present study reported in this thesis are:

-Implementation of a meanline axial compressor design for annulus sizing.

-Implementation of simple isentropic radial equilibrium to determine flow angles, blade cascade data from hub to tip.

-Implementation of simple isentropic radial equilibrium by taking into account radial variation of entropy in order to make a throughflow analysis of existing compressor geometry.

-Investigation of flow parameters from hub to tip. Comparison of adiabatic, axisymmetric throughflow analysis solution with 3-D Navier Stokes computation.

-Implementation of Genetic Algorithm assisted by Artificial Neural Network for optimization of an existing axial compressor stage.

-Investigation of effectiveness of the Artificial Neural Network in terms of prediction capability.

Present study has two main parts. First step includes design, throughflow analysis and 3-D CFD analysis for axial compressor. Design and throughflow analysis tools are developed in-house in C programming in the scope of thesis work. For 3-D Navier Stokes computations, commercially available software Numeca Fine Turbo is used. Second step includes design and optimization of a compressor stage. In this step design of the compressor stage is done with commercial software AxStream. Genetic Algorithm for optimization is developed in-house in the scope of thesis work. Artificial Neural Network to be used as metamodel in optimization is developed in-house. For 3-D Navier Stokes computations in optimization, commercial software Numeca Fine Turbo is used. Parametric modeling of the compressor stage is done in commercial CAD software Unigraphics. Statistical analysis is carried with commercial software Minitab 16 for metamodel effectiveness study.

3. DESIGN AND ANALYSIS

The approach used in the present investigation is based on design, throughflow analysis, 3-D Navier Stokes analysis and optimization steps of axial compressor.

Design is based on a meanline approach and based on determination of blade cascade data from hub to tip by simple isentropic radial equilibrium. Inputs for this step are inlet total quantities, pressure ratio, rotational speed, mass flow rate, stage number, first stage rotor hub to tip ratio etc. Outputs for this step are annulus

dimensions, variation of blade parameters from hub to tip, variation of flow parameters from hub to tip without taking into account losses.

Throughflow analysis is based on simple isentropic radial equilibrium by taking into account radial variation of entropy. Inputs for this step are inlet total quantities, pressure ratio, rotational speed, mass flow rate, stage number, annulus dimensions, blade cascade data, loss parameters etc. Outputs for this step are variation of flow parameters from hub to tip by considering losses, deviations etc.

3-D CFD computation is based on steady Reynolds Averaged Navier Stokes computations by commercial software Numeca Fine Turbo.

Optimization is based on Genetic Algorithm assisted by Artificial Neural Network. Inputs for the Genetic Algorithm are population information, optimization constraints, crossover conditions, mutation conditions. Output of the genetic algorithm is the parameter set obtained after given number of iterations. Inputs for the Artificial Neural Network are number of inputs, number of hidden layers, number of outputs, convergence criteria, iteration number, number of outputs, number of training sets and number of testing sets. Output of the trained Artificial Neural Network is the signal that is generated according to set of inputs.

3.1.Elementary Theory

Elementary theory about compressor design is governed by the two dimensional approach which is based on that flow velocity has two components. These components are the axial and tangential components of the flow. Velocity triangle notation and flowpath definition are given in Figure 3.1 and Figure 3.2.

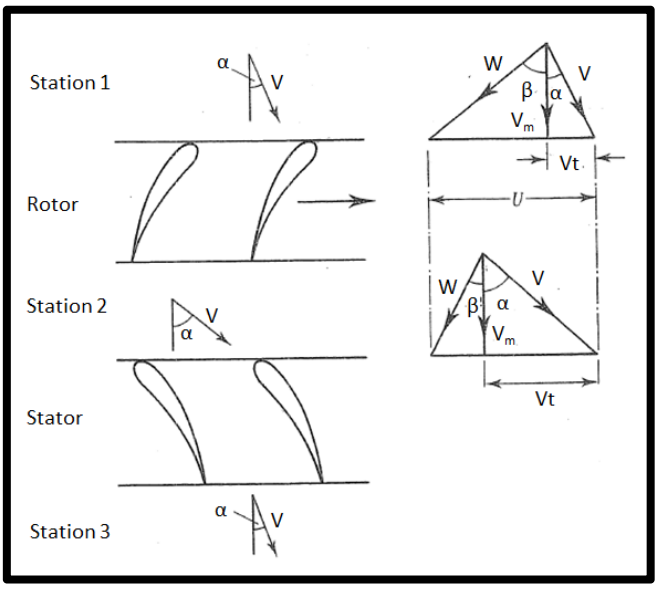

Figure 3.1. Velocity triangle notation [1]

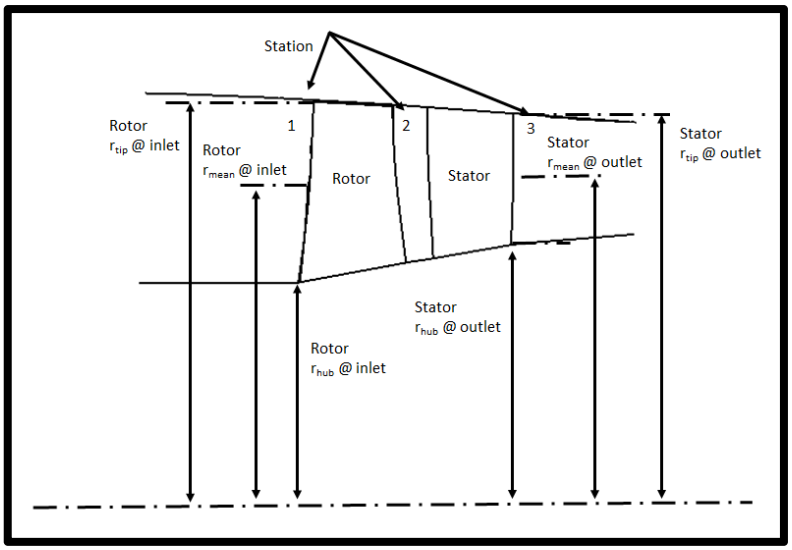

Figure 3.2. Flowpath definition

Applying steady flow energy equation to the rotor and assuming the entire process is adiabatic, power input to the compressor or control volume can be given as:

$$\dot{W} = \dot{m}.C_p.(T_{02} - T_{01}) \tag{3.1}$$

Power input can also be written in terms of rate of change of angular momentum to the rotor.

$$\dot{W} = \dot{m}.U.(V_{t2} - V_{t1}) \tag{3.2}$$

For initial design issues assuming axial component of the flow does not change from station 1 to station 2.

$$V_{m1} = V_{m2} = V_{m3} = V_m \tag{3.3}$$

$$\tan(\alpha_1) = \frac{V_{t1}}{V_{m1}} \tag{3.4}$$

$$\tan(\alpha_2) = \frac{V_{t2}}{V_{m2}} \tag{3.5}$$

$$\tan(\beta_1) = \frac{U - V_{t1}}{V_{m1}} \tag{3.6}$$

$$\tan(\beta_2) = \frac{U - V_{t2}}{V_{m2}} \tag{3.7}$$

$$\dot{W} = \dot{m}.U.\{(U - V_{m1}.\tan(\alpha_1)) - (U - V_{m2}.\tan(\alpha_2))\} \tag{3.8}$$

$$\dot{W} = \dot{m}.U.V_m.(\tan(\alpha_2) - \tan(\alpha_1)) \tag{3.9}$$

For rotor flow power input can also be written in terms of flow angles in relative frame.

$$\tan(\alpha_1) + \tan(\beta_1) = \tan(\alpha_2) + \tan(\beta_2) = \frac{U}{V_m} \tag{3.10}$$

$$\dot{W} = \dot{m}.U.V_m(\tan(\beta_1) - \tan(\beta_2)) \tag{3.11}$$

Stage total temperature rise will be written in the form;

$$T_{02} - T_{01} = \frac{U.V_m}{C_p}.(\tan(\beta_1) - \tan(\beta_2)) \tag{3.12}$$

Change of total enthalpy with respect to radius will be written as;

$$\frac{dh_0}{dr} = \frac{d\{U.V_m.(\tan(\beta_1) - \tan(\beta_2))\}}{dr} \tag{3.13}$$

$$\frac{dh_0}{dr} = \frac{d\{w.r.V_m.(\tan(\beta_1) - \tan(\beta_2))\}}{dr} \tag{3.14}$$

3.2.Meanline Design of Axial Flow Compressor

In this part flow parameters of axial compressor at the mean radius will be determined. Total enthalpy change can be written with flow parameters in absolute frame as:

$$\Delta h_{0,mean} = N_{mean}.r_{mean}.\{V_{m2,mean}.\tan(\alpha_{2,mean}) - V_{m1,mean}.\tan(\alpha_{1,mean})\} \quad (3.15)$$

Total enthalpy change can be written with flow parameters in relative frame as:

$$\Delta h_{0,mean} = N_{mean}.r_{mean}.\left\{V_{m2,mean}.\left(\frac{U_{mean}}{V_{m2,mean}} - \tan(\beta_{2,mean})\right) - V_{m1,mean}.\left(\frac{U_{mean}}{V_{m1,mean}} - \tan(\beta_{1,mean})\right)\right\} \quad (3.16)$$

$$\Delta h_{0,mean} = N_{mean}.r_{mean}.\{U_{mean} - V_{m2,mean}.\tan(\beta_{2,mean}) - U_{mean} + V_{m1,mean}.\tan(\beta_{1,mean})\} \quad (3.17)$$

$$\Delta h_{0,mean} = N_{mean}.r_{mean}.\{V_{m1,mean}.\tan(\beta_{1,mean}) - V_{m2,mean}.\tan(\beta_{2,mean})\} \quad (3.18)$$

Total enthalpy change of the stage is directly associated with rotor flow. Because external work is done on the fluid only at rotor, total enthalpy change will be related with temperature to find flow angles. The term degree of reaction is used to define the contribution of rotor on the static enthalpy rise in the stage.

Total enthalpy rise is obtained at only rotor because external work is done on the fluid at rotor. After rotor flow the static enthalpy is increased by decelerating the flow on stator.

The efficiency is determined by the amount of total enthalpy loss both in rotor and stator. This is also considered as total pressure losses on the stage.

Degree of Reaction, Λ

$$\Lambda = \frac{Static\_Enthaly\_Rise\_in\_the\_Rotor}{Static\_Enthaly\_Rise\_in\_the\_Stage} \quad (3.19)$$

$$\Lambda = \frac{h_2 - h_1}{h_{02} - h_{o1}} \quad (3.20)$$

Degree of reaction will be written in terms of velocities and flow angles as follows:

$$h_o = h + \frac{V^2}{2} = h + \frac{1}{2}.(V_m^2 + V_t^2) \quad (3.21)$$

$$\Lambda = \frac{U.(V_{t2} - V_{t1}) - \frac{1}{2}.(V_2^2 - V_1^2)}{U.(V_{t2} - V_{t1})} \quad (3.22)$$

$$\Lambda = 1 - \frac{(V_{m2}^2 - V_{m1}^2)}{2.U.(V_{t2} - V_{t1})} - \frac{(V_{t2}^2 - V_{t1}^2)}{2.U.(V_{t2} - V_{t1})} \quad (3.23)$$

Two equations, one coming from first law of thermodynamics the other coming from conservation of angular momentum, define the power input per mass flow to the stage. Power input to the stage and degree of reaction will be related in order to have an equation with primary design inputs.

$$U.(V_{t2}-V_{t1}) = Cp.(T_{02}-T_{01}) = Cp.\Delta T_{stage} \tag{3.24}$$

$$\Lambda = 1 - \frac{(V_{m2}^2 - V_{m1}^2)}{2.Cp.\Delta T_{stage}} - \frac{(V_{t2}-V_{t1}).(V_{t2}+V_{t1})}{2.U.(V_{t2}-V_{t1})} \tag{3.25}$$

$$\Lambda = 1 - \frac{(V_{m2}^2 - V_{m1}^2)}{2.Cp.\Delta T_{stage}} - \frac{V_{t2}+V_{t1}}{2.U} \tag{3.26}$$

Velocity components will be written in terms of the flow angles.

$$\Lambda = 1 - \frac{(V_{m2}^2 - V_{m1}^2)}{2.Cp.\Delta T_{stage}} - \frac{V_{m2}.\tan(\alpha_2)+V_{m1}.\tan(\alpha_2)}{2.U} \tag{3.27}$$

$$\Lambda = 1 - \frac{(V_{m2}^2 - V_{m1}^2)}{2.Cp.\Delta T_{stage}} - \frac{V_{m2}.\left\{\frac{U}{V_{m2}} - \tan(\beta_2)\right) + V_{m1}.(\frac{U}{V_{m1}} - \tan(\beta_1)\right\}}{2.U} \tag{3.28}$$

$$\Lambda = 1 - \frac{(V_{m2}^2 - V_{m1}^2)}{2.Cp.\Delta T_{stage}} - \frac{\left\{U - V_{m2}.\tan(\beta_2)+U - V_{m1}.\tan(\beta_1)\right\}}{2.U} \tag{3.29}$$

$$\Lambda = 1 - \frac{(V_{m2}^2 - V_{m1}^2)}{2.Cp.\Delta T_{stage}} - \frac{2.U}{2.U} + \frac{V_{m1}.\tan(\beta_1)+V_{m2}.\tan(\beta_2)}{2.U} \tag{3.30}$$

$$\Lambda = \frac{V_{m1}.\tan(\beta_1)+V_{m2}.\tan(\beta_2)}{2.U} - \frac{(V_{m2}^2 - V_{m1}^2)}{2.Cp.\Delta T_{stage}} \tag{3.31}$$

Because of the adverse pressure gradient in the compressor, the boundary layers along the annulus (flow path) walls thicken as the flow progresses [1]. This results in a change in radial distribution of meridional velocity. Meridional velocity is lower in boundary layers. These effects get dominant in the later stages of compressor and the work capacity of the stage decreases. With the same flow turning the stage enthalpy rise in later stages will be lower than stage enthalpy rise in front stages. The amount is defined by work done factor of the stage (λ).

Equation (3.32) and Equation (3.33) include flow angles in absolute frame. Equation (3.34) and Equation (3.35) include flow angles in relative frame. If one

of the two sets are solved simultaneously α_1, α_2, β_1, β_2 and other flow parameters will be obtained at mean radius.

First set of equations,

$$V_{m2,mean}.\tan(\alpha_{2,mean})-V_{m1,mean}.\tan(\alpha_{1,mean})=\frac{Cp.\Delta T_{stage,mean}}{N.r_{mean}}.\frac{1}{\lambda} \quad (3.32)$$

$$V_{m2,mean}.\tan(\alpha_{2,mean})+V_{m1,mean}.\tan(\alpha_{1,mean})=\left(1-\frac{V_{m2,mean}^2-V_{m1,mean}^2}{2.Cp.\Delta T_{stage,mean}}-\Lambda\right).2.N.r_{mean} \quad (3.33)$$

Second set of equations,

$$V_{m1,mean}.\tan(\beta_{1,mean})-V_{m2,mean}.\tan(\beta_{2,mean})=\frac{Cp.\Delta T_{stage,mean}}{N.r_{mean}}.\frac{1}{\lambda} \quad (3.34)$$

$$V_{m1,mean}.\tan(\beta_{1,mean})+V_{m2,mean}.\tan(\beta_{2,mean})=\left(\Lambda+\frac{V_{m2,mean}^2-V_{m1mean}^2}{2.Cp.\Delta T_{stage,mean}}\right).2.N.r_{mean} \quad (3.35)$$

3.3.Radial Component of Flow

Elementary theory is based on the assumption that there is no radial component of flow in the compressor flowpath. This assumption is quite reasonable when the blade height is small relative to the mean diameter of flowpath. Rear stages of an axial compressor where hub to tip ratio is high around 0.8 will be a typical situation for this assumption [1].

When the blade height is relatively high (lower hub to tip ratios, front stages of a compressor), forces on the flow in radial direction gets larger and cause the flow streamlines shift in radial direction. This occurs especially at front stages of an axial compressor where hub to tip ratio is low about 0.4 [1].

In this case where radial movement of the flow cannot be ignored, Equation (3.13) which represents the radial change of total enthalpy will not be enough. Inertia forces acting on a fluid element in radial direction which shifts streamlines in radial direction are given as follows.

-Circumferential flow produces a centripetal force in radial direction at r-θ plane. This force is named as Radial Force 1.

-Flow along the streamline produces a centripetal force in radial direction at r-z plane. This force is named as Radial Force 2.

-Linear acceleration of flow along streamline requires a force and this force has a radial component at r-z plane. This force is named as Radial Force 3.

Gravitational forces are ignored since magnitudes of other forces are large when compared to them [1]. These inertia forces are balanced with pressure forces which are named as Radial Force 4.

3.3.1. Radial force 1

Radial Force F_1 acts in negative direction. Width of the fluid element is considered as unity.

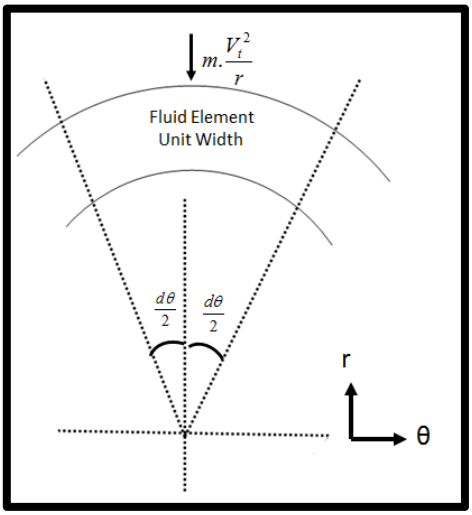

Figure 3.3. Radial force 1

$$F_1 = m.\frac{V_t^2}{r} \tag{3.36}$$

$$mass = density.volume \tag{3.37}$$

$$volume = area.width \tag{3.38}$$

Periphery of a circle is given as,

$$\int_0^{2.\pi}\int_0^{r} dr.d\theta = \int_0^{2.\pi} d\theta.\{r(0 \to r)\} = r.\{\theta(0 \to 2.\pi)\} = 2.\pi.r \tag{3.39}$$

Area of a circle is given as,

$$\int_0^{2.\pi}\int_0^{r} r.dr.d\theta = \int_0^{2.\pi} d\theta.\left\{\frac{r^2}{2}(0 \to r)\right\} = \frac{r^2}{2}.\{\theta(0 \to 2.\pi)\} = \pi.r^2 \tag{3.40}$$

$$F_1 = \rho.area.width.\frac{V_t^2}{r} \tag{3.41}$$

$$F_1 = -\rho.r.dr.d\theta.\frac{V_t^2}{r} \tag{3.42}$$

Considering the direction a negative sign is added to the force.

3.3.2. Radial force 2

$$F_2 = m.\frac{V_s^2}{r_s}.\cos(\alpha_s) \tag{3.43}$$

$$F_2 = -\rho.r.dr.d\theta.\frac{V_s^2}{r_s}.\cos\alpha_s \tag{3.44}$$

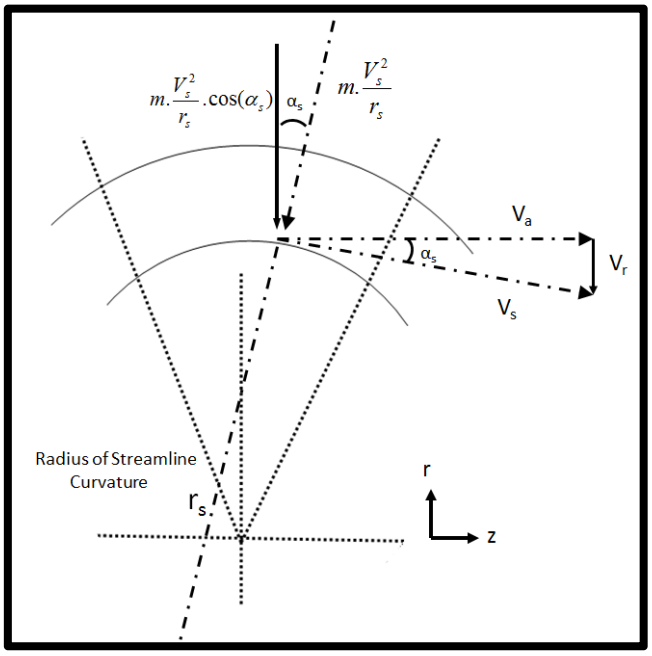

Figure 3.4. Radial force 2

Considering the direction a negative sign is added to the force.

3.3.3. Radial force 3

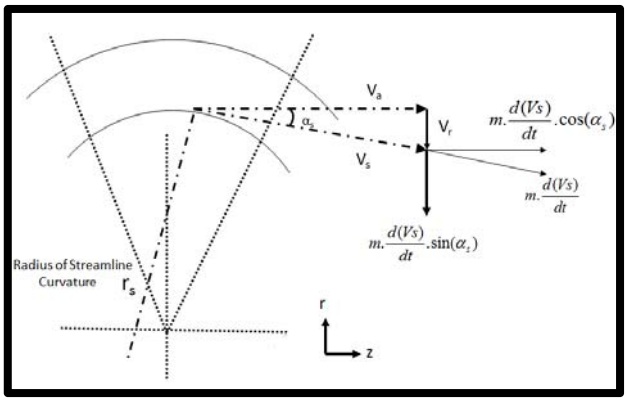

Figure 3.5. Radial force 3

$$F_3 = m.\frac{dV_s}{dt}.\sin(\alpha_s) \tag{3.45}$$

$$F_3 = -\rho.r.dr.d\theta.\frac{dV_s}{dt}.\sin(\alpha_s) \tag{3.46}$$

Considering the direction a negative sign is added to the force. These three forces are the inertia forces acting on the fluid element in the radial direction. These forces are balanced by the pressure forces acting on the fluid element.

3.3.4. Radial force 4

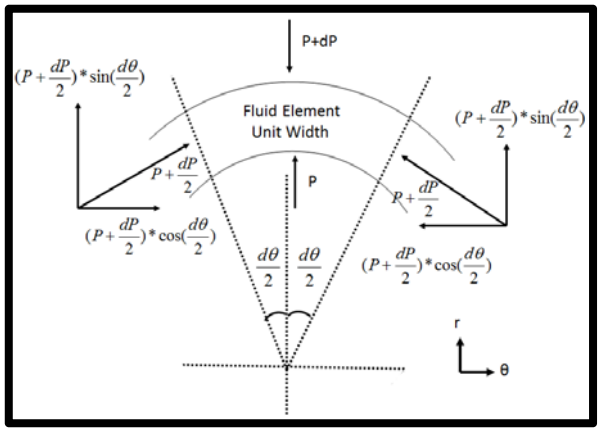

Figure 3.6. Radial force 4

$$(P+dP).Area = (P+dP).length_1.length_2 \tag{3.47}$$

$length_1 = r.d\theta$ (3.48)

$length_1$ is calculated from periphery of a circle

$length_2 = 1$ (3.49)

length$_2$ is calculated as unity from unit width fluid element.

$$F_4 = -(P+dP).(r+dr)d\theta + P.r.d\theta + (P+\frac{dP}{2}).\sin\left(\frac{d\theta}{2}\right).dr + (P+\frac{dP}{2}).\sin\left(\frac{d\theta}{2}\right).dr \tag{3.50}$$

since dθ/2 is a small angle

$$\sin\left(\frac{d\theta}{2}\right) = \frac{d\theta}{2} \tag{3.51}$$

$$F_4 = -P.r.d\theta - P.dr.d\theta - dP.r.d\theta - dP.dr.d\theta + P.r.d\theta + P.dr.d\theta + \frac{dP}{2}.d\theta.dr \tag{3.52}$$

(1, 3, 2, 1, 3, 4)

The terms called 1 cancel each other and the terms called 3 cancel each other. The terms 2 and 4 are product of three infinitesimal terms, so these are neglected. Side forces which have the cosine terms are neglected.

Then Radial Force 4 is calculated as,

$$F_4 = -dP.r.d\theta \tag{3.53}$$

3.4.Equilibrium of Forces on the Fluid Element in Radial Direction

Equilibrium of resultant pressure forces and resultant inertia forces acting on the fluid element in radial direction are given as follows.

$$\vec{F_1} + \vec{F_2} + \vec{F_3} = \vec{F_4} \tag{3.54}$$

$$-\rho.r.dr.d\theta.\frac{V_t^2}{r} - \rho.r.dr.d\theta.\frac{V_s^2}{r_s}.\cos(\alpha_s) - \rho.r.dr.d\theta.\frac{dV_s}{dt}.\sin(\alpha_s) = -dP.r.d\theta \tag{3.55}$$

r and dθ terms are cancelled since they exist at all terms in the equation.

$$-\rho.dr\frac{V_t^2}{r} - \rho.dr.\frac{V_s^2}{r_s}.\cos(\alpha_s) - \rho.dr.\frac{dV_s}{dt}.\sin(\alpha_s) = -dP \tag{3.56}$$

Rearranging the terms,

$$\frac{1}{\rho}.\frac{dP}{dr} = \frac{V_t^2}{r} + \frac{V_s^2}{r_s}.\cos(\alpha_s) + \frac{dV_s}{dt}.\sin(\alpha_s) \tag{3.57}$$

Equation (3.57) is called the radial equilibrium equation. Radial equilibrium equation includes all contributory forces acting on a fluid element in radial direction.

For some design purposes second and third terms of the radial equilibrium equation can be neglected with the following assumptions [1].

-Radius of streamline curvature is too large and the second term gets very small.
-Radius of streamline curvature is too large and α_s gets too small and $\sin(\alpha_s)$ approaches zero.

Rewriting the simplified form of radial equilibrium equation;

$$\frac{1}{\rho}.\frac{dP}{dr}=\frac{V_t^2}{r} \tag{3.58}$$

Simplified form of radial equilibrium equation will be written in terms of change of total enthalpy in radial direction.

$$h_o=h+\frac{V^2}{2}=h+\frac{1}{2}.(V_m^2+V_t^2) \tag{3.59}$$

Taking the derivative of both sides with respect to radius will give the variation of total enthalpy with respect to radius;

$$\frac{dh_o}{dr}=\frac{dh}{dr}+V_m.\frac{dV_m}{dr}+V_t.\frac{dV_t}{dr} \tag{3.60}$$

Equation (3.60) will be related to the simplified form of radial equilibrium equation. Static enthalpy is related with the pressure, density and temperature by the relation from second law of thermodynamics [8].

$$Tds=dh-\frac{dP}{\rho} \tag{3.61}$$

Taking the derivative of both sides with respect to radius will relate the terms with simplified form of radial equilibrium equation.

$$\frac{dh}{dr}=T.\frac{ds}{dr}+ds.\frac{dT}{dr}+\frac{1}{\rho}\frac{dP}{dr}-\frac{1}{\rho^2}\frac{d\rho}{dr}dP \tag{3.62}$$

The second order terms can be dropped since they are small.

$$\frac{dh}{dr}=T.\frac{ds}{dr}+\frac{1}{\rho}\frac{dP}{dr} \tag{3.63}$$

When variation of static enthalpy with respect to radius is inserted to the equation, variation of total enthalpy with respect to radius will be obtained.

$$\frac{dh_o}{dr} = T.\frac{ds}{dr} + \frac{1}{\rho}\frac{dP}{dr} + V_m.\frac{dV_m}{dr} + V_t.\frac{dV_t}{dr} \tag{3.64}$$

Equation [64] is called the non-isentropic radial equilibrium equation (NISRE), giving the variation of total enthalpy with respect to radius.

$$\frac{dh_o}{dr} = \frac{1}{\rho}\frac{dP}{dr} + V_m.\frac{dV_m}{dr} + V_t.\frac{dV_t}{dr} \tag{3.65}$$

Equation (3.65) is called the isentropic radial equilibrium equation (ISRE), giving the variation of total enthalpy with respect to radius by neglecting entropy change across radial direction.

3.5.Distributions of Flow Parameters in Radial Direction

In the previous part the flow angles in absolute frame and relative frame were obtained at the mean radius. In this part variation of parameters in radial direction will be investigated.

For a given tangential velocity distribution in the form;

$$V_{t1} = a.r^n - \frac{b}{r} \quad \text{At inlet of rotor blade} \tag{3.66}$$

$$V_{t2} = a.r^n + \frac{b}{r} \quad \text{At exit of rotor blade} \tag{3.67}$$

$$\Delta h_0 = U.(V_{t2} - V_{t1}) \quad \text{Conservation of angular momentum} \tag{3.68}$$

$$\Delta h_0 = N.r.(a.r^n + \frac{b}{r} - a.r^n + \frac{b}{r}) \tag{3.69}$$

$$\Delta h_0 = N.r.\frac{2.b}{r} \tag{3.70}$$

Δh_0=2.N.b=constant (3.71)

In this form of velocity distribution, since Δh_0=2.N.b=constant

$$\frac{d(\Delta h_0)}{dr} = 0 \tag{3.72}$$

3.5.1. Free vortex velocity distribution

In this part radial distribution of parameters will be investigated for n=-1. This tangential velocity distribution is called Free Vortex Distribution [1] .

Radial equilibrium equation in isentropic form (ISRE)

$$\frac{dh_o}{dr} = \frac{1}{\rho}\frac{dP}{dr} + V_m.\frac{dV_m}{dr} + V_t.\frac{dV_t}{dr} \tag{3.73}$$

$\frac{d(\Delta h_0)}{dr} = 0$ In the form of velocity distribution at inlet and exit

(3.74)

At rotor inlet (Station1)

$$V_{t1} = a.r^n - \frac{b}{r} = \frac{a-b}{r} \tag{3.75}$$

$$\frac{d(V_{t1})}{dr} = -\frac{1}{r^2}(a-b) = \frac{b-a}{r^2} \tag{3.76}$$

Inserting tangential component of absolute velocity into the isentropic radial equilibrium equation;

$$0 = \frac{a^2 - 2.a.b + b^2}{r^2}.\frac{1}{r} + V_m.d(V_m) + \frac{a-b}{r}.\frac{b-a}{r^2} \tag{3.77}$$

rearranging the equation

$$0 = \frac{a^2 - 2.a.b + b^2 + a.b - a^2 - b^2 + a.b}{r^3} + V_m.d(V_m) \tag{3.78}$$

the first term cancels since nominator is zero

$$0 = \int_{r_m}^{r} V_m.d(V_m) = \frac{1}{2}V_m^2\{r_m \to r\} = 0 \tag{3.79}$$

$$\frac{1}{2}.(V_{mr}^2 - V_{mr\,m}^2) = 0 \tag{3.80}$$

$(V_{m,r}^2 - V_{m,r\,m}^2) = 0$ at inlet (3.81)

At rotor exit (Station 2)

$$V_{t2} = a.r^n + \frac{b}{r} = \frac{a+b}{r} \tag{3.82}$$

$$\frac{d(V_{t2})}{dr} = -\frac{1}{r^2}(a-b) = \frac{b-a}{r^2} \tag{3.83}$$

$$0 = \frac{a^2 + 2.a.b + b^2}{r^2}.\frac{1}{r} + V_m.d(V_m) - \frac{a+b}{r}.\frac{b+a}{r^2} \tag{3.84}$$

$$0 = \int_{r_m}^{r} V_m.d(V_m) = \frac{1}{2}V_m^2\{r_m \to r\} = 0 \tag{3.85}$$

$$(V_{mr}^2 - V_{mr\,m}^2) = 0 \text{ at exit} \tag{3.86}$$

$$(V_{m,r}^2 - V_{m,rm}^2)_2 - (V_{m,r}^2 - V_{m,rm}^2)_1 = 0 \tag{3.87}$$

Degree of Reaction for n=-1 (free vortex)

$$\Lambda = \frac{U.(V_{t2} - V_{t1}) - \frac{1}{2}.(V_2^2 - V_1^2)}{U.(V_{t2} - V_{t1})} \tag{3.88}$$

$$\Lambda = 1 - \frac{(V_{m2}^2 - V_{m1}^2)}{2.U.(V_{t2} - V_{t1})} - \frac{(V_{t2}^2 - V_{t1}^2)}{2.U.(V_{t2} - V_{t1})} \tag{3.89}$$

Rearranging equation by writing N.r in terms of U and rewriting tangential components of absolute velocity,

$$\Lambda = 1 - \frac{(V_{m2}^2 - V_{m1}^2)}{2.N.r.(V_{t2} - V_{t1})} - \frac{\left\{(\frac{a+b}{r})^2 - (\frac{a-b}{r})^2\right\}}{2.N.r.(\frac{a+b}{r} - \frac{a-b}{r})} \tag{3.90}$$

$$\Lambda = 1 - \frac{(V_{m2}^2 - V_{m1}^2)}{2.N.r.(V_{t2} - V_{t1})} - \frac{\frac{a^2 + b^2 + 2.a.b - a^2 + 2.a.b - b^2}{r^2}}{2.N.r.(\frac{a+b-a+b}{r})} \tag{3.91}$$

$$\Lambda = 1 - \frac{1}{2}.(\frac{V_{m2}^2 - V_{m1}^2}{2.N.b} + \frac{2.a}{N.r^2}) \tag{3.92}$$

$\frac{d(\Delta h_0)}{dr} = 0$ In the form of velocity distribution. (3.93)

$\Delta h_0 = 2.N.b = \text{constant}$ (3.94)

$$b = \frac{Cp.\Delta T_{stage}}{2.N} \tag{3.95}$$

from inlet to exit meridionalvelocity distribution,

$$V_{m2}^2 - V_{m1}^2 = V_{m2,m}^2 - V_{m1,m}^2 \tag{3.96}$$

Changing the value of b in the degree of reaction equation;

$$\Lambda = 1 - \frac{1}{2}.(\frac{V_{m2}^2 - V_{m1}^2}{Cp.\Delta T_{stage}} + \frac{2.a}{N.r^2}) \quad (3.97)$$

Writing the equation in terms of a; (3.98)

$$a = (1 - \Lambda_m - \frac{1}{2}.\frac{V_{m2,m}^2 - V_{m1,m}^2}{Cp.\Delta T_{stage}}).N.r_m^2 \quad (3.99)$$

Parameters a and b are found. Since a and b are known, radial distribution of the parameters will be calculated.

3.5.2. Exponential velocity distribution

In this part radial distribution of parameters will be investigated for n=0. This tangential velocity distribution is called Exponential Velocity Distribution [1].

$$V_{t1} = a.r^n - \frac{b}{r} \quad (3.100)$$

with n=0 at inlet,

$$V_{t1} = a - \frac{b}{r} \quad (3.101)$$

$$\frac{d(V_{t1})}{dr} = \frac{b}{r^2} \quad (3.102)$$

$$\frac{dh_o}{dr} = \frac{1}{\rho}\frac{dP}{dr} + V_m.\frac{dV_m}{dr} + V_t.\frac{dV_t}{dr} \quad (3.103)$$

and

$$\frac{d(\Delta h_0)}{dr} = 0 \quad (3.104)$$

Inserting tangential component of absolute velocity into the isentropic radial equilibrium equation;

$$0 = \left(a^2 - \frac{2.a.b}{r} + \frac{b^2}{r^2}\right).\frac{1}{r} + V_m.\frac{d(V_m)}{dr} + \left(a - \frac{b}{r}\right).\frac{b}{r^2} \quad (3.105)$$

$$0 = \frac{a^2}{r} - \frac{2.a.b}{r^2} + \frac{b^2}{r^3} + V_m.\frac{d(V_m)}{dr} + \frac{a.b}{r^2} - \frac{b^2}{r^3} \quad (3.106)$$

$$0 = \frac{a^2}{r} - \frac{a.b}{r^2} + V_m.\frac{d(V_m)}{dr} \quad (3.107)$$

$$V_m.d(V_m)=\left(\frac{a.b}{r^2}-\frac{a^2}{r}\right).dr \tag{3.108}$$

integrating from r_m to any r,

$$\int_{r_m}^{r} V_m.d(V_m)=\int_{r_m}^{r}\left(\frac{a.b}{r^2}-\frac{a^2}{r}\right).dr \tag{3.109}$$

$$\frac{1}{2}.V_m.\{r_m \to r\}=-\frac{a.b}{r^2}-a^2.\ln(r)\{r_m \to r\} \tag{3.110}$$

$$V_{m,r}^2-V_{m,r_m}^2=2.\left(-\frac{a.b}{r}-a^2.\ln(r)+\frac{a.b}{r_m}+a^2.\ln(r_m).\right) \tag{3.111}$$

$$V_{m,r}^2-V_{m,r_m}^2=2.a.b.\left(\frac{1}{r_m}-\frac{1}{r}\right)+2.a^2.\ln\left(\frac{r_m}{r}\right) \tag{3.112}$$

at exit,

$$V_{t1}=a+\frac{b}{r} \tag{3.113}$$

$$\frac{d(V_{t1})}{dr}=-\frac{b}{r^2} \tag{3.114}$$

$$\frac{dh_o}{dr}=\frac{1}{\rho}\frac{dP}{dr}+V_m.\frac{dV_m}{dr}+V_t.\frac{dV_t}{dr} \tag{3.115}$$

and

$$\frac{d(\Delta h_0)}{dr}=0 \tag{3.116}$$

Inserting tangential component of absolute velocity into the isentropic radial equilibrium equation;

$$0=\left(a^2+\frac{2.a.b}{r}+\frac{b^2}{r^2}\right).\frac{1}{r}+V_m.\frac{d(V_m)}{dr}+\left(a+\frac{b}{r}\right).\left(\frac{-b}{r^2}\right) \tag{3.117}$$

$$0=\frac{a^2}{r}+\frac{2.a.b}{r^2}+\frac{b^2}{r^3}+V_m.\frac{d(V_m)}{dr}-\frac{a.b}{r^2}-\frac{b^2}{r^3} \tag{3.118}$$

$$0=\frac{a^2}{r}+\frac{a.b}{r^2}+V_m.\frac{d(V_m)}{dr} \tag{3.119}$$

$$V_m.d(V_m)=\left(\frac{-a.b}{r^2}-\frac{a^2}{r}\right).dr \tag{3.120}$$

integrating from r_m to any r,

$$\int_{r_m}^{r} V_m.d(V_m) = \int_{r_m}^{r}\left(\frac{-a.b}{r^2} - \frac{a^2}{r}\right).dr \tag{3.121}$$

$$\frac{1}{2}.V_m.\{r_m \to r\} = \frac{a.b}{r^2} - a^2.\ln(r)\{r_m \to r\} \tag{3.122}$$

$$V_{m,r}^2 - V_{m,r_m}^2 = 2.\left(\frac{a.b}{r} - a^2.\ln(r) - \frac{a.b}{r_m} + a^2.\ln(r_m).\right) \tag{3.123}$$

$$V_{m,r}^2 - V_{m,r_m}^2 = 2.a.b.\left(\frac{1}{r} - \frac{1}{r_m}\right) + 2.a^2.\ln\left(\frac{r_m}{r}\right) \tag{3.124}$$

Degree of Reaction for n=0 (exponential)

$$\Lambda = \frac{U.(V_{t2} - V_{t1}) - \frac{1}{2}.(V_2^2 - V_1^2)}{U.(V_{t2} - V_{t1})} \tag{3.125}$$

$$\Lambda = 1 - \frac{(V_{m2}^2 - V_{m1}^2)}{2.U.(V_{t2} - V_{t1})} - \frac{(V_{t2}^2 - V_{t1}^2)}{2.U.(V_{t2} - V_{t1})} \tag{3.126}$$

Rearranging equation by writing N.r in terms of U and rewriting tangential components of absolute velocity,

$$\Lambda = 1 - \frac{(V_{m2}^2 - V_{m1}^2)}{2.N.r.\left(\left(a + \frac{b}{r}\right) - \left(a - \frac{b}{r}\right)\right)} - \frac{\left\{\left(a + \frac{b}{r}\right)^2 - \left(a - \frac{b}{r}\right)^2\right\}}{2.N.r.\left(\left(a + \frac{b}{r}\right) - \left(a - \frac{b}{r}\right)\right)} \tag{3.127}$$

$$\Lambda = 1 - \frac{(V_{m2}^2 - V_{m1}^2) + a^2 + \frac{2.a.b}{r} + \frac{b^2}{r^2} - a^2 + \frac{2.a.b}{r} - \frac{b^2}{r}}{2.N.r.\left(a + \frac{b}{r} - a + \frac{b}{r}\right)} - \tag{3.128}$$

$$\Lambda = 1 - \frac{1}{2}.\left(\frac{V_{m2}^2 - V_{m1}^2}{2.N.b} + \frac{2.a}{N.r}\right) \tag{3.129}$$

from inlet to exit

$$V_{m2}^2 - V_{m1}^2 = 2.a.b.\left(\frac{1}{r} - \frac{1}{r_m}\right) + 2.a^2.\ln\left(\frac{r_m}{r}\right) - 2.a.b.\left(\frac{1}{r_m} - \frac{1}{r}\right) - 2.a^2.\ln\left(\frac{r_m}{r}\right) + V_{m,2m}^2 - V_{m,1m}^2$$

(3.130)

$$V_{m2}^2 - V_{m1}^2 = 4a.b.\left(\frac{1}{r} - \frac{1}{r_m}\right) + V_{m,2m}^2 - V_{m,1m}^2 \tag{3.131}$$

$$\frac{d(\Delta h_0)}{dr} = 0 \tag{3.132}$$

$$\Delta h_o = U.(V_{t2} - V_{t1}) \tag{3.133}$$

$$\Delta h_o = U.\left(a + \frac{b}{r} - a + \frac{b}{r}\right) \tag{3.134}$$

$$\Delta h_o = U.\left(\frac{2.b}{r}\right) = c_p.\Delta T_{o,stage} \tag{3.135}$$

$$b = \frac{Cp.\Delta T_{stage}}{2.N} \tag{3.136}$$

$$\Lambda = 1 - \frac{1}{2}.\left(\frac{4.a.b.\left(\frac{1}{r} - \frac{1}{r_m}\right) + V_{m,2m}^2 - V_{m,1m}^2}{2.N.b} + \frac{2.a}{N.r}\right) \tag{3.137}$$

Evaluate a @ mean and fix it

$$\Lambda_m = 1 - \frac{1}{2}.\left(\frac{V_{m,2m}^2 - V_{m,1m}^2}{c_c.\Delta T_{o,stage}} + \frac{2.a}{N.r_m}\right) \tag{3.138}$$

$$a = \left(1 - \Lambda_m - \frac{V_{m,2m}^2 - V_{m,1m}^2}{c_c.\Delta T_{o,stage}}\right).N.r_m \tag{3.139}$$

Since a and b are known, radial distribution of the parameters can be calculated.

3.5.3. First power velocity distribution

In this part radial distribution of parameters will be investigated for n=1. This tangential velocity distribution is called First Power Velocity Distribution [1].

At inlet,

$$V_{t1} = a.r^n - \frac{b}{r} \tag{3.140}$$

$$V_{t1} = a.r - \frac{b}{r} \tag{3.141}$$

$$\frac{d(V_{t1})}{dr} = a + \frac{b}{r^2} \tag{3.142}$$

$$\frac{dh_o}{dr} = \frac{1}{\rho}\frac{dP}{dr} + V_m.\frac{dV_m}{dr} + V_t.\frac{dV_t}{dr} \tag{3.143}$$

and

$$\frac{d(\Delta h_0)}{dr} = 0 \tag{3.144}$$

$$0 = \left(a^2.r^2 - 2.a.b + \frac{b^2}{r^2}\right).\frac{1}{r} + V_m.\frac{d(V_m)}{dr} + \left(a.r - \frac{b}{r}\right).\left(a + \frac{b}{r^2}\right) \tag{3.145}$$

$$0 = \left(a^2.r - \frac{2.a.b}{r} + \frac{b^2}{r^3}\right) + V_m.\frac{d(V_m)}{dr} + a^2.r + \frac{a.b}{r} - \frac{a.b}{r} - \frac{b^2}{r^3} \tag{3.146}$$

$$V_m.d(V_m) = \left(\frac{2.a.b}{r} - 2.a^2.r\right).dr \tag{3.147}$$

integrating from r_m to any r,

$$\int_{r_m}^{r} V_m.d(V_m) = \int_{r_m}^{r}\left(\frac{2.a.b}{r} - 2.a^2.r\right).dr \tag{3.148}$$

$$\frac{1}{2}.V_m^2.\{r_m \to r\} = 2.a.b.\ln(r) - 2.a^2.\frac{r^2}{2}\{r_m \to r\} \tag{3.149}$$

$$\frac{1}{2}.\left(V_{m,r}^2 - V_{m,rm}^2\right) = 2.a.b.\ln(r) - a^2.r^2 - 2.a.b.\ln(r_m) + a^2.r_m^2 \tag{3.150}$$

$$V_{m,r}^2 - V_{m,rm}^2 = 4.a.b.\ln\left(\frac{r}{r_m}\right) + 2.a^2.\left(r_m^2 - r^2\right) \quad @ \text{ inlet} \tag{3.151}$$

At exit,

$$V_{t1} = a.r^n + \frac{b}{r}; \tag{3.152}$$

$$V_{t1} = a.r + \frac{b}{r} \tag{3.153}$$

$$\frac{d(V_{t1})}{dr} = a - \frac{b}{r^2} \tag{3.154}$$

$$\frac{dh_o}{dr} = \frac{1}{\rho}\frac{dP}{dr} + V_m.\frac{dV_m}{dr} + V_t.\frac{dV_t}{dr} \tag{3.155}$$

and

$\frac{d(\Delta h_0)}{dr} = 0$ In the form of velocity distribution at inlet and exit (3.156)

$$0 = \left(a^2.r^2 + 2.a.b + \frac{b^2}{r^2} \right).\frac{1}{r} + V_m.\frac{d(V_m)}{dr} + \left(a.r + \frac{b}{r} \right).\left(a - \frac{b}{r^2} \right) \tag{3.157}$$

$$0 = \left(a^2.r + \frac{2.a.b}{r} + \frac{b^2}{r^3} \right) + V_m.\frac{d(V_m)}{dr} + a^2.r - \frac{a.b}{r} + \frac{a.b}{r} - \frac{b^2}{r^3} \tag{3.158}$$

$$V_m.d(V_m) = \left(-\frac{2.a.b}{r} - 2.a^2.r \right).dr \tag{3.159}$$

integrating from r_m to any r,

$$\int_{r_m}^{r} V_m.d(V_m) = \int_{r_m}^{r} \left(-\frac{2.a.b}{r} - 2.a^2.r \right).dr \tag{3.160}$$

$$\frac{1}{2}.V_m^2.\{r_m \to r\} = -2.a.b.\ln(r) - 2.a^2.\frac{r^2}{2}\{r_m \to r\} \tag{3.161}$$

$$\frac{1}{2}.\left(V_{m,r}^2 - V_{m,rm}^2 \right) = -2.a.b.\ln(r) - a^2.r^2 + 2.a.b.\ln(r_m) + a^2.r_m^2 \tag{3.162}$$

$$V_{m,r}^2 - V_{m,rm}^2 = 4.a.b.\ln\left(\frac{r_m}{r} \right) + 2.a^2.\left(r_m^2 - r^2 \right) \quad @ \text{ exit} \tag{3.163}$$

Degree of Reaction for n=1 (first power)

$$\Lambda = \frac{U.(V_{t2} - V_{t1}) - \frac{1}{2}.(V_2^2 - V_1^2)}{U.(V_{t2} - V_{t1})} \tag{3.164}$$

$$\Lambda = 1 - \frac{(V_{m2}^2 - V_{m1}^2)}{2.U.(V_{t2} - V_{t1})} - \frac{(V_{t2}^2 - V_{t1}^2)}{2.U.(V_{t2} - V_{t1})} \tag{3.165}$$

Rearranging equation by writing N.r in terms of U and rewriting tangential components of absolute velocity

$$\Lambda = 1 - \frac{(V_{m2}^2 - V_{m1}^2) + \left(a^2.r^2 + 2.a.b + \frac{b^2}{r^2} - a^2.r^2 + 2.a.b - \frac{b^2}{r^2} \right)}{2.N.r.\left(a.r + \frac{b}{r} - a.r + \frac{b}{r} \right)} \tag{3.166}$$

$$\Lambda = 1 - \frac{(V_{m2}^2 - V_{m1}^2) + 4.a.b}{2.N.r.\frac{2.b}{r}} \tag{3.167}$$

$$\Lambda = 1 - \frac{1}{2}.\left(\frac{V_{m2}^2 - V_{m1}^2}{2.N.b} + \frac{2.a}{N}\right) \tag{3.168}$$

from inlet to exit

$$V_{m2}^2 - V_{m1}^2 = 4.a.b.\ln\left(\frac{r_m}{r}\right) + 2.a^2.\left(r_m^2 - r^2\right) - 4.a.b.\ln\left(\frac{r}{r_m}\right) - 2.a^2.\left(r_m^2 - r^2\right) + V_{m,2m}^2 - V_{m,1m}^2 \tag{3.169}$$

$$V_{m2}^2 - V_{m1}^2 = 8a.b.\ln\left(\frac{r_m}{r}\right) + V_{m,2m}^2 - V_{m,1m}^2 \tag{3.170}$$

$\frac{d(\Delta h_0)}{dr} = 0$ In the form of velocity distribution at inlet and exit (3.171)

$$\Delta h_o = U.\left(V_{t2} - V_{t1}\right) \tag{3.172}$$

$$\Delta h_o = U.\left(a + \frac{b}{r} - a + \frac{b}{r}\right) \tag{3.173}$$

$$\Delta h_o = U.\left(\frac{2.b}{r}\right) = c_p.\Delta T_{o,stage} \tag{3.174}$$

$$b = \frac{Cp.\Delta T_{stage}}{2.N} \tag{3.175}$$

$$\Lambda = 1 - \frac{1}{2}.\left(\frac{V_{m2}^2 - V_{m1}^2}{2.N.b} + \frac{2.a}{N}\right) \tag{3.176}$$

$$\Lambda = 1 - \frac{1}{2}.\frac{8.a.b.\ln\left(\frac{r_m}{r}\right)}{2.N.b} - \frac{1}{2}.\frac{V_{m2,m}^2 - V_{m1,m}^2}{2.N.b} - \frac{a}{N} \tag{3.177}$$

Evaluate a @ mean and fix it

$$\Lambda_m = 1 - \frac{1}{2}.\frac{V_{m,2m}^2 - V_{m,1m}^2}{C_p.\Delta T_{o,stage}} - \frac{a}{N} \tag{3.178}$$

$$a = \left(1 - \Lambda_m - \frac{V_{m,2m}^2 - V_{m,1m}^2}{C_p.\Delta T_{o,stage}}\right).N \tag{3.179}$$

Since a and b are known, radial distribution of the parameters can be calculated.

3.6.Loss and Deviation Correlations

3.6.1. Design incidence angle and design angle of attack

Design incidence angle or design angle of attack defines near optimum or minimal loss inlet angle for the cascade. Formula for the design angle of attack is given below [2].

$$\alpha^* = \left(3.6K_{sh}.K_{ti} + 0.3532.\theta.\left(\frac{a}{c}\right)^{0.25} \right).\sigma^e \tag{3.180}$$

$$e = 0.65 - 0.002.\theta \tag{3.181}$$

K_{sh}=1 for NACA 65

K_{sh}=1.1 for C4 profiles

K_{sh}=0.7 for DCA profiles

Formula for the design incidence angle is given below.

$$i^* = K_{sh}.K_{ti}.\left(i_0^*\right)_{10} + n.\theta \tag{3.182}$$

$$\left(i_0^*\right)_{10} = \frac{\beta_1^p}{5 + 46 * \exp(-2.3\sigma)} - 0.1\sigma^3.\exp\left(\frac{\beta_1 - 70}{4}\right) \tag{3.183}$$

$$p = 0.914 + \frac{\sigma^3}{160} \tag{3.184}$$

$$n = 0.025.\sigma - 0.06 - \frac{\left(\frac{\beta_1}{90}\right)^{(1+1.2*\sigma)}}{1.5 + 0.43\sigma} \tag{3.185}$$

3.6.2. Design deviation angle

Empirical model for the design deviation angle, corresponding to operation at the design incidence angle is given by Lieblien [3]. Formula for the design deviation angle is given below [3].

$$\delta^* = K_{sh}.K_{t,\delta}.\left(\delta_0^*\right)_{10} + m.\theta \tag{3.186}$$

$$\left(\delta_0^*\right)_{10} = 0.01\sigma.\beta_1 + \left(0.74\sigma^{1.9} + 3.\sigma\right).\left(\frac{\beta_1}{90}\right)^{(1.67+1.09*\sigma)} \tag{3.187}$$

$$m = \frac{m_{1.0}}{\sigma^b} \tag{3.188}$$

For NACA 65 Series profiles,

$$m_{1.0} = 0.17 - 0.0333.\frac{\beta_1}{100} + 0.333.\left(\frac{\beta_1}{100}\right)^2 \tag{3.189}$$

For circular arc camberlines,

$$m_{1.0} = 0.249 - 0.074\frac{\beta_1}{100} + 0.132\left(\frac{\beta_1}{100}\right)^2 + 0.316\left(\frac{\beta_1}{100}\right)^3 \tag{3.190}$$

$$b = 0.9625 - 0.17\frac{\beta_1}{100} - 85\left(\frac{\beta_1}{100}\right)^3 \tag{3.191}$$

$$K_{t,\delta} = 6.25*(\frac{t_b}{c}) + 37.5*(\frac{t_b}{c})^2 \tag{3.192}$$

3.6.3. Design loss coefficients and diffusion factors

Sources of total pressure losses are diffusion on blade, tip clearance, leakage in shrouded stators, end-wall boundary layers, Mach number effects, Reynolds number effects and secondary flows [3]. Loss coefficients due to diffusion on blade are considered as profile loss coefficients.

Diffusion Factor (D factor)

$$D = 1 - \frac{W_2}{W_1} + \frac{W_{\theta 1} - W_{\theta 2}}{2.W_1.\sigma} \tag{3.193}$$

Equivalent Diffusion Factor (D_{eq} factor)

$$D_{eq} \approx \frac{W_{\max}}{W_2} \tag{3.194}$$

$$D_{eq}^* = \left(\frac{W_{\max}}{W_1}\right)^* .\frac{W_1^*}{W_2^*} = \left(\frac{W_{\max}}{W_1}\right)^* .\frac{\cos\left(\beta_2^*\right)}{\cos\left(\beta_1^*\right)}.\frac{W_{m1}}{W_{m2}} \tag{3.195}$$

$$\left(\frac{W_{\max}}{W1}\right)^* = 1.12 + 0.61\frac{\cos^2\left(\beta_1^*\right)}{\sigma}.\left\{\tan\left(\beta_1^*\right) - \tan\left(\beta_2^*\right)\right\} \tag{3.196}$$

$$\frac{\omega^* * \cos\left(\beta_2^*\right)}{2.\sigma} = K_1.(K_2 + 3.5.D^* + 37.\left(D^*\right)^4 \tag{3.197}$$

$$\frac{\omega^*.\cos\left(\beta_2\right)}{2.\sigma}.\left(\frac{W_1^*}{W_2^*}\right)^2 = K_1.\left\{K_2 + 3.1\left(D_{eq}^* - 1\right)^2 + 0.4(D_{eq}^* - 1)^8\right\} \tag{3.198}$$

The parameters K1 and K2 can be used to calibrate the profile loss calculations of the throughflow model with experimental data. In the thesis work

they are kept constant and additional scaling factors from hub to tip are used for calibration of the throughflow model.

3.6.4. End-wall and secondary losses

Drag effects due to annulus walls and secondary losses are modeled according to [24]. Formulation for the losses due to annulus and secondary losses are given in [2]. Losses due to annulus drag and secondary flow effects are shown in Figure 3.7 [1].

$$C_{D,\sec ondary} = 0.018.C_L^2 \tag{3.199}$$

$$C_L = \left(\frac{2}{\sigma}\right).\cos\beta_m.\{\tan(\beta_1) - \tan(\beta_2)\} \tag{3.200}$$

$$\tan\beta_m = \frac{\tan(\beta_1) + \tan(\beta_2)}{2} \tag{3.201}$$

$$\omega_{\sec ondary} = C_{D,\sec ondary}.\frac{1}{2}.\rho.V^2 \tag{3.202}$$

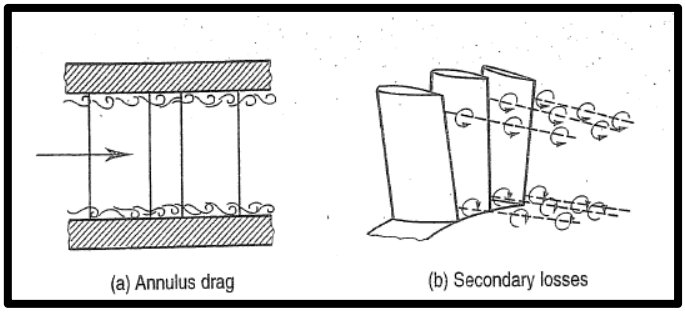

Figure 3.7. Losses due to annulus drag and secondary flow effects [1]

3.6.5. Positive and negative stall incidence angles

Figure 3.8 shows the change of loss coefficient with respect to incidence angles. Loss coefficient grows rapidly when the cascade goes far from the design operating condition. Positive incidence corresponds to pressure side incidence where negative incidence corresponds to suction side incidence. As the compressor cascade goes from choke to stall, incidence changes from negative direction to positive direction. Positive and negative stall incidences are determined according to the incidence where pressure loss coefficient is twice the minimum value [2].

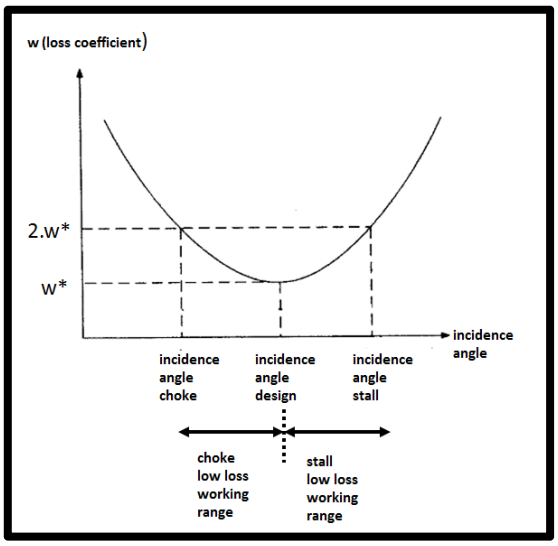

Figure 3.8. Effect of incidence angles on profile loss coefficient

Empirical equations for minimum and maximum loss angles are applied according to [2].

$$\alpha_c - \alpha^* = -9 + \left(1 - \left(\frac{30}{\beta 1_c}\right)^{0.48}\right) \cdot \frac{\theta}{4.176} \tag{3.203}$$

$$\alpha_s - \alpha^* = 10.3 + \left(2.92 - \frac{\beta 1_c}{15.6}\right) \cdot \frac{\theta}{8.2} \tag{3.204}$$

3.6.6. Mach number effects

When calculating blade element loss data from low speed correlations, Mach number corrections are necessary since low loss working ranges of the cascade decreases with increasing inlet Mach number. Figure 3.9 shows the effect of Mach number on losses [1].

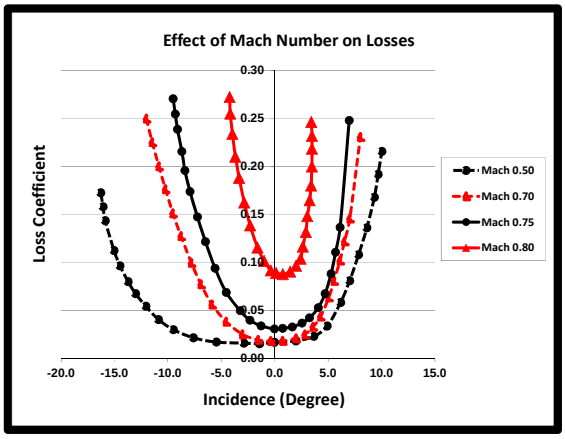

Figure 3.9. Effect of mach number on losses [1]

Low loss working ranges are R_s and R_c. R_s correspond to the stall side where positive incidence occurs in the blade. R_c corresponds to the choke side where negative incidence occurs in the blade.

$$R_c = \alpha^* - \alpha_c = i^* - i_c \tag{3.205}$$

$$R_s = \alpha_s - \alpha^* = i_s - i^* \tag{3.206}$$

$$i_c = i^* - \frac{R_c}{1 + \frac{M_1^3}{2}} \tag{3.207}$$

$$i_s = i^* + \frac{R_s}{1 + \frac{\left(K_{sh}.M_1^3\right)^3}{2}} \tag{3.208}$$

With negative and positive stall incidence angles, minimum loss incidence angle will be also adjusted for Mach number effects.

$$i_m = i_c + \frac{(i_s - i_c).R_c}{R_c + R_s} \tag{3.209}$$

When the cascade operates at moderate Mach numbers far from choking condition design incidence angle and minimum loss incidence angles are equal to each other. For high Mach number cascade operation minimum loss incidence angle is greater than the design incidence angle. If incidence angle is smaller than or equal to minimum loss incidence angle

$$\omega = \omega_m + \omega_m.\left(\frac{i - i_m}{i_c - i_m}\right)^2 \tag{3.210}$$

If incidence angle is bigger than or equal to minimum loss incidence angle

$$\omega = \omega_m + \omega_m\left(\frac{i - i_m}{i_s - i_m}\right)^2 \tag{3.211}$$

Minimum correction for minimum loss coefficient is

$$\omega_m = \omega^*.\left(1 + \frac{(i_m - i^*)^2}{R_s^2}\right) \tag{3.212}$$

Until fluid velocities become supersonic on blade surfaces, loss coefficients at the minimum loss incidence angle change less with the change in Mach number. After the critical Mach number, where the flow becomes

supersonic on blade surfaces, minimum loss coefficient is estimated from Equation (3.214).

Critical Mach number at blades M_c is calculated as;

$$M_c = \left(\frac{M_1 . W^*}{W_{\max}} \right) \tag{3.213}$$

$$\omega_m = \omega^* . \left(1 + \frac{\left(i_m - i^* \right)^2}{R_s^2} \right) + K_{sh} . \left(\frac{\left(\frac{M_1}{M_c - 1} \right) . W^*}{W_1} \right)^2 \tag{3.214}$$

$$\frac{W_{\max}}{W_1} = 1.12 + 0.61 . \frac{\cos^2(\beta_1)}{\sigma} \left(\tan(\beta_1) - \tan(\beta_2) \right) + \alpha . \left(i - i^* \right)^{1.43} \tag{3.215}$$

For the Mach numbers higher than the critical Mach number , minimum loss coeficient fomulation is valid until M_1 is smaller than sonic Mach number 1.

For the far off design conditions, profile loss coefficient is calculated according to equations below.

$$\xi = \frac{i - i_m}{i_s - i_m} \tag{3.216}$$

Equation [217] is valid for i is greater or bigger than i_m

$$\xi = \frac{i - i_m}{i_m - ic} \tag{3.217}$$

Equation [218] is valid for i is smaller than i_m

$$\omega = \omega_m \left(1 + \xi^2 \right) \qquad \text{for } -2 \le \xi \le 1 \tag{3.218}$$

$$\omega = \omega_m \left(5 - 4 . \left(2 + \xi \right) \right) \qquad \text{for } \xi < -2 \tag{3.219}$$

$$\omega = \omega_m \left(2 + 2 . \left(\xi - 1 \right) \right) \qquad \text{for } \xi > 1 \tag{3.220}$$

Off design deviation angles are also adjusted according to change in design incidence angle.

$$\delta = \delta^* + \left(\frac{\partial \delta}{\partial i} \right)^* . \left(i - i^* \right) + 10 . \left(1 - \frac{W_{m2}}{W_{m1}} \right) \tag{3.221}$$

$$\left(\frac{\partial \delta}{\partial i} \right)^* = \frac{\left[1 + \left(\sigma + 0.25\sigma^4 \right) . \left(\frac{\beta_1}{53} \right)^{2.5} \right]}{\exp(3.1\sigma)} \tag{3.222}$$

3.6.7. Boundary layer analysis

End wall boundary analysis is done according to Pachidis [5]. Pachidis used a simplified two-dimensional boundary layer approach given by Barbosa [32] for calculation of blockage factors due to endwall boundary layers. Boundary layer momentum thickness is calculated from Equation (3.223) and Equation (3.224). Boundary layer shape factor is calculated from Equation (3.225). Boundary layer displacement thickness is calculated from Equation (3.226). Blockage factors for hub and tip are calculated from Equation (3.227) and Equation (3.228). Overall blockage factor is calculated from Equation (3.229).

$$\theta(z) = \theta(z_0) + k_{factor}\left(\frac{\int_{z\_inlet}^{z\_outlet} V_m^4(z)dz}{V_m^{3.2}}\right)^{0.8} \tag{3.223}$$

$$\theta(z_0) = \frac{\delta^*(z_0)}{H(z_0)}$$

$$H(z) = 1.5 + 30\frac{d\theta}{dz} \tag{3.224}$$

(3.225)

$$\delta^*(z) = \theta(z).H(z) \tag{3.226}$$

$$k_B @ hub = \frac{(r_{hub} + \delta^*_{hub})^2 - r_{hub}^2}{r_{tip}^2 - r_{hub}^2} \tag{3.227}$$

$$k_B @ tip = \frac{r_{tip}^2 - (r_{tip} - \delta^*_{tip})^2}{r_{tip}^2 - r_{hub}^2} \tag{3.228}$$

$$k_B = 1 - (k_B @ tip + k_B @ hub) \tag{3.229}$$

3.6.8. Shock losses

For the shock loss calculations assumptions made are given as:

-Unique incidence condition

-Bow oblique shock is attached to the leading edge

-Shock inside the passage is a normal shock perpendicular o the mean streamline and is at the mid of two blades.

Shock loss calculations are given in step by step method.

Shock loss model 1

Shock loss calculation at this model is done according to Pachidis[5]. Pachidis used shock loss model of Schwenk et al. [33].

Step 1:

Calculate supersonic turning, τ from Equation (3.230). τ is also called Prandtl Meyer expansion angle.

$$\nu_B(M_B) - \nu_1(M_1) = \tau \tag{3.230}$$

Prandtl-Meyer function for the flow at inlet (1) and before (B) the normal shock is calculated form Equation (3.231).

$$\nu(M) = \sqrt{\frac{k+1}{k-1}} * \tan^{-1}\sqrt{\frac{k-1}{k+1}*(M^2-1)} - \tan^{-1}\sqrt{M^2-1} \tag{3.231}$$

Step 2:

Calculate supersonic turning, τ from Equation (3.232). τ is also called Prandtl Meyer expansion angle.

$$\tau = \alpha_1 - \zeta + \xi \tag{3.232}$$

ζ is the stagger angle and ξ is calculated form Equation (3.233).

$$\xi = \sin\left(\left(\frac{2.x}{c'} - 1\right).\sin\left(\frac{\phi_s}{2}\right)\right) \tag{3.233}$$

c' is calculated from Equation (3.234).

$$c' = chord - 2.r_{le} \tag{3.234}$$

φ_s is calculated from Equation (3.235).

$$\phi_s = 4.\tan^{-1}\left(\frac{1-\cos\left(\frac{\theta}{2}\right)}{\sin\left(\frac{\theta}{2}\right)} + \frac{t_{\max\_blade} - 2.r_{le}}{c'}\right) \tag{3.235}$$

x is calculated from Equation (3.236).

$$\frac{2.x}{c'} = 1 + \sin(2.\Sigma).\cot\left(\frac{\theta}{2}\right) - \cos(2.\Sigma) \tag{3.236}$$

Σ is calculated from Equation (3.237).

$$\Sigma = \tan^{-1}\left(\frac{\sin(K_1).\sin(\frac{\theta}{2})}{\frac{c'}{s}+\cos(K_1).\sin\left(\frac{\theta}{2}\right)}\right) \tag{3.237}$$

Step 3:

Calculate Mach number before shock through an iterative process between step 1 and step 2. False Position Iteration [25] is used for calculation of M_B in the thesis work .

Step 4:

Calculate an average Mach Number before normal shock by averaging inlet Mach number (M_1) and mach number of Prandtl Meyer analysis (M_B) .

$$M_{BS} = \frac{M_1 + M_B}{2} \tag{3.238}$$

Step 5:

Calculate Mach Number after normal shock, M_A from Equation (3.239).

$$M_A = \sqrt{\frac{(k-1).M_{BS}^2 + 2}{2.k.M_{BS}^2 - (k-1)}} \tag{3.239}$$

Calculate total pressure after normal shock, Po_A from Equation (3.240)

$$\frac{Po_A}{Po_{BS}} = \left(\frac{\frac{k+1}{2}.M_{BS}^2}{1+\frac{k-1}{2}.M_{BS}^2}\right)^{\frac{k}{k-1}} .\left(\frac{2.k}{k+1}.M_{BS}^2 - \frac{k-1}{k+1}\right)^{\frac{k}{1-k}} \tag{3.240}$$

With the known values of Po_{BS}, M_{BS}, calculate Ps_{BS} from Equation (3.241).

$$\frac{Po_{BS}}{Ps_{BS}} = \left(1+\frac{k-1}{2}.M_{BS}^2\right)^{\frac{k-1}{k}} \tag{3.241}$$

Step 6:

Calculate shock loss coefficient from Equation (3.242)

$$w_s = \frac{Po_{BS} - Po_A}{Po_{BS} - Ps_{BS}} \tag{3.242}$$

Shock loss model 2

Shock loss calculation at this model is done according to Aungier [2]. Aungier's calculations are based on shock loss model of Swan [31] . Figure 3.10 and Figure 3.11 give the nomenclature for the shock loss model.

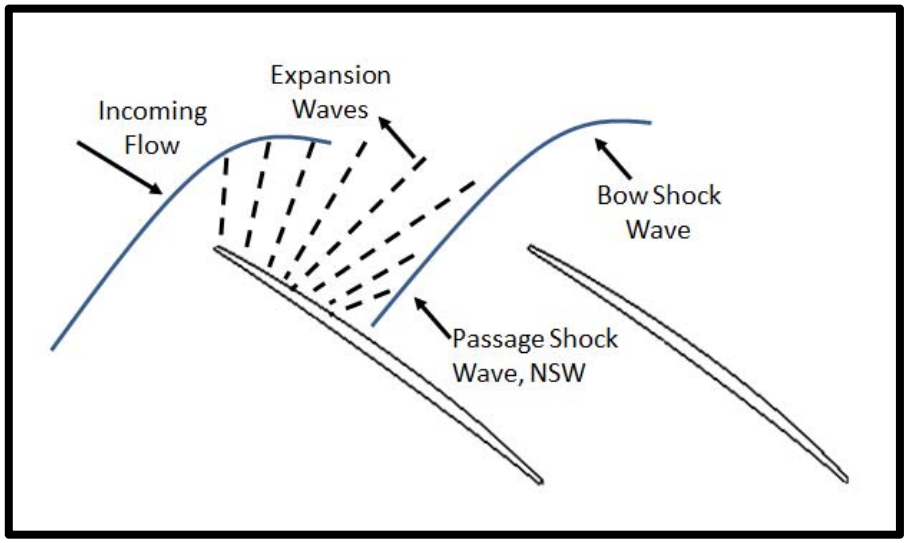

Figure 3.10. Shock structure for shock loss model 2 [2]

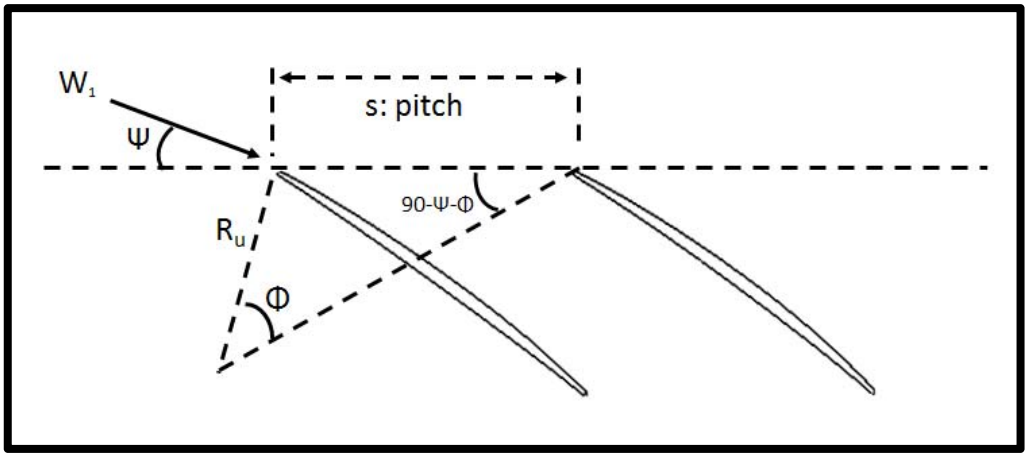

Figure 3.11. Cascade nomenclature for the shock loss model 2 [2]

Step 1:

Calculate Prandtl-Meyer expansion angle τ from Equation (3.243).

$$\tan(\tau) = \frac{s.\cos(\psi)}{s.\sin(\psi) + R_u} \tag{3.243}$$

$$2.\frac{R_u}{c} = \sin\left(\frac{\theta_u}{2}\right) \tag{3.244}$$

$$\tan\left(\frac{\theta_u}{4}\right)=\tan\left(\frac{\theta}{4}\right)+\frac{t_b}{c} \tag{3.245}$$

$$90-\psi=\frac{\theta_u}{2}+\gamma \tag{3.246}$$

Prandtl-Meyer function for the flow at inlet (1) and before (B) the normal shock is calculated form Equation (3.247).

$$\nu(M)=\sqrt{\frac{k+1}{k-1}}*\tan^{-1}\sqrt{\frac{k-1}{k+1}*(M^2-1)}-\tan^{-1}\sqrt{M^2-1} \tag{3.247}$$

Step 2:

Calculate Prandtl-Meyer function for the flow before (B) the normal shock from Equation (3.248)

$$\nu_B(M_B)-\nu_1(M_1)=\tau \tag{3.248}$$

Step 3:

Calculate an average Mach Number before normal shock by by averaging inlet Mach number (M_1) and Mach number of Prandtl Meyer analysis (M_B) .

$$M_{BS}=\sqrt{M_1.M_B} \tag{3.249}$$

Step 4:

Calculate Mach Number after normal shock, M_A from Equation (3.250).

$$M_A=\sqrt{\frac{(k-1).M_{BS}^2+2}{2.k.M_{BS}^2-(k-1)}} \tag{3.250}$$

Calculate total pressure after normal shock, Po_A from Equation (3.251).

$$\frac{Po_A}{Po_{BS}}=\left(\frac{\frac{k+1}{2}.M_{BS}^2}{1+\frac{k-1}{2}.M_{BS}^2}\right)^{\frac{k}{k-1}}.\left(\frac{2.k}{k+1}.M_{BS}^2-\frac{k-1}{k+1}\right)^{\frac{k}{1-k}} \tag{3.251}$$

With the known values of Po_{BS}, M_{BS}, calculate Ps_{BS} from Equation (3.252).

$$\frac{Po_{BS}}{Ps_{BS}}=\left(1+\frac{k-1}{2}.M_{BS}^2\right)^{\frac{k-1}{k}} \tag{3.252}$$

Step 5:

Calculate shock loss coefficient from Equation (3.253).

$$w_s = \frac{Po_{BS} - Po_A}{Po_{BS} - Ps_{BS}} \tag{3.253}$$

Shock loss model 3

Shock loss calculation at this model is done according to Cetin et al.[4]. Cetin's calculations are based on shock loss model of Swan [31] .

Step 1:

Calculate supersonic turning, τ from Equation (3.254). τ is also called Prandtl Meyer expansion angle.

$$\nu_B(M_B) - \nu_1(M_1) = \tau \tag{3.254}$$

Prandtl-Meyer function for the flow at inlet (1) and before (B) the normal shock is calculated form Equation (3.255),

$$\nu(M) = \sqrt{\frac{k+1}{k-1}} * \tan^{-1}\sqrt{\frac{k-1}{k+1}*(M^2-1)} - \tan^{-1}\sqrt{M^2-1} \tag{3.255}$$

Step 2:

Calculate supersonic turning, τ from Equation (3.256). τ is also called Prandtl Meyer expansion angle.

$$\tau = \tan^{-1}\left(\frac{s.\sin(\alpha_1)}{s.\cos(\alpha_1) + R_u}\right) \tag{3.256}$$

R_u is the blade upper surface radius of curvature. R_u is calculated from Equation (3.257)

$$R_u = \frac{r_{le}}{2} + \left[\frac{\left\{\frac{t_{max\_blade}}{2} - \frac{r_{le}}{2} + \left(\frac{chord}{2} - \frac{r_{le}}{2}\right).\tan\left(\frac{\theta}{4}\right)\right\}^2 + \left\{\frac{chord}{2} - \frac{r_{le}}{2}\right\}}{2.\left\{\left(\frac{chord}{2}\right).\tan\left(\frac{\theta}{4}\right) + \frac{t_{max\_blade}}{2} - \frac{r_{le}}{2}\right\}}\right] \tag{3.257}$$

Step 3:

Calculate Mach number before shock through an iterative process between step 1 and step 2. False Position Iteration [25] is used for calculation of M_B . Alternatively use approximate value for M_B from Equation (3.258).

$$M_B = 1.0 + 0.0432\nu_B(M_B) \tag{3.258}$$

Step 4:

Calculate an average Mach Number before norrmal shock by by averaging inlet Mach number (M_1) and Mach number of Prandtl Meyer analysis (M_B) **.**

$$M_{BS} = \frac{M_1 + M_B}{2} \tag{3.259}$$

Step 5:

Calculate Mach Number after normal shock, M_A from Equation (3.260)

$$M_A = \sqrt{\frac{(k-1).M_{BS}^2 + 2}{2.k.M_{BS}^2 - (k-1)}} \tag{3.260}$$

Calculate total pressure after normal shock, Po_A from Equation (3.261)

$$\frac{Po_A}{Po_{BS}} = \left(\frac{\frac{k+1}{2}.M_{BS}^2}{1+\frac{k-1}{2}.M_{BS}^2} \right)^{\frac{k}{k-1}} .\left(\frac{2.k}{k+1}.M_{BS}^2 - \frac{k-1}{k+1} \right)^{\frac{k}{1-k}} \tag{3.261}$$

With the known values of Po_{BS}, M_{BS}, calculate Ps_{BS} from Equation (3.262).

$$\frac{Po_{BS}}{Ps_{BS}} = \left(1+\frac{k-1}{2}.M_{BS}^2 \right)^{\frac{k-1}{k}} \tag{3.262}$$

Step 6:

Calculate shock loss coefficient from Equation (3.263).

$$w_s = \frac{Po_{BS} - Po_A}{Po_{BS} - Ps_{BS}} \tag{3.263}$$

Shock loss model 4

For shock loss model 4 calculations are done according to [1]. In Figure 3.12 cascade nomenclature for shock loss model is given [1]. In Figure 3.13 shock loss coefficents for shock loss model 4 is given [1]. For this model supersonic turning angle is assumed to be half of the camber.

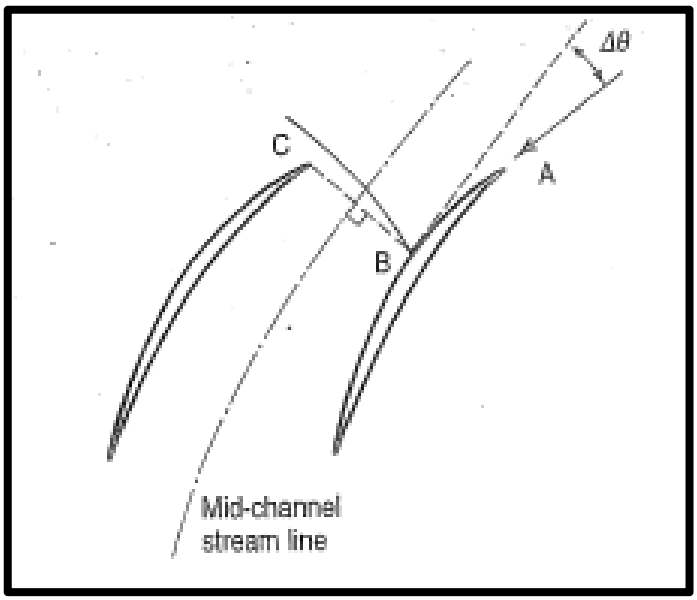

Figure 3.12. Cascade nomenclature for the shock loss model 4 [1]

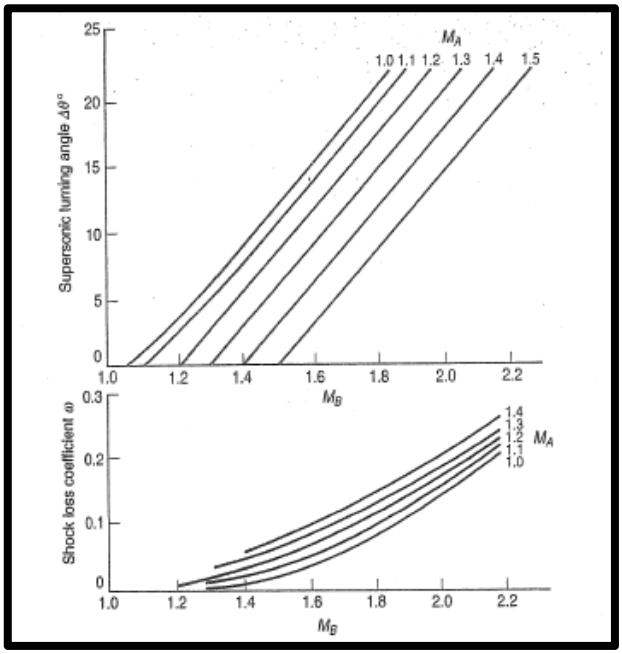

Figure 3.13. Shock loss coefficients for sock loss model 4 [1]

Step 1:

Calculate shock Mach number at point B.

$$M_B = 3.10985 - 5.58148M_A + 4.59534M_A^2 - 1.05699M_A^3 + 0.0606884\Delta\theta - 0.00076839\Delta\theta^2 + 4.54814e^{-6}\Delta\theta^3 - 0.0257165M_A.\Delta\theta + 0.0057339M_A^2.\Delta\theta + 0.00043224.M_A.\Delta\theta^2 \quad (3.264)$$

Step 2:

Calculate shock loss coefficient.

$$\omega_s = 0.919337 - 0.188945M_A - 0.428293M_A^2 + 0.0990409M_A^3 - 1.69524.M_B + 0.6423332.M_B^2 - 0.0293283.M_B^3 + 0.930183.M_A.M_B + 0.0518149.M_A^2.M_B - 0.291765.M_A.M_B^2 \quad (3.265)$$

Additional to these shock loss models there are available shock loss models that take into accont effect of incidence [7] [6], shock position [6] and shock inclination [6] as normal shock or oblique shock.

3.6.9. Overall loss coefficient

Oveall loss coefficient is calculated by adding profile losses, secondary losses and shock losses. Profile losses have Mach Number corrections to take into account compressibility effects. In the throughflow analysis scaling factors from hub to tip for all loss coefficients are used to be able to calibrate analysis results according to experimental results or CFD.

3.7.Blade Design

With the determined annulus dimansions and given blade aspect ratios at mean radius, blade chord is determined.

$$c = \frac{r_{tip} - r_{hub}}{A.R} \quad (3.266)$$

Solidity is determined from flow turning, chord and target diffusion factor for the blade. Target diffusion factor is input for the throughflow program when it is running in design mode.

$$D = 1 - \frac{W_2}{W_1} + \frac{W_{\theta 1} - W_{\theta 2}}{2.W_1.\sigma} \quad (3.267)$$

Pitch is ratio of chord to solidity.

$$s = \frac{c}{\sigma} \quad (3.268)$$

Blade number is defined by periphery of the flowpath at meanline and pitch.

$$Blade_{number} = \frac{2.\pi.r_{mean}}{s} \quad (3.269)$$

Construction of blade profiles are done according to Aungier [2]. Cascade nomenclature is given in Figure 3.14.

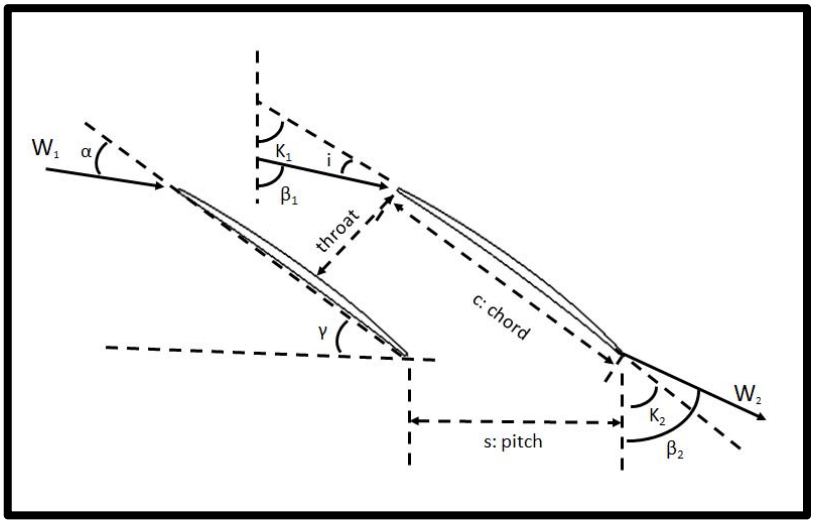

Figure 3.14. Cascade nomenclature

3.7.1. Circular arc camberline

Circular arc camberlines are used in British C4 series blade profiles and in double circular arc (DCA) profiles. Camberline is constructed using camber angle and chord length.

Radius of curvature of the circular arc camberline is calculated from Equation (3.270).

$$R_c = \frac{c/2}{\sin(\theta/2)} \tag{3.270}$$

y-coordinate of radius of curvature is calculated from Equation (3.271).

$$y_c = -R_c.\cos\left(\frac{\theta}{2}\right) \tag{3.271}$$

x-coordinate of chord is defined from –c/2 to c/2. y-coordinate of the circular arc camberline will be calculated from Equation (3.272).

$$y = y_c + \sqrt{R_c^2 - x^2} \tag{3.272}$$

3.7.2. Parabolic arc camberline

Parabolic arc camberlines are used in British C4 series blade profiles. Camberline is constructed using camber angle, chord length and point of maximum camber.

y-coordinate of point of maximum camber is calculated from Equation (3.273).

$$\frac{b}{c}=\frac{\sqrt{1+(4.\tan(\theta))^2\left[\frac{a}{c}-\left(\frac{a}{c}\right)^2-\frac{3}{16}\right]}-1}{4.\tan(\theta)} \tag{3.273}$$

x-coordinate and y-coordinates of camberline are calculated from Equation (3.274).

$$x^2+\frac{c-2.a}{b}.xy+\frac{(c-2.a)^2}{4.b^2}.y^2-c.x-\frac{c^2-4.a.c}{4.b}.y=0 \tag{3.274}$$

3.7.3. Double circular arc camberline

Double circular arc profile is constructed by two circular arcs defining upper and lower surfaces.Radius of curvature of the circular arc camberline is calculated from Equation (3.275)

$$R_c=\frac{c/2}{\sin(\theta/2)} \tag{3.275}$$

y-coordinate of radius of curvature is calculated from Equation (3.276)

$$y_c=-R_c.\cos\left(\frac{\theta}{2}\right) \tag{3.276}$$

x-coordinate of chord is defined from –c/2 to c/2. y-coordinate of the circular arc camberline are calculated from Equation (3.277).

$$y=y_c+\sqrt{R_c^2-x^2} \tag{3.277}$$

y(0) is calculated by inserting x=0 to above equation

$$y(0)=y_c+R_c \tag{3.278}$$

For calculation of upper and lower surface radius of curvature values ,

$$d=y(0)+\frac{t_{\max\_blade}}{2}-r_{le}.\sin\left(\frac{\theta}{2}\right) \tag{3.279}$$

$$R_u=\frac{d^2-r_{le}^2+\left[\frac{c}{2}-r_{le}.\cos\left(\frac{\theta}{2}\right)\right]^2}{2.(d-r_{le})} \tag{3.280}$$

$$R_l = \frac{d^2 - r_{le}^2 + \left[\frac{c}{2} + r_{le}.\cos\left(\frac{\theta}{2}\right)\right]^2}{2.(d + r_{le})} \tag{3.281}$$

x-coordinate of chord is defined from –c/2 to c/2. y-coordinates of the upper and lower surfaces are calculated from Equation (3.282) and Equation (3.283).

$$y_u = y_c + \sqrt{R_u^2 - x^2} \tag{3.282}$$

$$y_l = y_c + \sqrt{R_l^2 - x^2} \tag{3.283}$$

3.8.Velocity Distribution in Meridional Plane

Velocity distribution in meridional plane is determined according to the following procedure.

-Blade cascade data and flow path information is given.

-Mass flow rate, rotational speed, inlet total pressure and total temperature is given.

-Inlet flow angle is given.

-Inlet meridional velocity is calculated according to annulus dimansions and inlet flow field inputs.

-Keeping the meridional velocity constant or by specifying a an axial velocity ratio across blade row, outlet flow field is calculated in terms of losses and deviations.

-With the flow field information at the exit of the blade row meridional velocity is specified at tip [3].

-Meridional velocity is distributed from tip to hub according to ISRE or NISRE equations.

-Convergence for the mass flow rate is checked.

-Iterations continue by changing exit meridional velocity at tip until continuity is satisfied.

Meridional velocity distribution is given in Equation (3.284) according to simple radial equilibrium equation taking into account entropy gradients in radial direction [3].

ISRE

$$V_m^2 = V_{m,i}^2 + 2.c_p\left(T - T_i\right) - \left(V_t^2 - V_{t,i}^2\right) - \left(\frac{V_t^2}{r} + \frac{V_{t,i}^2}{r_i}\right).\left(r - r_i\right) \tag{3.285}$$

NISRE

$$V_m^2 = \left\{\frac{1}{1 - \frac{k-1}{2k}.\ln\left(\frac{\left(\frac{T}{T_i}\right)^{\frac{k}{k-1}}}{\frac{P}{Pi}}\right)}\right\}\left\{\begin{array}{l} V_{m,i}^2.\left\{1 + \frac{k-1}{2k}.\ln\left[\frac{\left(\frac{T}{T_i}\right)^{\frac{k}{k-1}}}{\frac{P}{P_i}}\right]\right\} + 2.c_p\left(T - T_i\right) - \left(V_t^2 - V_{t,i}^2\right) \\ - \left(\frac{V_t^2}{r} + \frac{V_{t,i}^2}{r_i}\right).\left(r - r_i\right) - \ln\left[\frac{\left(\frac{T}{T_i}\right)^{\frac{k}{k-1}}}{\frac{P}{P_i}}\right].\left[\left(T + T_i\right) - \frac{k-1}{2.k}.\left(V_t^2 + V_{t,i}^2\right)\right] \end{array}\right\} \tag{3.284}$$

Meridional velocity distribution is given in Equation (3.285) according to simple radial equilibrium [3].

4. OPTIMIZATION

Optimization is done with coupling a metamodel to genetic algorithm. Metamodel is Artificial Neural Network in the optimization procedure.

4.1.Genetic Algorithm

Genetic Algorithm is a numerical search technique based on genetics. Genetic Algorithm simulates Darwin's evalutionary theory "survival of the fittest" [19] .

Application areas for Genetic Algorithms are in a wide range and a list of these application areas are listed [19] [27].

-Scheduling
-Engineering Optimisation
-Control Systems
-Time Series Prediction

Flowchart for the genetic algorithm is given in Figure 4.1.

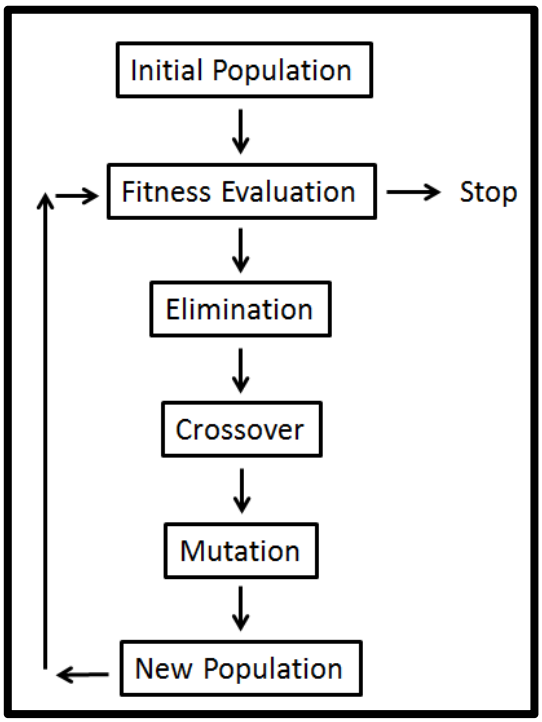

Figure 4.1. Genetic algorithm flow chart

In population initiation a set of design variables (chromosomes) are taken either by random number generation or by user specification. In fitness evaluation rank for design variable sets are sorted according to the way of optimization. Design variable sets are sorted either in ascending or descending order. In elimination , worst ranking variable sets are substrated from the population in order to evolve the population. In crossover remaining population is crossedover between each other in order to generate new chromosomes. In mutation population is changed by a factor defined by the user in order to have variety in the population. New population is again tested in terms of fitness values. Iterations continue until a predefined convergence criteria or iteration number limit is reached.

Fitness evaluation may be done either directly by numerical compuatation of the problem or can be done by an approximate model representing the real problem. Approximate models or metamodels such as Polynomial Response Surfaces , Artificial Neural Networks can be used in fitness evaluation.

After elimination while the variable sets are crossed over best ranking set or sets will be kept without change. This is called in Elitisim is Genetic Algorithm. This operation avoids loosing best ranking chromosome pairs.

4.2.Artificial Neural Network

Artificial Neural Network is an emulation of biological neural system. Artificial Neural Network is a collection of simple processors connected together that and named as Neural Net or ANN. Figure 4.2 [28] and Figure 4.3 give similarity between biological and artificial system of networks.

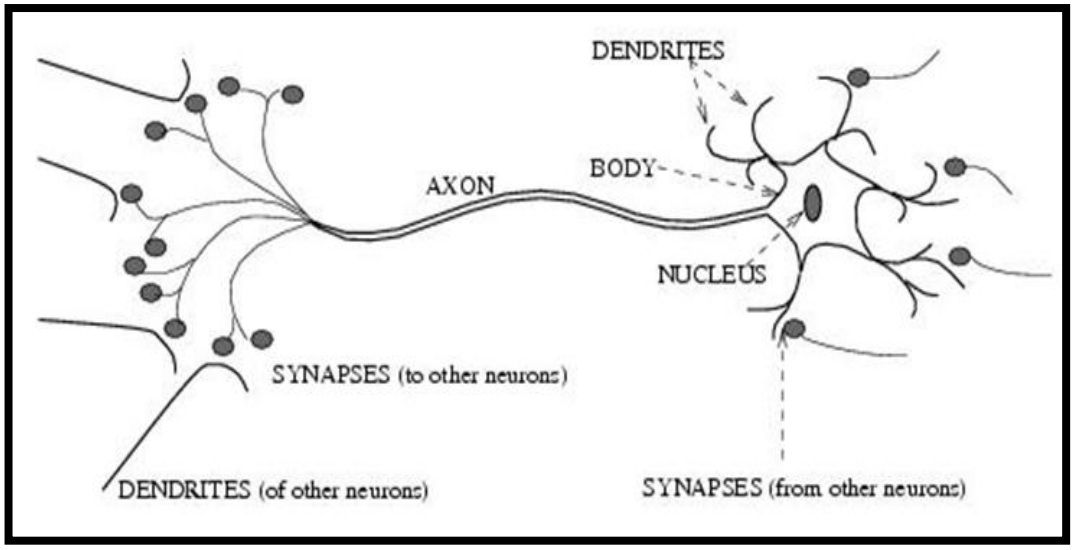

Figure 4.2. Neuron in a biological neural network [28]

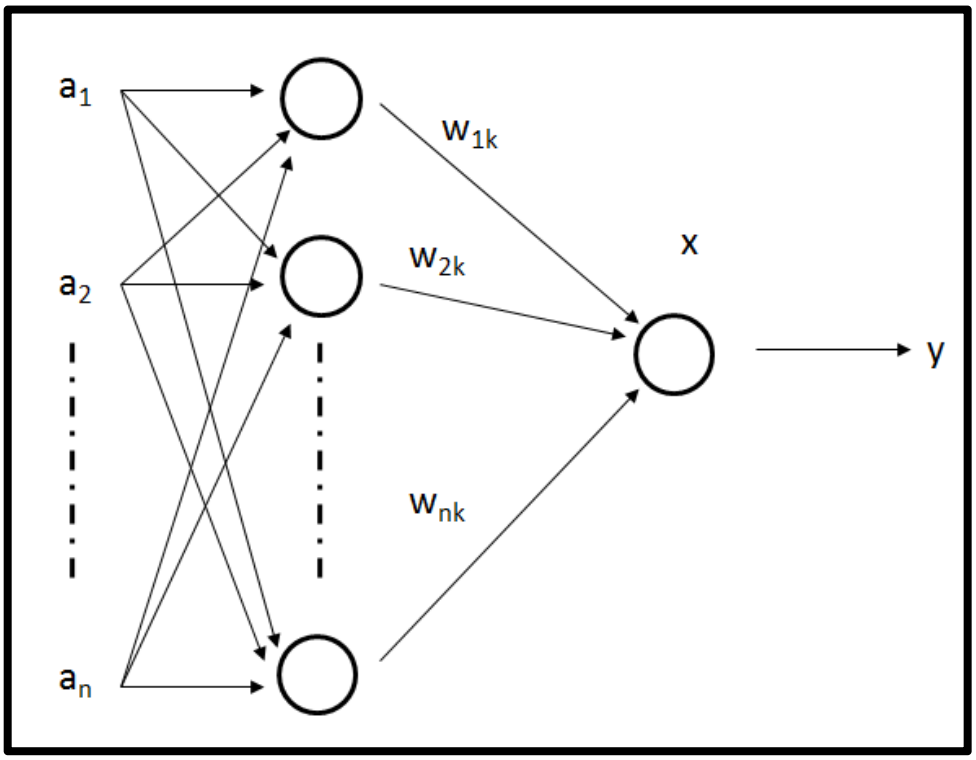

Figure 4.3. Neurons in an artificial neural network

4.3.Real Life Application of Artificial Neural Networks

Some application areas of Neural Networks are given below [28] [29]:

-Function Approximation

- -Interpolation
- -Extrapolation
- -Regression Analysis
- -Curve Fitting
- -Time Series Prediction

-Classification

- -Fault Detection of Components
- -Pattern Recognition (Face, Object Identification)
- -Sequence Recognition (Speech, Handwritten Text Identification)

-Data Processing

- -Filtering
- -Clustering

Structure of a Neural Network consists of simply three layers. Input layer includes input neuron(s). Hidden layer(s) are locations where calculation procedure is implemented. Output layer includes output neron(s).

Neurons of the network are interconnected to each other with weights. Weights can be considered as the synapses of a biological neural network.

Mainly there are two types of Neural Networks. Feedforward Networks where signals travel in one direction from input layer to output layer. Feedback Networks where signals travel left-right, right-left ,up-down and down-up directions with generating loops in the network.

Figure 4.4 and Figure 4.5 give structure of Feedforward and Feedback Neural Networks.

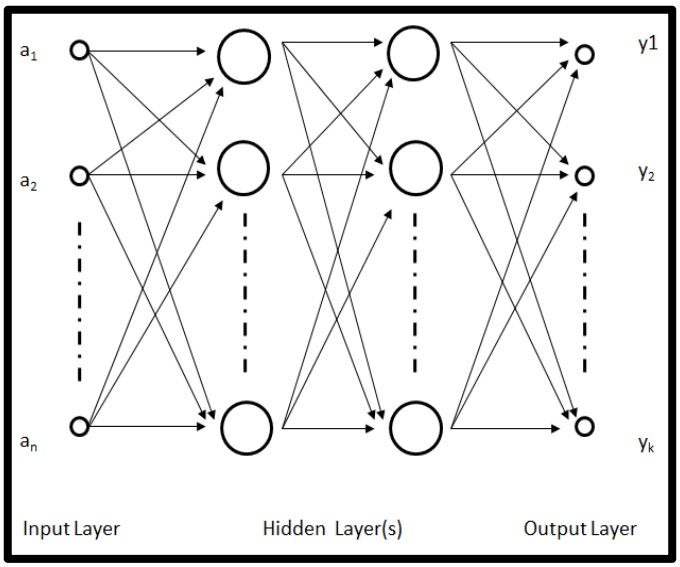

Figure 4.4. Feedforward neural network

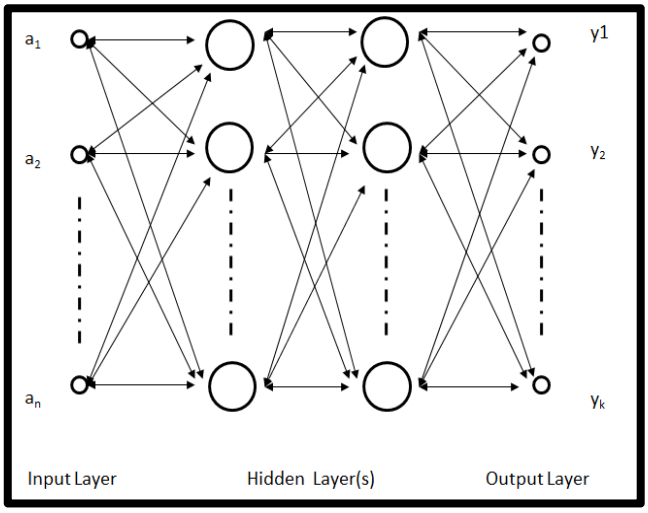

Figure 4.5. Feedback neural network

Teaching procedure of Neural Networks includes three steps.In the first step training sets are given to the network. In the second step ,how closely the actual output of the network matches to the desired output is determined. In the third step, weight of each connection is changed to have the network producing a better approximation of the desired output.

Activation function can be either in binary level or continuous. A binary level neural network produces two ouputs 0 or 1 for given inputs. Some continuous activation functions are Sigmoid , Hyperbolic Tangent and Gaussian functions. Table 4.1 gives som activation functions and derivatives used in Neural Nets.

Table 4.1. Some activation functions and derivatives used in neural nets

Name	Function	Graph
Linear	$y = f(x) = x$ $\frac{\partial y}{\partial x} = 1$	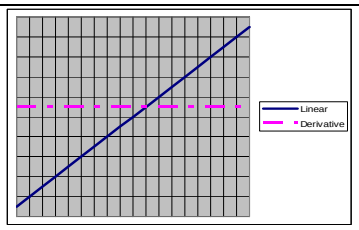
Sigmoid	$y = f(x) = \frac{1}{1+e^{-x}}$ $\frac{\partial y}{\partial x} = \frac{1}{1+e^{-x}} * (1 - \frac{1}{1+e^{-x}})$	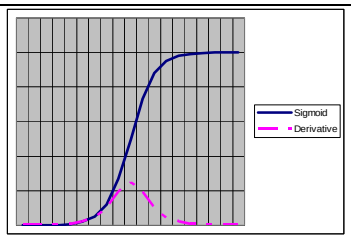
Tanh	$y = f(x) = Tanh(x)$ $\frac{\partial y}{\partial x} = 1 - (Tanh(x))^2$	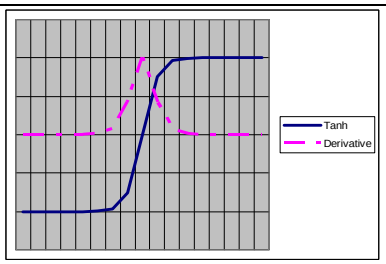
Gaussian	$y = f(x) = e^{-x^2/2}$ $\frac{\partial y}{\partial x} = -x * e^{-x^2/2}$	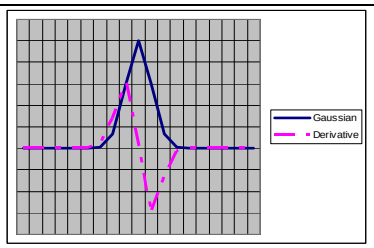
Log	$y = f(x) = \log(1+x)$ if x≥0 $y = f(x) = -\log(1-x)$ if x<0 $\frac{\partial y}{\partial x} = \frac{1}{1+x}$ if x≥0 $\frac{\partial y}{\partial x} = \frac{1}{1-x}$ if x<0	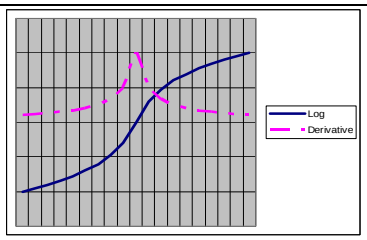

In order to decrease the difference between the actual output of the network and desired output weights must be changed. Different algorithms for

error uptade are used in Neural Nets. Figure 4.6 shows connections between neurons.

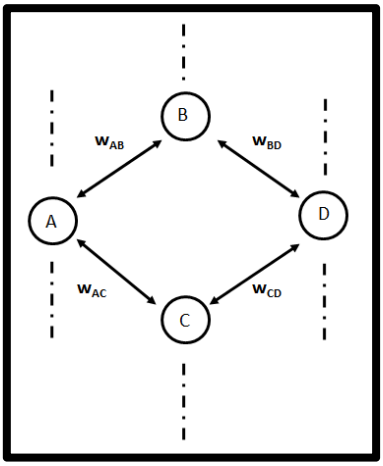

Figure 4.6. Connections between neurons

The algorithm procedure for a feedforwrd neural network with backpropagation algorithm is given as follows.

-Weights W_{AB} ,W_{AC} ,W_{BD}, W_{CD} are initialized randomly bewtween -1,+1

-$Output_C = f(W_{AC} * Output_A)$ (4.1)

-$Output_B = f(W_{AB} * Output_A)$ (4.2)

-$Output_D = f(W_{CD} * Output_C + W_{BD} * Output_B)$ (4.3)

-Actual output of the network is value of D.

-$Error_D = f'(Output_D) . (Desired_D - Output_D)$ (4.4)

-For sigmoid activation function, $f'(Output_D) = (Output_D) . (1 - Output_D)$ (4.5)

-New weights are calculated

-$W_{new,CD} = W_{CD} + \mu * Error_D . Output_B$ (4.6)

-$W_{new,BD} = W_{BD} + \mu * Error_D * Output_B$ (4.7)

-Error is backpropagated to calculte $Error_C$ and $Error_B$

-$Error_C = f'(Output_C) * (Error_D * W_{CD})$ (4.8)

-$Error_B = f'(Output_B) * (Error_D * W_{BD})$ (4.9)

-Error is backpropagated to calculte $Error_A$

-$Error_A = f'(Output_A) * (Error_C * W_{AC} + Error_B * W_{AB})$ (4.10)

-New weights are calculated.

$-W_{nw,AC} = W_{AC} + \mu * Error_C * Output_A$ (4.11)

$-W_{new,AB} = W_{AB} + \mu * Error_B * Output_A$ (4.12)

-Iteration will continue until $Error_D$ decreases to convergence criteria.

μ is learning rate which is used to speed up or slow down learning. Learning rate value changes from 0 to 1.

Backpropagation algorithm changes the error to fall in each iteration but error will not decrease in some cases where algorithm sticks to a local minimum. Weights can be initialized to different values or a new term Momentum (M) can be added to the weight adjustment calculation to leave local minimum. Momentum is a term similar to learning rate. Weight adjustment depend on the error of previous iteration [29]. Figure 4.7 shows local mimimum and global minimum for Neural Net training.

W_{new} = W + Current Change + Momentum . (Change on Previous Iteration) (4.13)

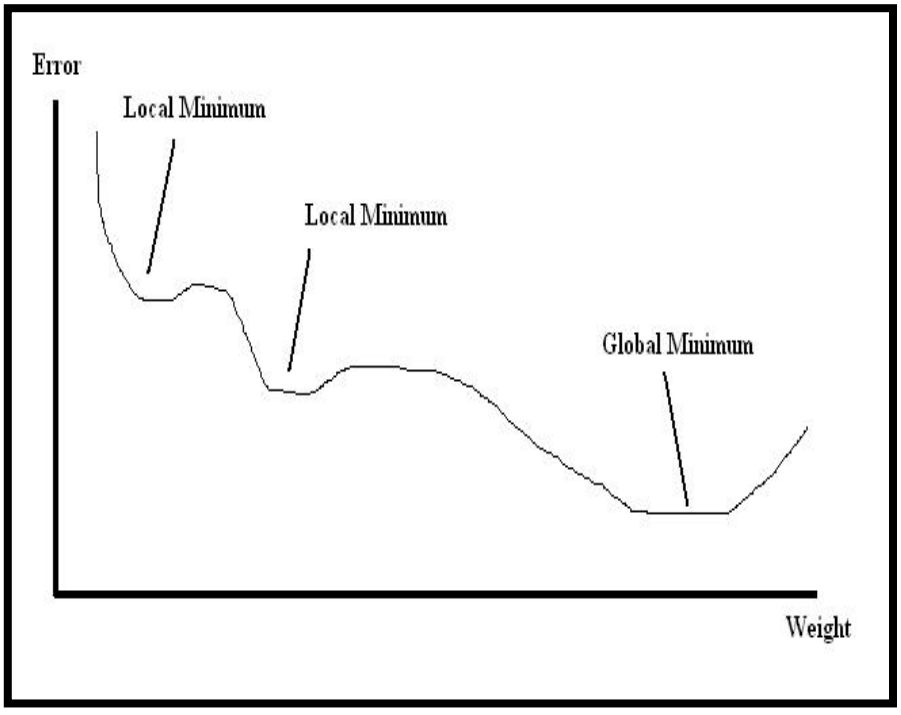

Figure 4.7. Local minimum and global minimum for neural net training [29]

Different error calculation and weight adjustment techniques for a feed forward network are given in Table 4.2

Table 4.2. Error calculation and weight adjustment techniques

Algorithm	Error Calculation	Weight Adjustment
BackProp.	*Last Layer* (Desired-Actual) *Intermediate Layers* $\sum_{i=1}^{j}\left(Error_i * Weight_{k,i}\right)_{n+}$	$w(t+1) = w(t) + \mu * \frac{\partial E}{\partial w}(t)$
BackProp. With Moment.	*Last Layer* (Desired-Actual) *Intermediate Layers* $\sum_{i=1}^{j}\left(Error_i * Weight_{k,i}\right)_{n+}$	$w(t+1) = w(t) + \mu * \frac{\partial E}{\partial w}(t) + \mathrm{M} * \frac{\partial E}{\partial w}(t-1)$
Quick Prop.	*Last Layer* (Desired-Actual) *Intermediate Layers* $\sum_{i=1}^{j}\left(Error_i * Weight_{k,i}\right)_{n+}$	$w(t+1) = w(t) + \frac{\frac{\partial E}{\partial w}(t)}{\frac{\partial E}{\partial w}(t-1) + \frac{\partial E}{\partial w}(t)} * \Delta w(t-1) - \mu * \frac{\partial E}{\partial w}(t)$

For intermediate layers,

$$\left(\frac{\partial E}{\partial w}(t)\right)_{k,n} = Output_{k,n-1} * f'\left(Output_{k,n}\right) * \sum_{i=1}^{j}\left(Error_i * Weight_{k,i}\right)_{n+1} \tag{4.14}$$

For last layer,

$$\left(\frac{\partial E}{\partial w}(t)\right)_{k,last} = Output_{k,last-1} * f'\left(Output_{k,last}\right) * Error_{k,last} \tag{4.15}$$

5. CALCULATIONS

A two stage axial compressor is designed in the design mode of throughflow program. Througflow analysis and 3-D RANS analysis are carried out. Point where throughflow and CFD results are coincident on the performance curve of the compressor is selected for flow field investigation. Spanwise distributions of interstage flow parameters are compared.

For optimization a one stage axial compressor is designed. Blades are parametrized in suction and pressure sides. Feed forward Artificial Neural Network with back propagation algorithm assisted to Genetic Algorithm for optimization. After optimization loop Artificial Neural Network is retrained before the next optimization step.

5.1.Design and Analysis

Flowcharts for design and analysis modes are given in Figure 5.1 , Figure 5.2 and Figure 5.3. In design mode with the given inputs throughflow program generates a compressor geometry without loss calculations. Losses and deviations are introduced in throughflow analysis at existing geometry analysis mode. With the known cascade information blades are generated with profiling mode of design programme.

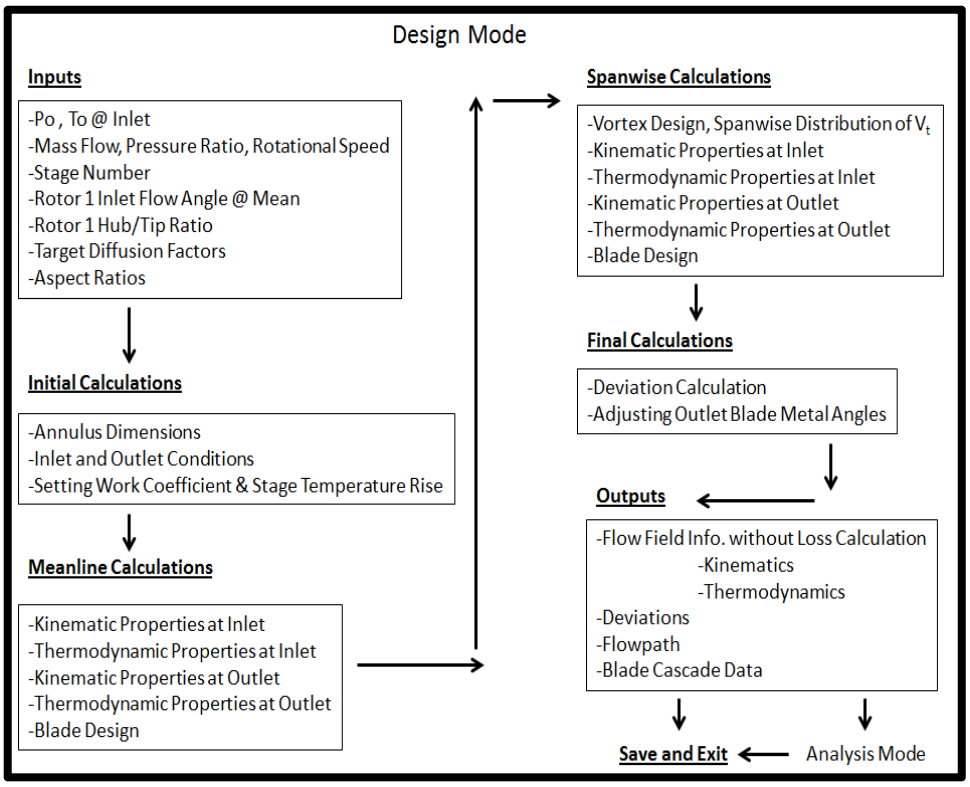

Figure 5.1. Flowchart for design mode calculations

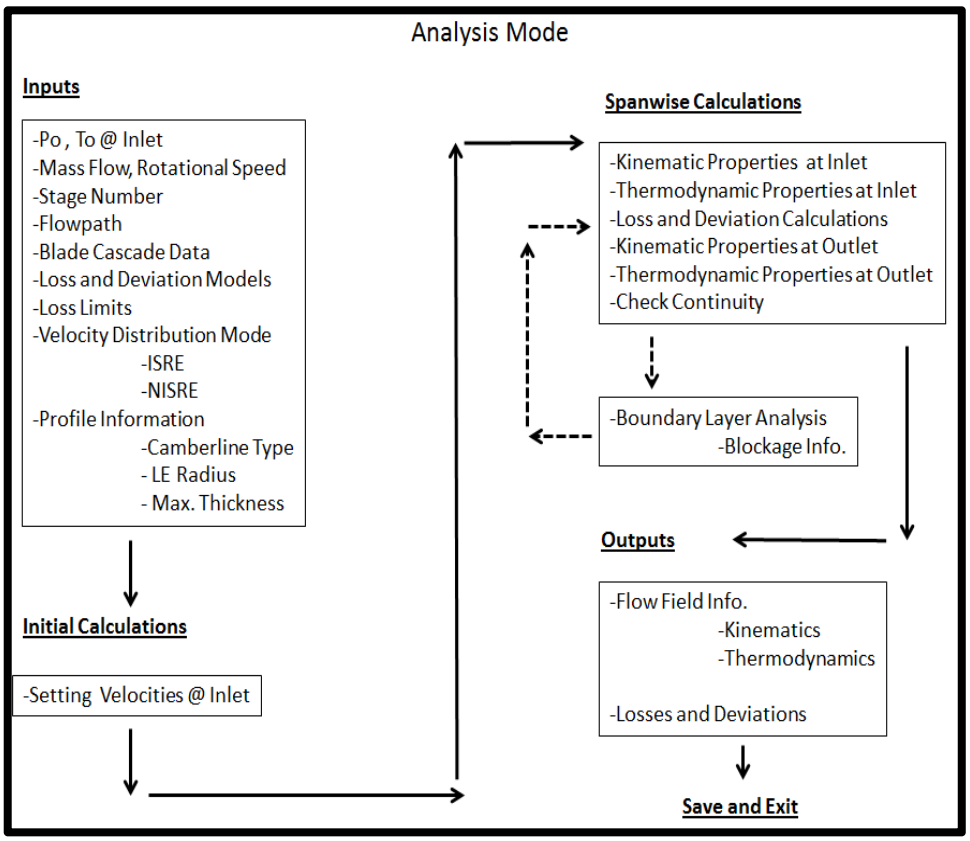

Figure 5.2. Flowchart for analysis mode calculations

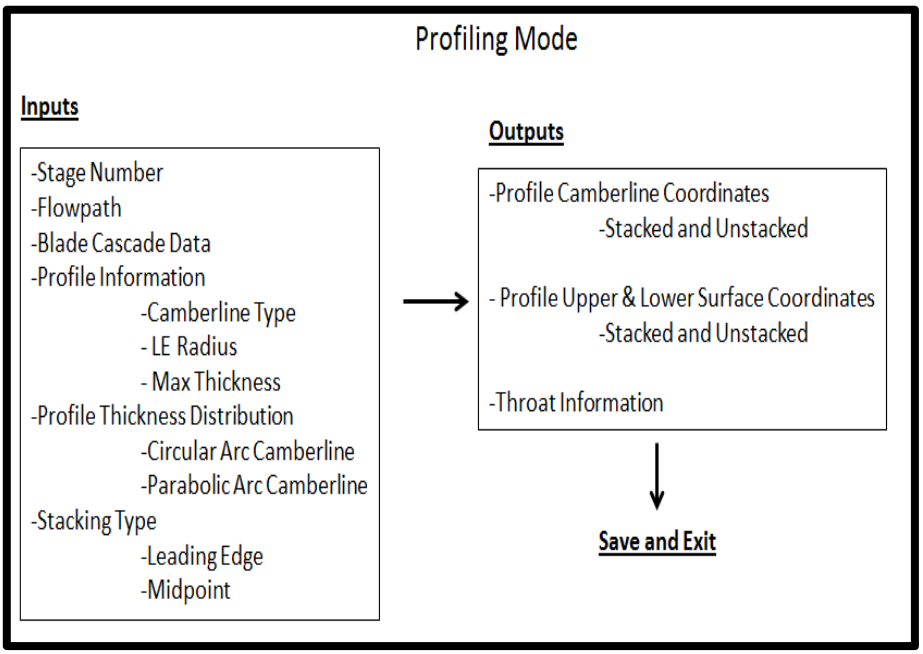

Figure 5.3. Flowchart for blade profiling mode calculations

Two stage axial compressor design conditions and geometry information are given in Table 5.1and Table 5.2 . Flowpath and pitchwise averaged data locations of CFD calculation are shown in Figure 5.1.

Table 5.1. Two stage axial compressor design conditions

Inlet Po	Pa	101325
Inlet To	Kelvin	288
Mass Flow Rate	kg/s	3.2
Rotational Speed	RPM	39000
Total to Total Pressure Ratio		2.1

Table 5.2. Two stage axial compressor geometry information

	Rotor 1			Rotor 2			Stator 1			Stator 2		
	Hub	Mean	Tip	Hub	Mean	Tip	Hub	Mean	Tip	Hub	Mean	Tip
Metal Angle @ Inlet (°)	52.77	61.38	66.95	50.63	55.51	58.55	49.74	44.64	55.29	45.30	40.52	49.61
Metal Angle @ Outlet (°)	7.00	37.40	57.00	9.00	35.00	47.00	0.00	0.00	0.00	0.00	0.00	0.00
Solidity	1.90	1.45	1.05	1.54	1.42	1.09	1.18	0.91	0.74	1.43	1.21	1.05
Aspect Ratio	1.32	1.22	1.31	1.22	1.09	1.21	1.74	1.74	1.74	1.34	1.34	1.34
Chord (mm)	31.70	34.27	32.00	21.70	24.30	22.00	19.00	19.00	19.00	17.00	17.00	17.00
Radius @ Inlet (mm)	50.50	71.40	92.30	60.40	73.65	86.90	56.50	73.00	89.50	62.30	73.70	85.10
Radius @ Outlet (mm)	56.00	73.30	90.60	62.10	74.00	85.90	60.00	73.75	87.50	63.40	73.50	83.60
Blade Type	DCA	DCA	DCA	DCA	DCA	DCA	DCA	DCA	DCA	DCA	DCA	DCA

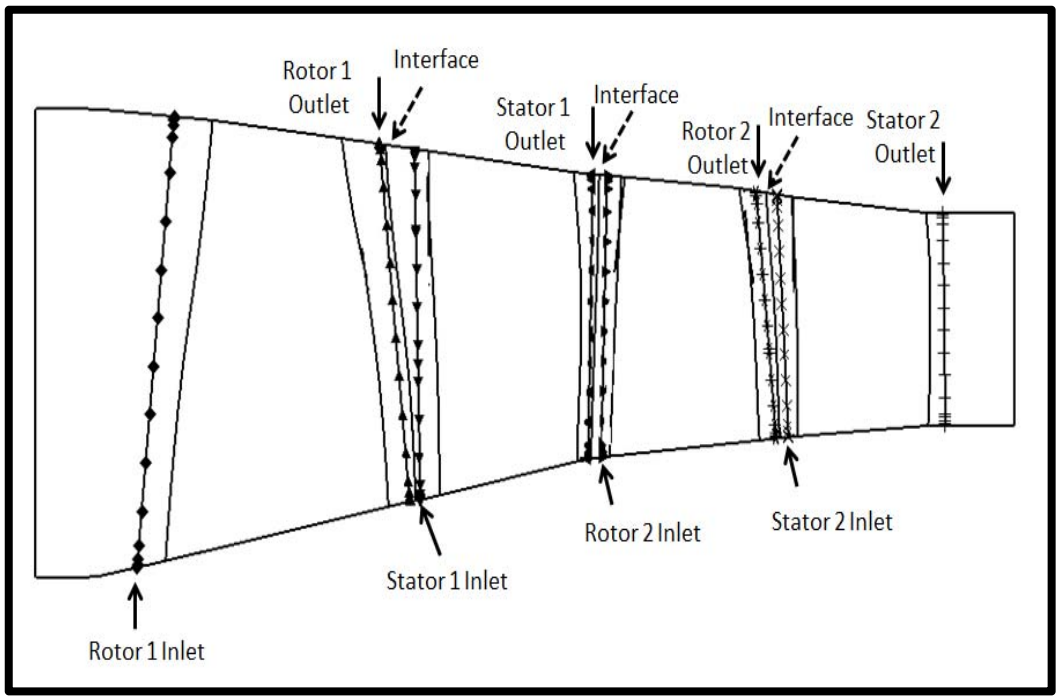

Figure 5.4. Flowpath and pitchwise averaged data locations of CFD calculation

In Figure 5.5 and Figure 5.6 Rotor 1 blade stacked from midpoint and leading edge are given. For these figure rotor blade is considered as a circular arc blade.

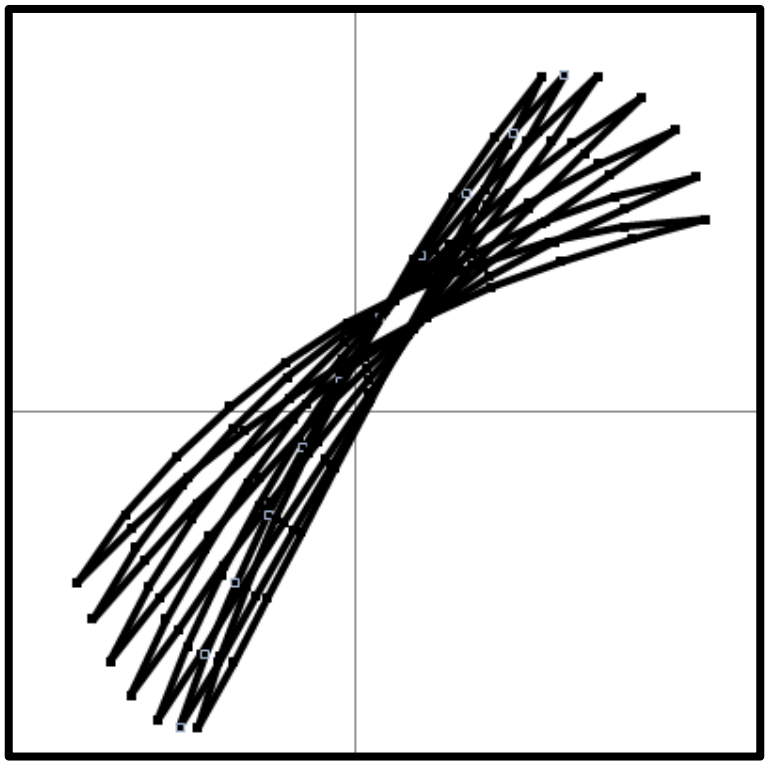

Figure 5.5. Blade stacked from midpoint

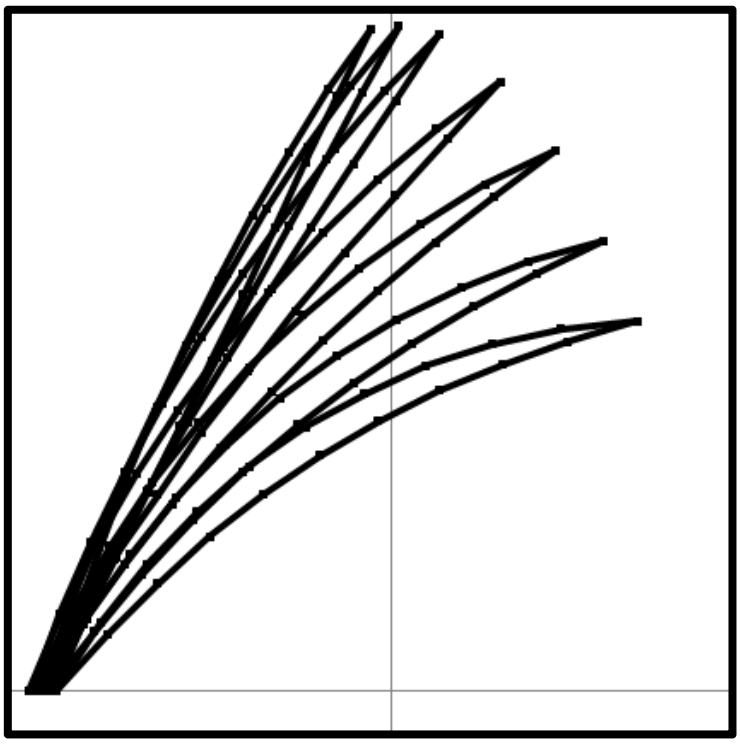

Figure 5.6. Blade stacked from leading edge

In Figure 5.7 computational grid of stage 2 CFD calculation in blade to blade plane is given. In Figure 5.8 computational grid of 2 stage axial compressor CFD calculation in 3-D view is given.

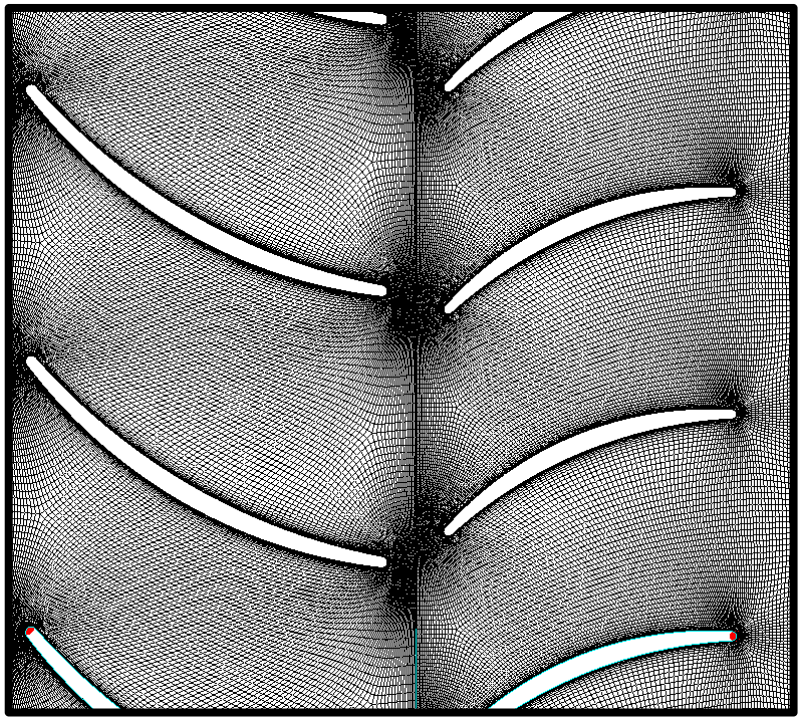

Figure 5.7. Computational grid of CFD calculation in blade to blade plane

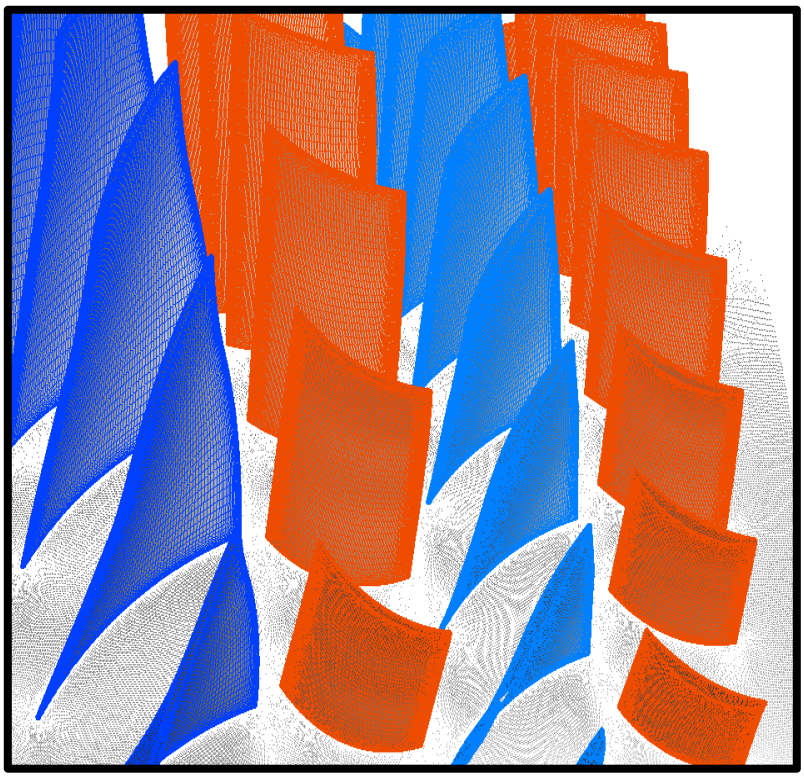

Figure 5.8. Computational grid of CFD calculation in 3-D view

In Table 5.3 CFD analysis conditions for the 2 stage compressor are given. Performance maps for througflow calculation and 3-D CFD calculations are given in Figure 5.4. Throughflow calculations are named as “DP”. In spanwise distributions “Normalized Arc Length” corresponds to normalized blade height. In blade to blade distributions “Normalized Arc Length” corresponds normalized chord length.

Table 5.3. 3-D CFD analysis conditions for the 2 stage compressor

Air Model	Perfect Gas
Mathemetical Model	Turbulent Navier Stokes
Turbulence Model	Spalart Allmaras
Rotor-Stator Interface	Conservative Coupling by Pitchwise Row (Mixing Plane Approach)
Outlet Conditions	Static Pressure Imposed with Radial Equilibrium Condition
Wall y+ After Solution	~ 1

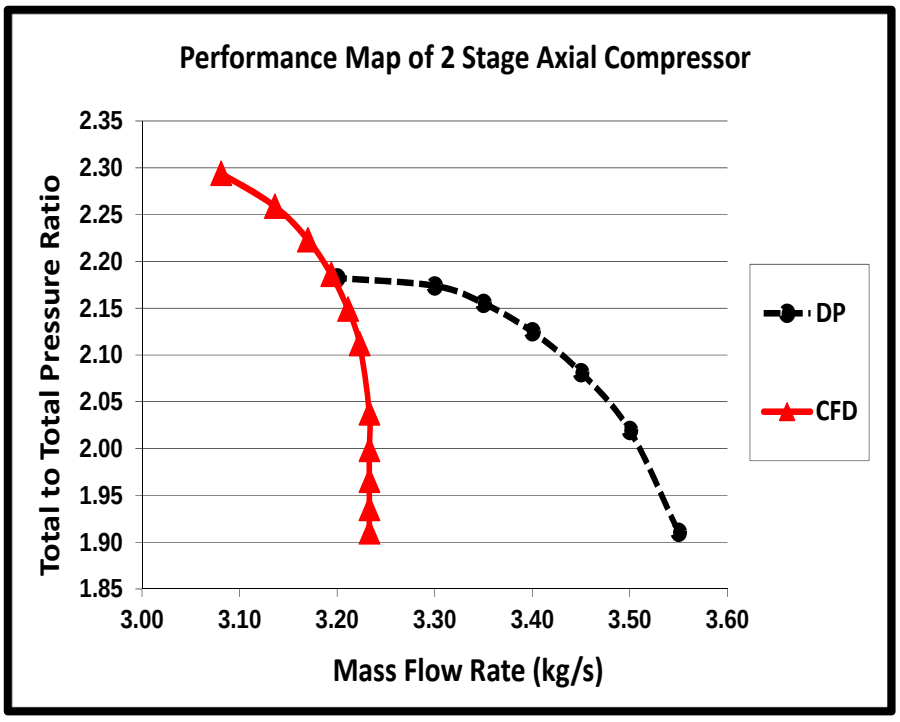

Figure 5.9. Performance maps for throughflow and 3-D CFD calculation

Flow field information and comparisons between the throughflow analysis and CFD analysis are given in the below figures.

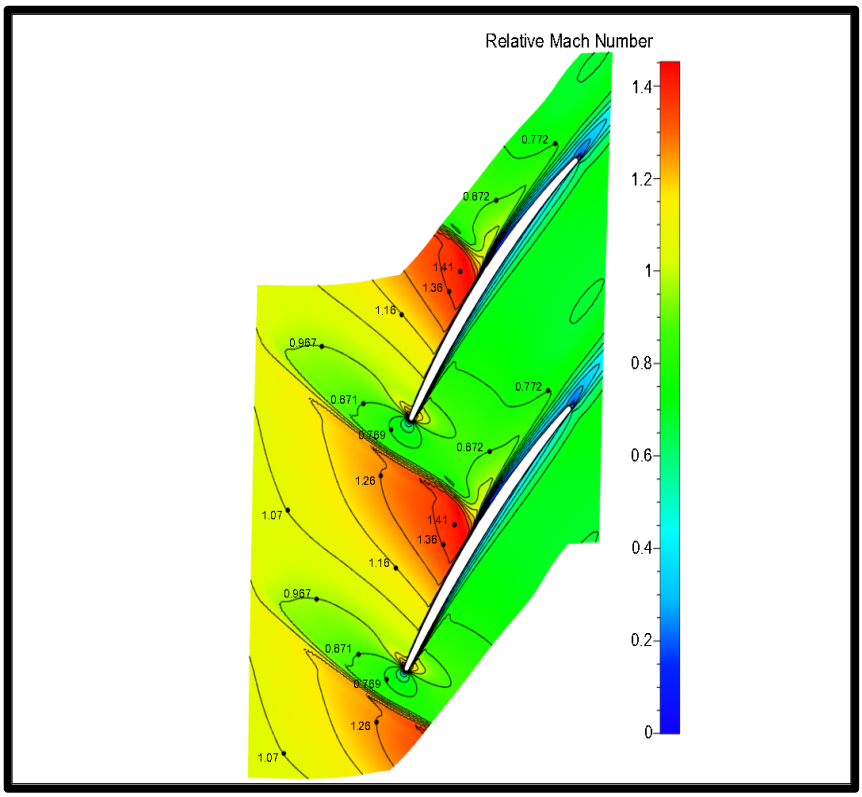

Figure 5.10. Isentropic mach number distribution of rotor 1 @ 66% span

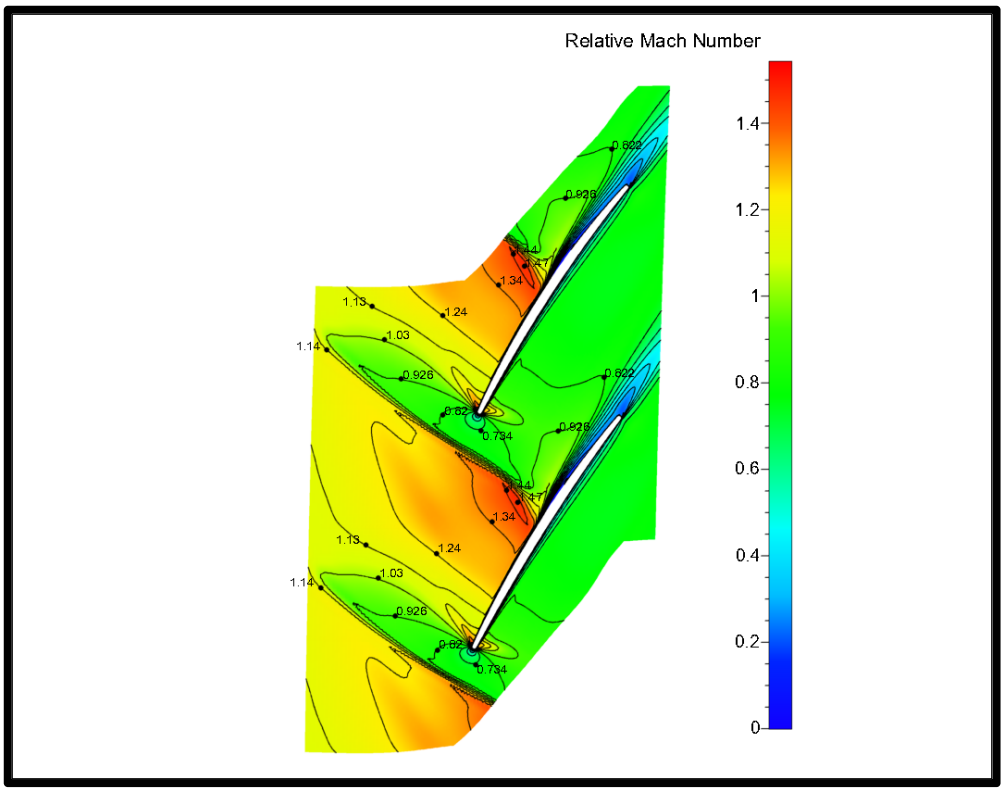

Figure 5.11. Isentropic mach number distribution of rotor 1 @ 83% span

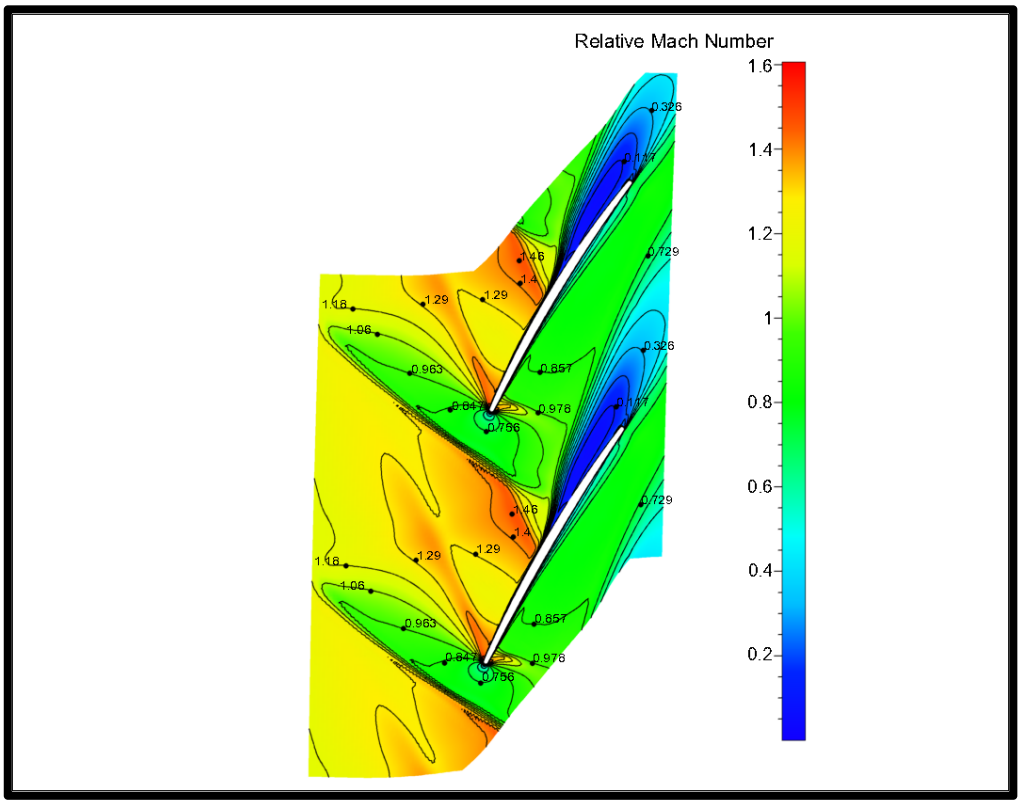

Figure 5.12. Isentropic mach number distribution of rotor 1 @ 95% span

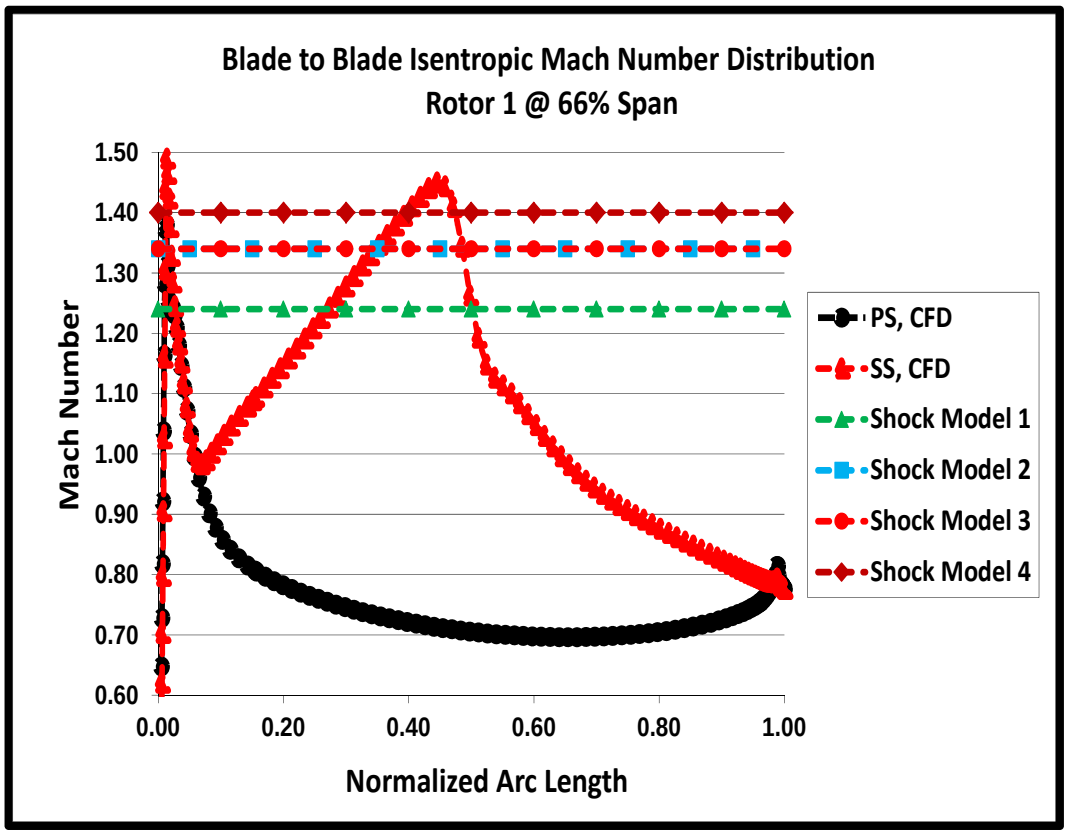

Figure 5.13. Throughflow shock mach number predictions at rotor 1 66% span

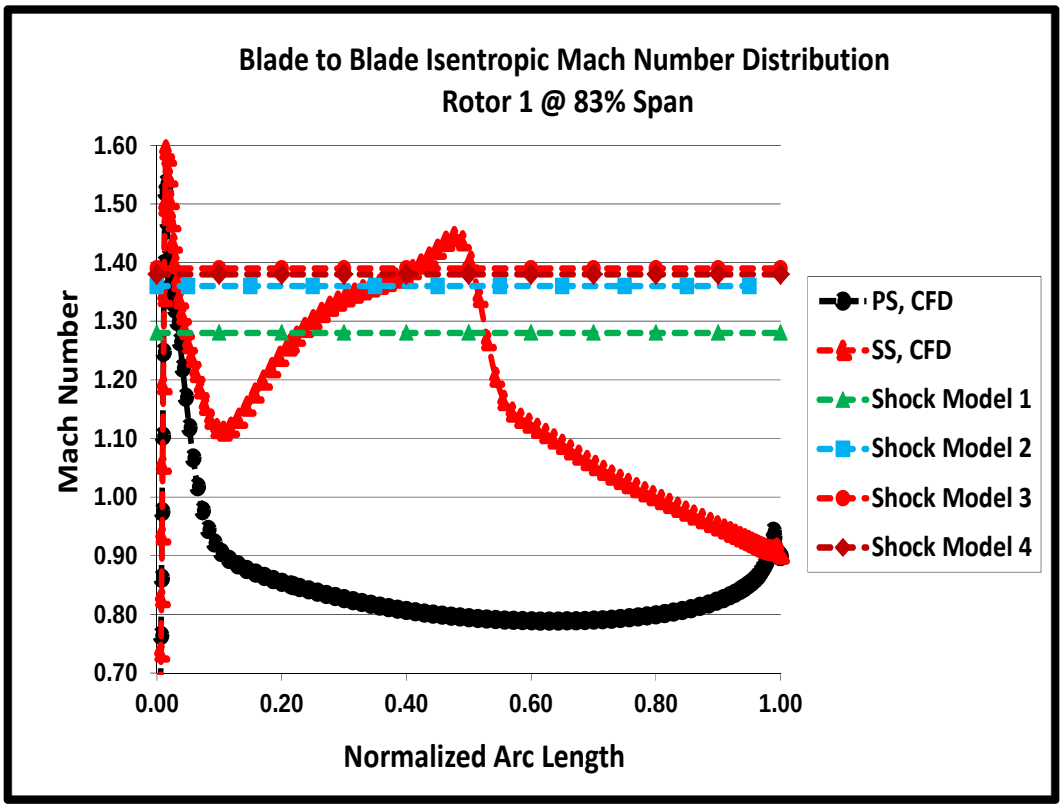

Figure 5.14. Throughflow shock mach number predictions at rotor 1 83% span

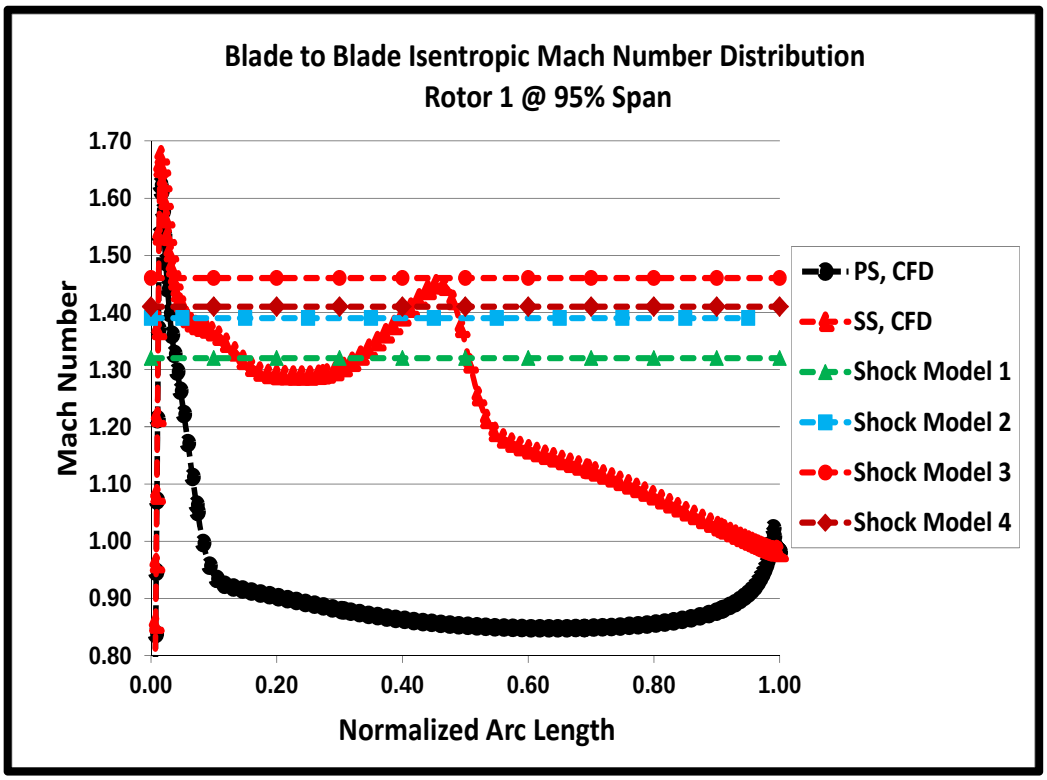

Figure 5.15. Throughflow shock mach number predictions at rotor 1 95% span

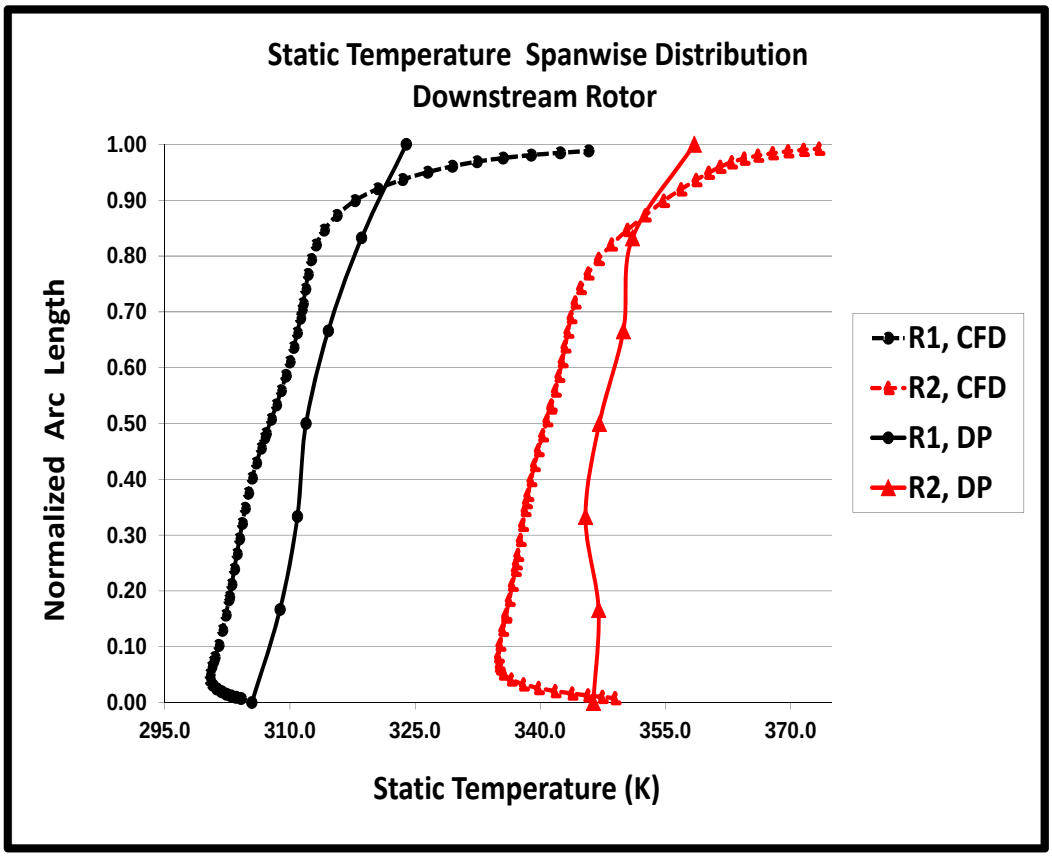

Figure 5.16. Static temperature spanwise distribution downstream rotor

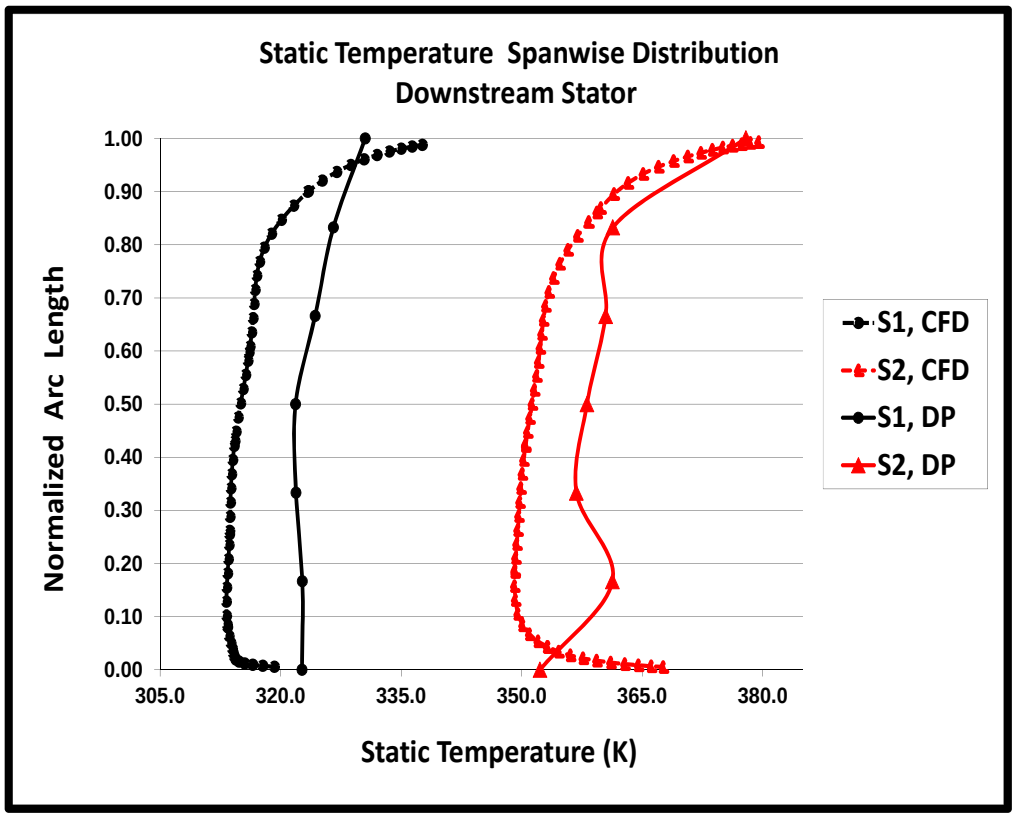

Figure 5.17. Static temperature spanwise distribution downstream stator

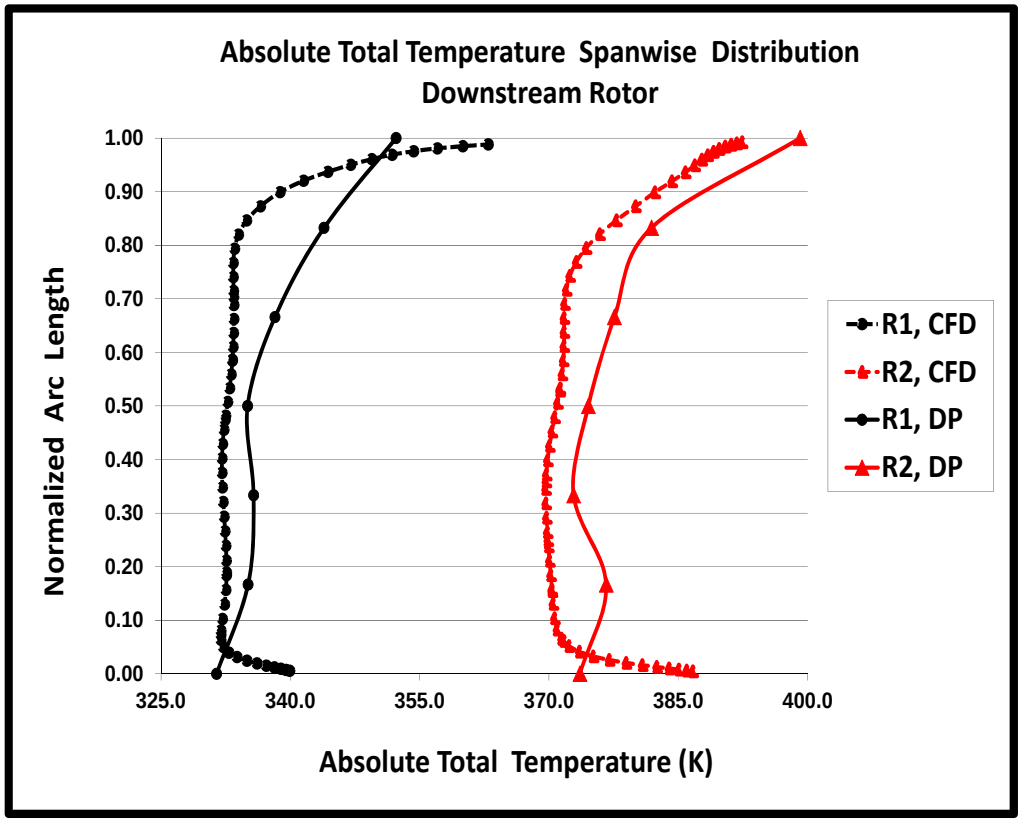

Figure 5.18. Absolute To spanwise distribution downstream rotor

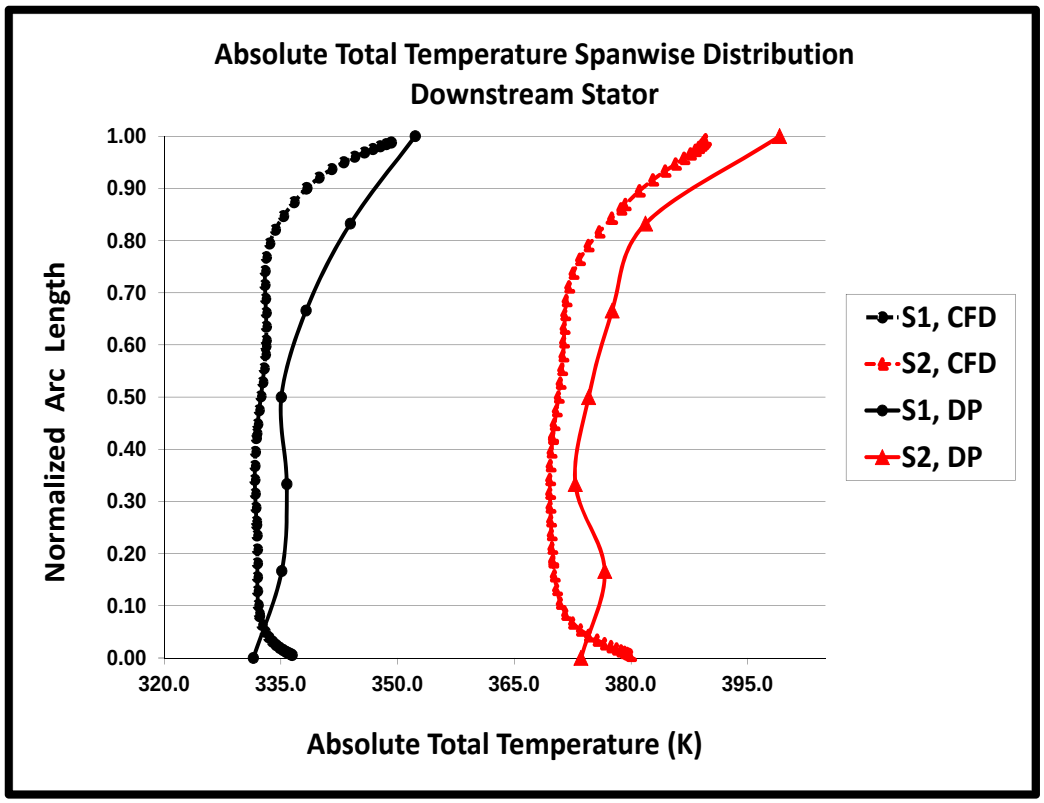

Figure 5.19. Absolute To spanwise distribution downstream stator

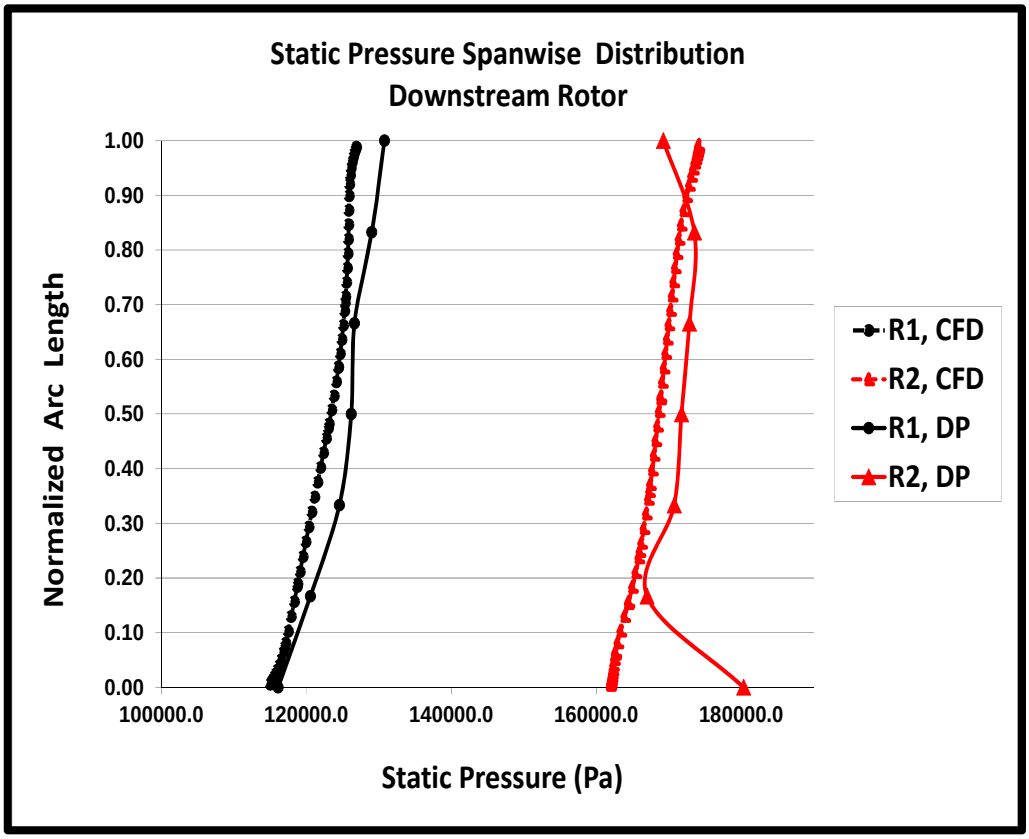

Figure 5.20. Static pressure spanwise distribution downstream rotor

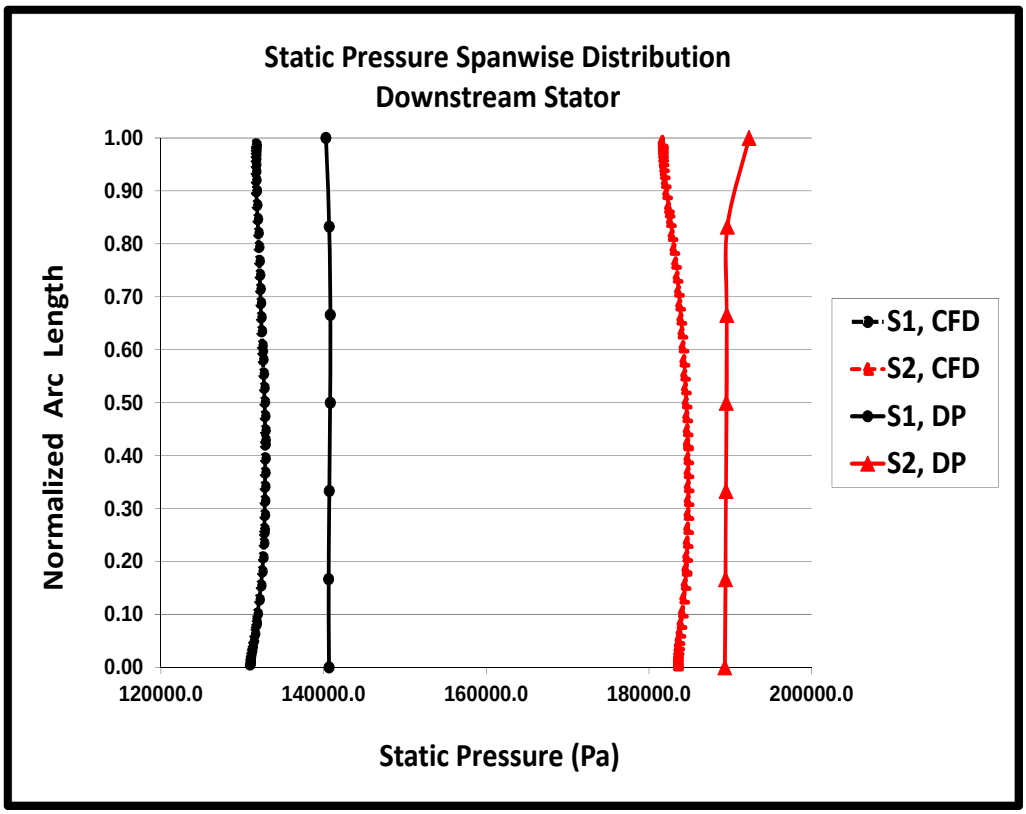

Figure 5.21. Static pressure spanwise distribution downstream stator

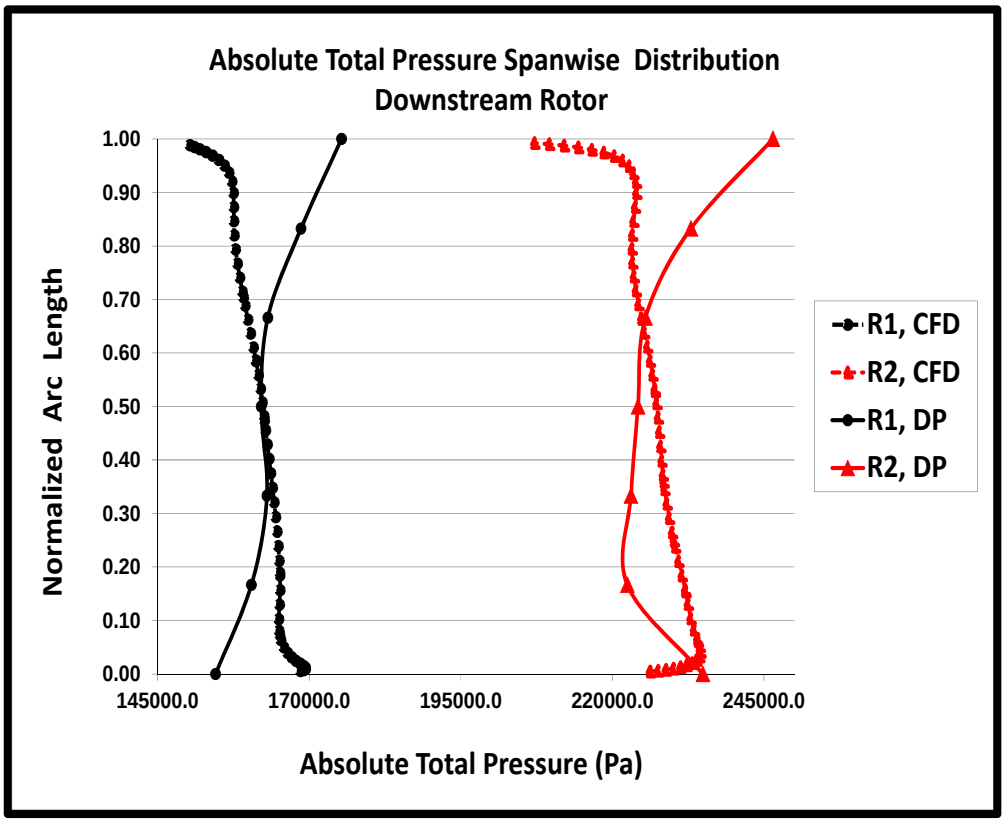

Figure 5.22. Absolute total pressure spanwise distribution downstream rotor

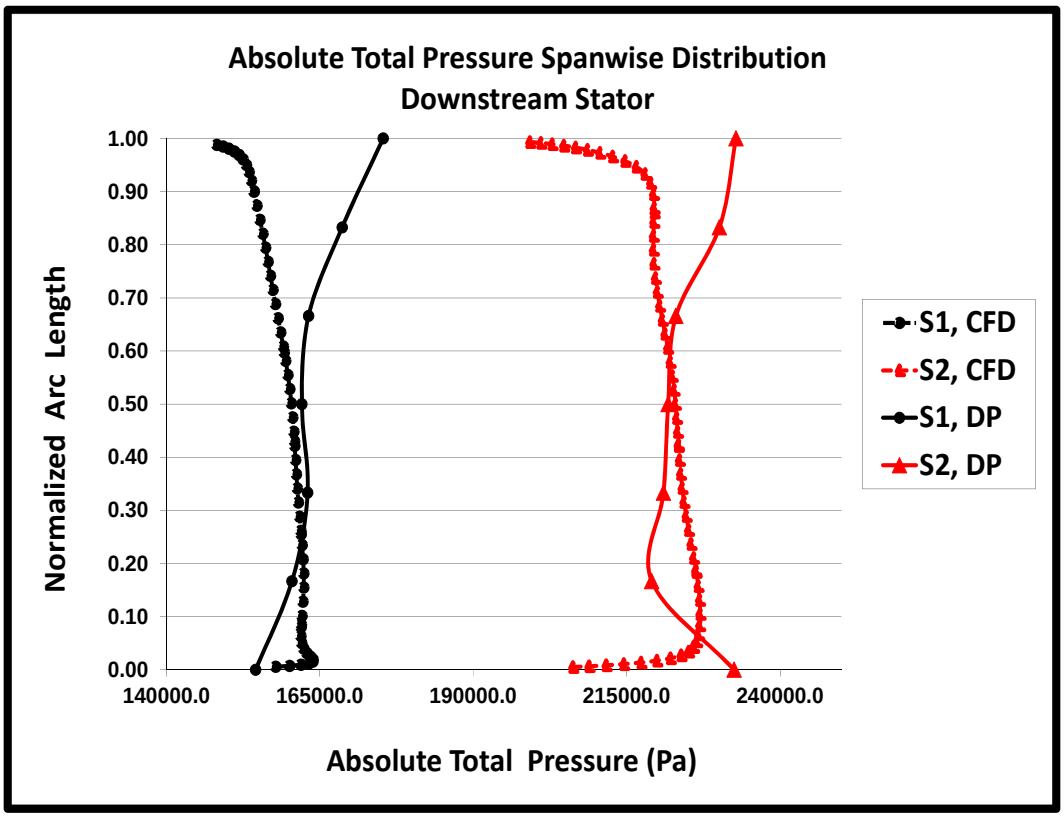

Figure 5.23. Absolute total pressure spanwise distribution downstream stator

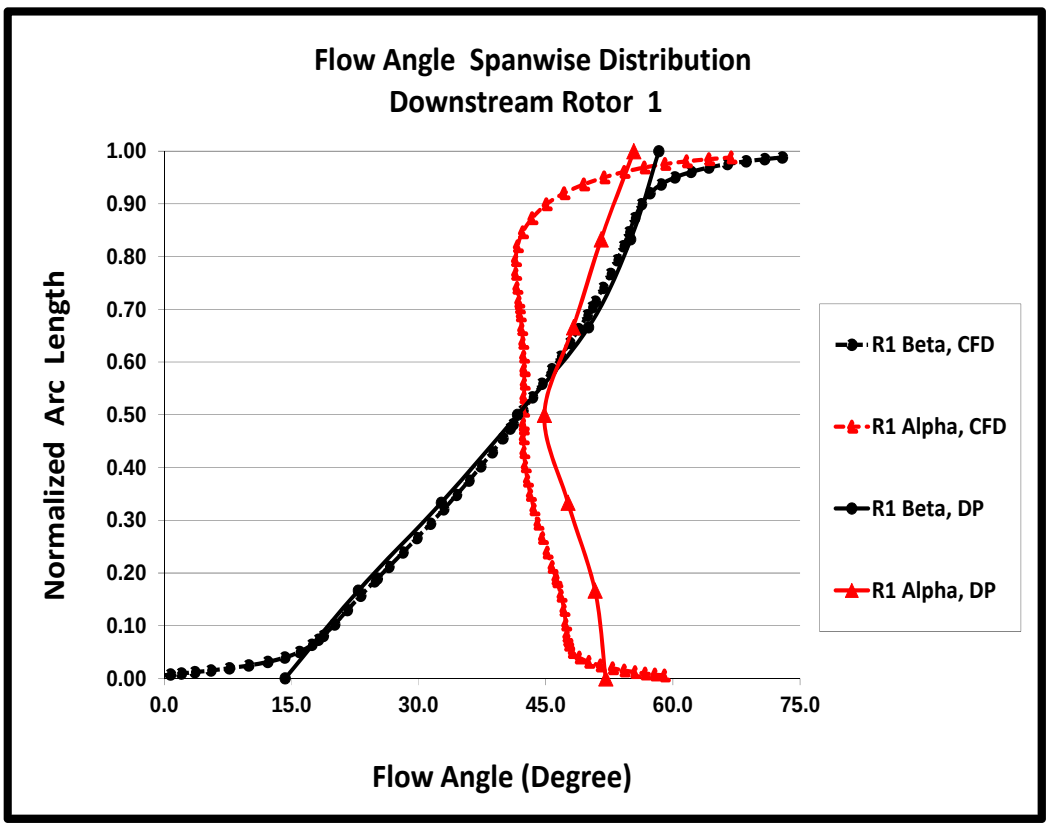

Figure 5.24. Flow angle spanwise distribution downstream rotor 1

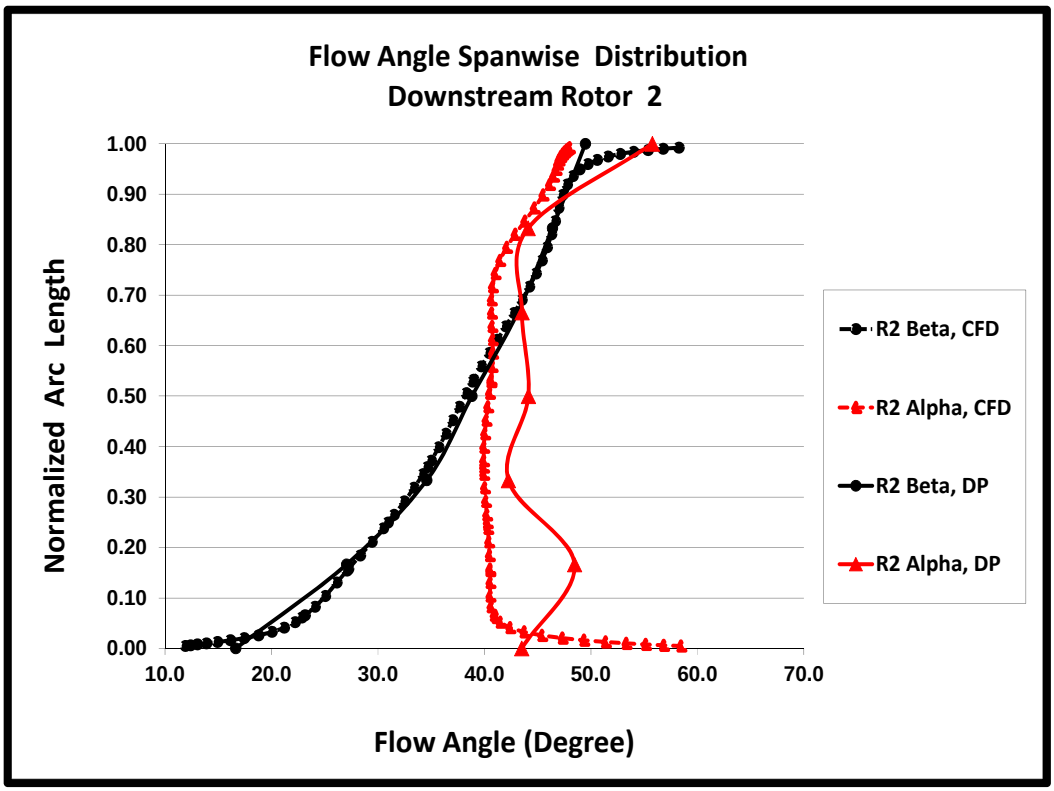

Figure 5.25. Flow angle spanwise distribution downstream rotor 2

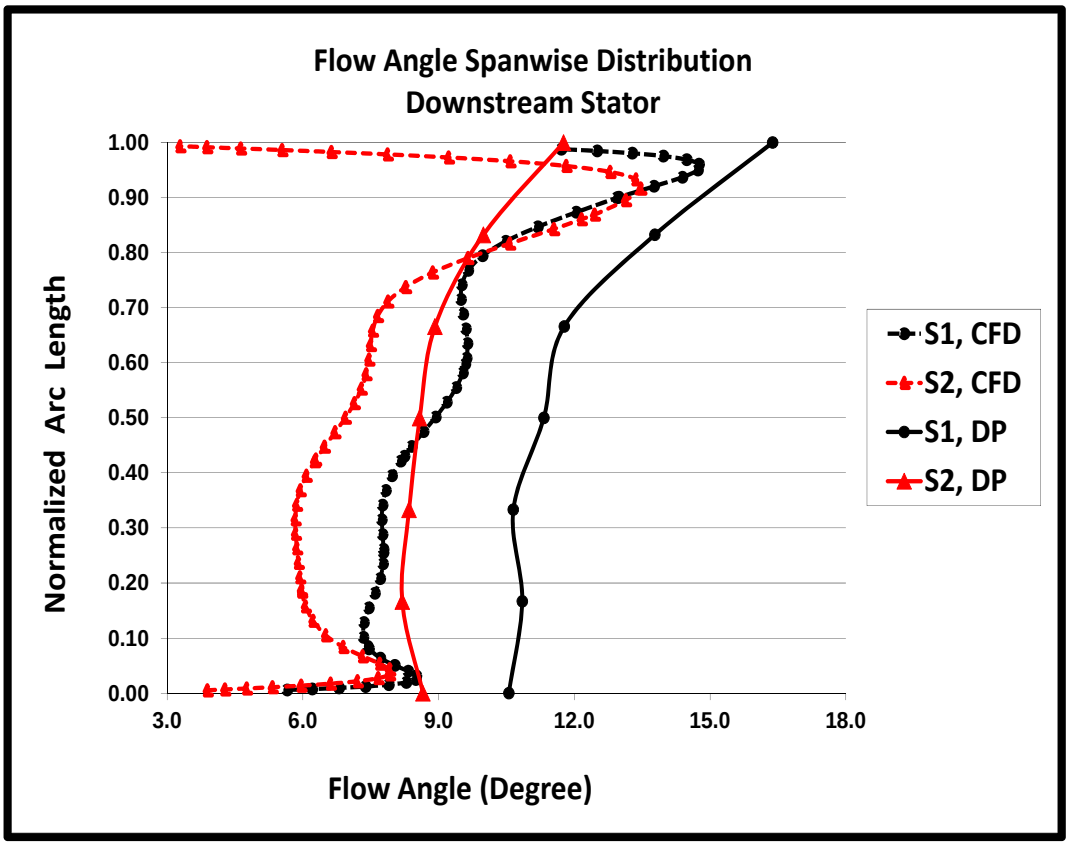

Figure 5.26. Flow angle spanwise distribution downstream stator

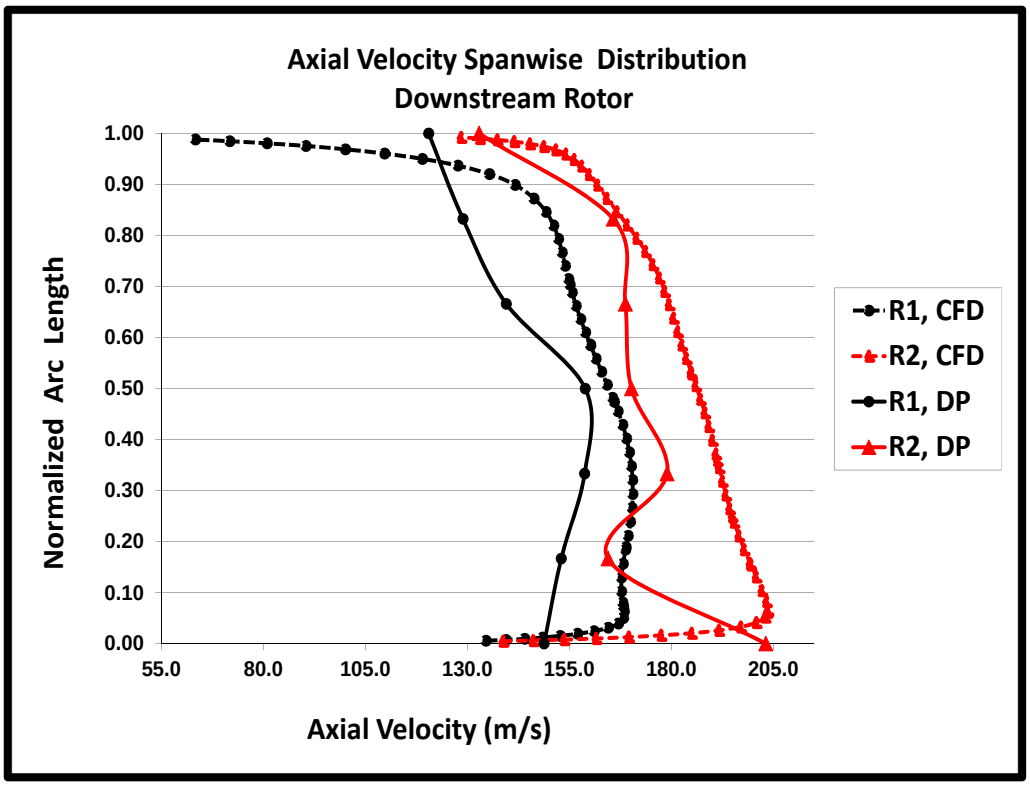

Figure 5.27. Axial velocity spanwise distribution downstream rotor

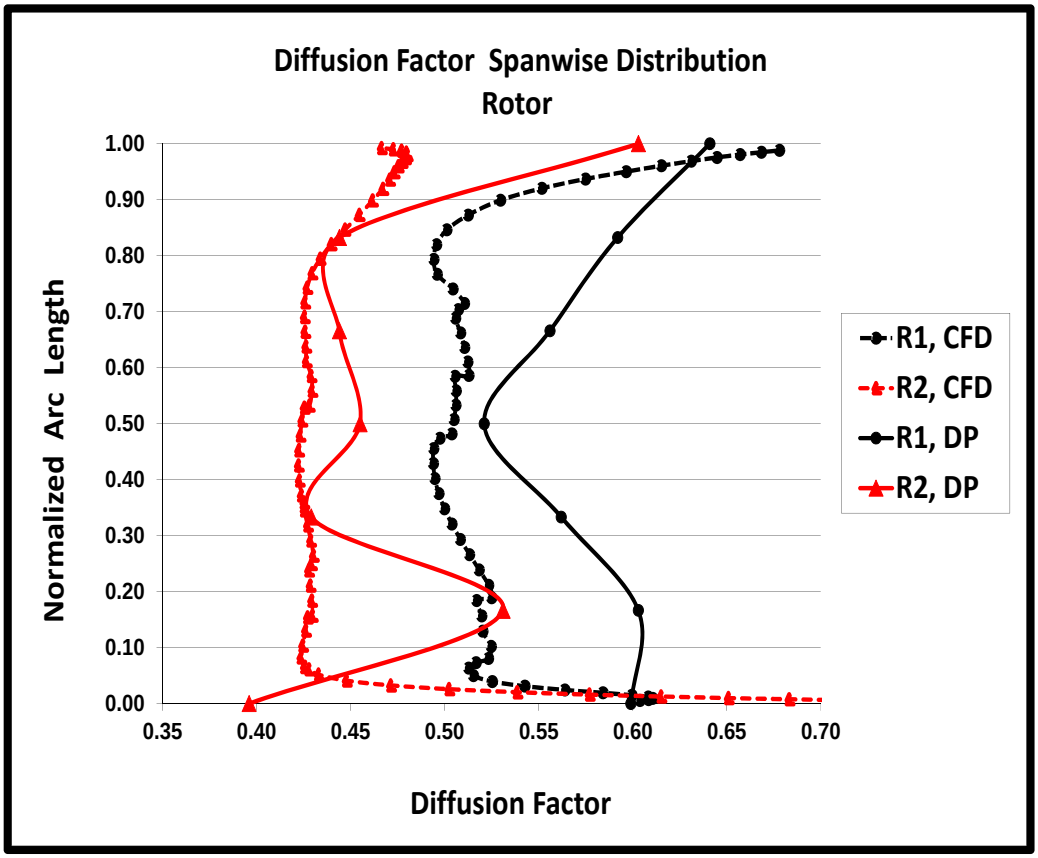

Figure 5.28. Diffusion factor spanwise distribution downstream rotor

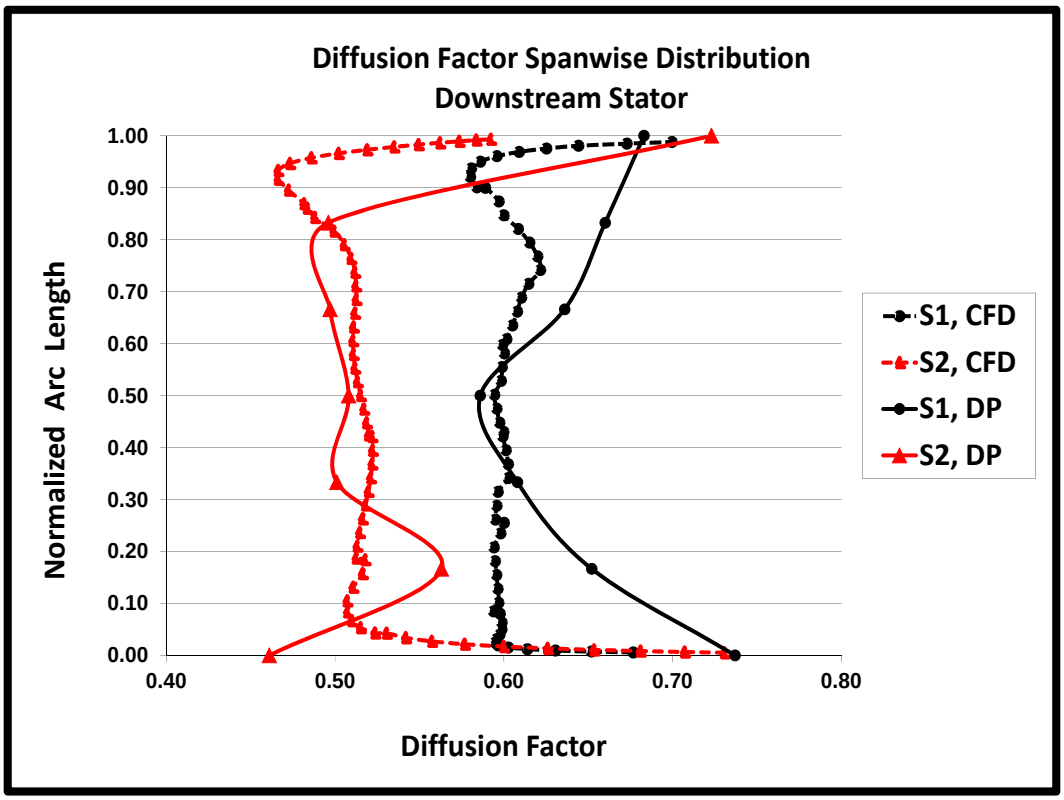

Figure 5.29. Diffusion factor spanwise distribution downstream stator

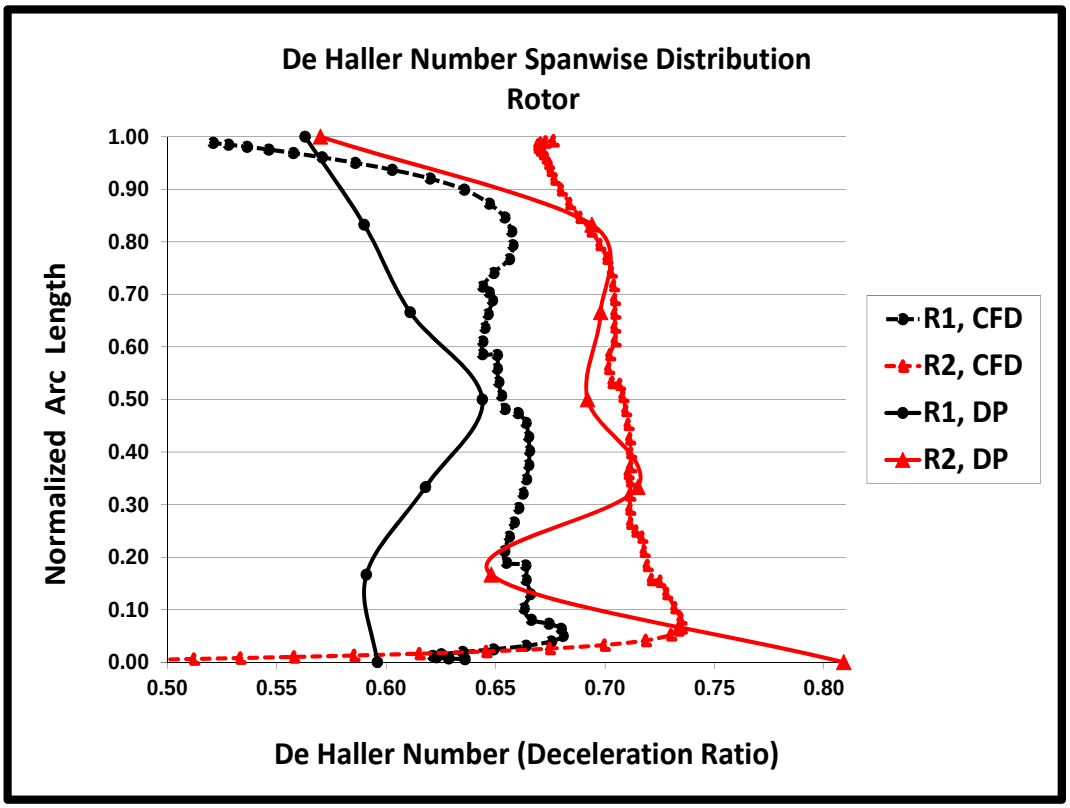

Figure 5.30. De Haller number spanwise distribution downstream rotor

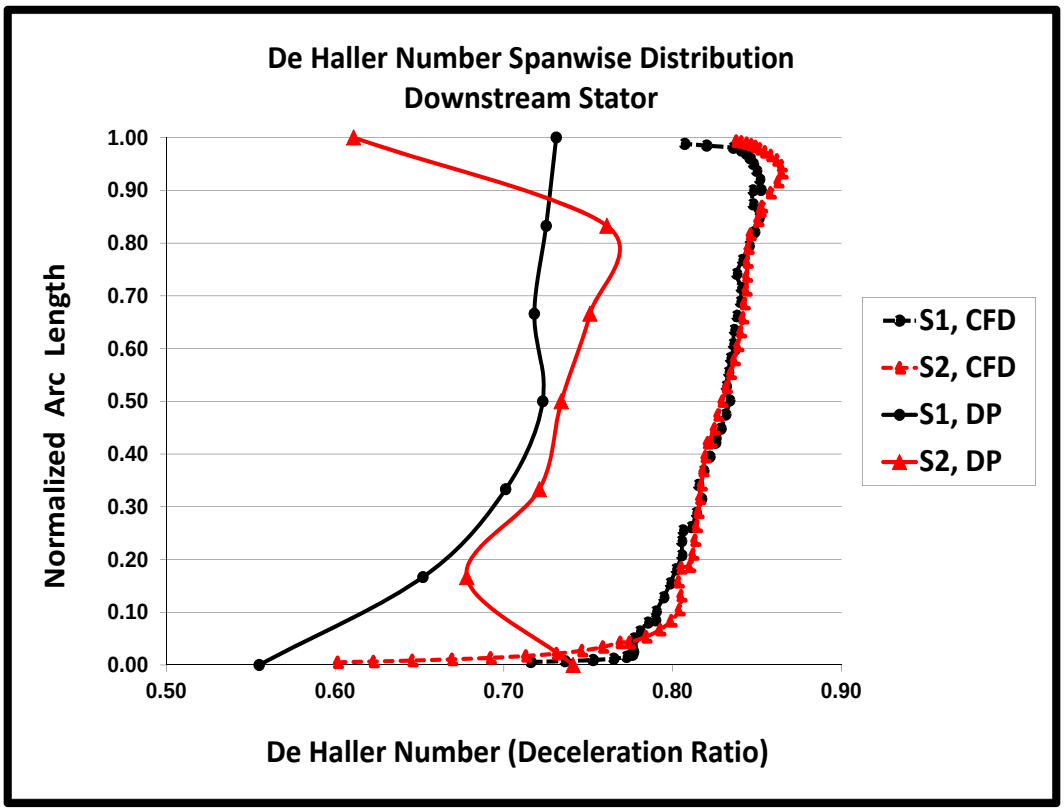

Figure 5.31. De Haller number spanwise distribution downstream stator

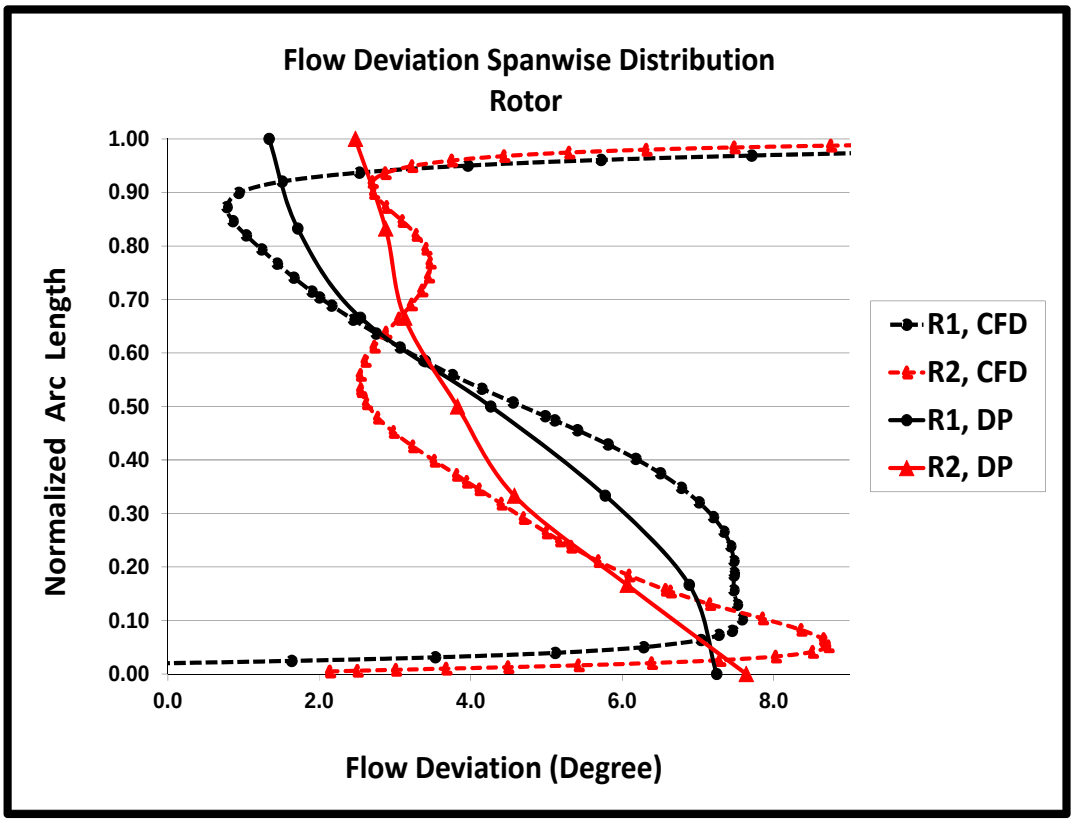

Figure 5.32. Flow deviation spanwise distribution downstream rotor

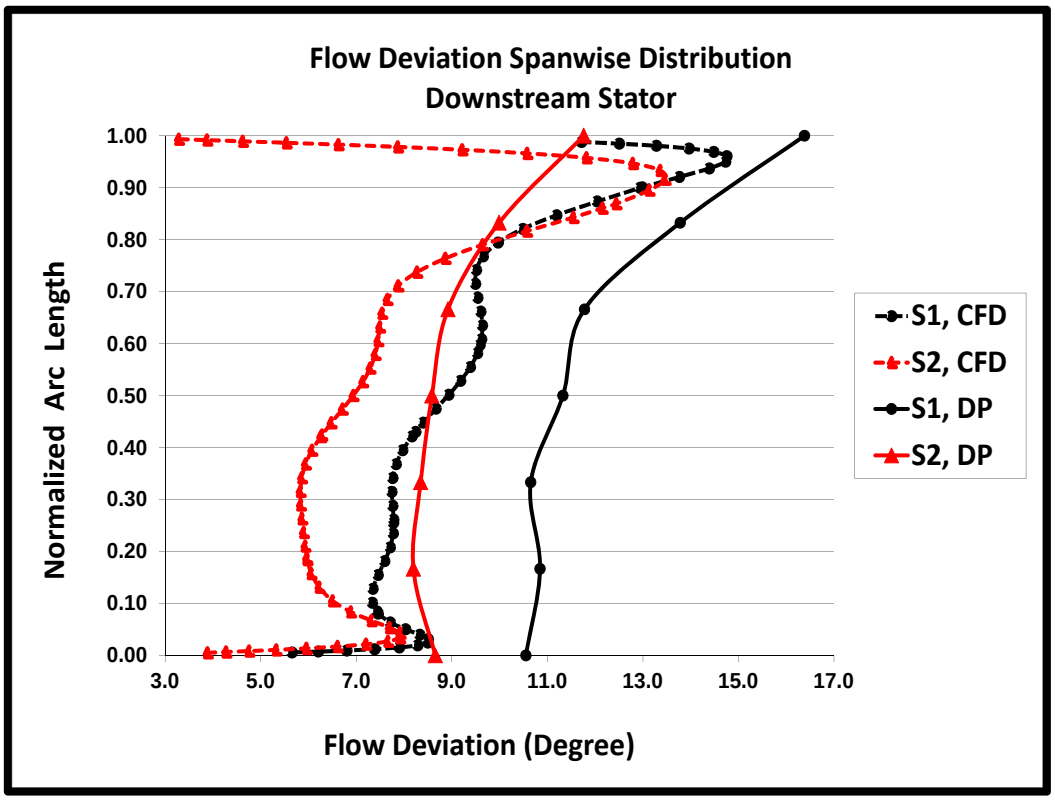

Figure 5.33. Flow deviation spanwise distribution downstream stator

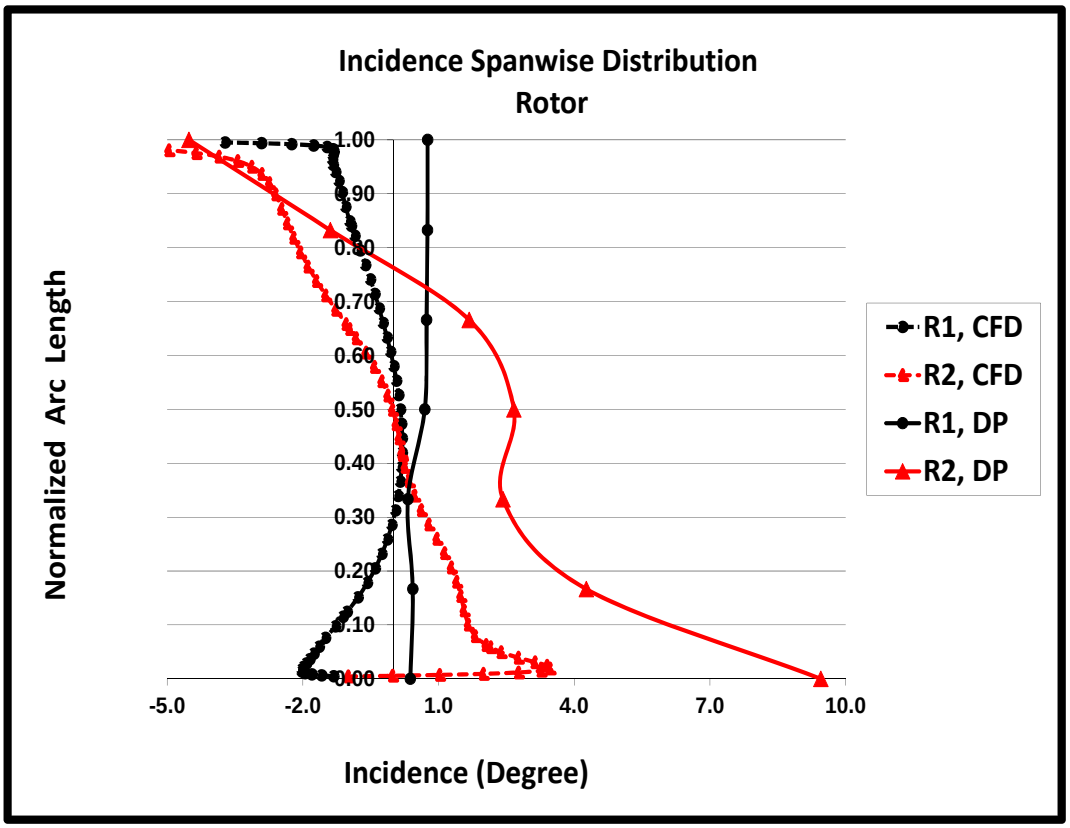

Figure 5.34. Incidence spanwise distribution downstream rotor

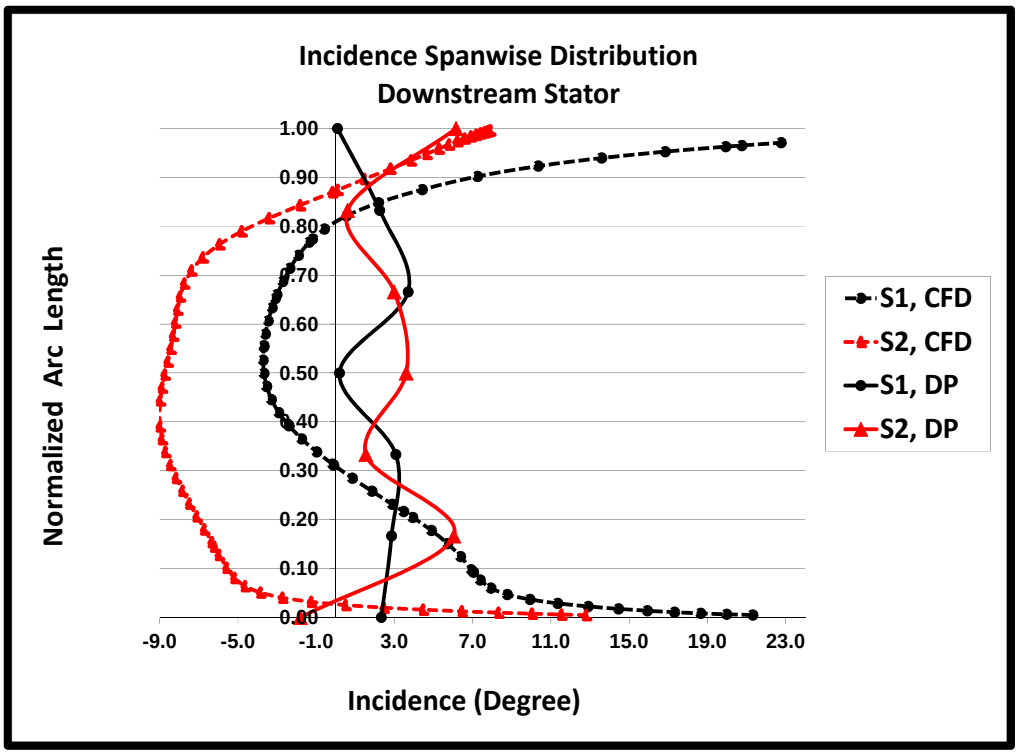

Figure 5.35. Incidence spanwise distribution downstream stator

Investigation of flow field in throughflow analysis depend on the succes in loss prediction, success in deviation prediction and method in radial equilibrium solution. When results of throughflow and CFD calculations are compared, prediction of pressure and temperature field can be considered as satisfactory. Prediction of flow field can be improved by tuning the loss and deviaiton values by added scale factors from hub to tip in the programme input file. Deviation predictions seem well when they are compared with CFD calculations but incidence situation show differences between throughflow and CFD calculations. One of the reason for the difference is caused from the meridional velocity calculations from radial equilibrium equation. The other reason is the added errors from loss and deviation calculations. Choking is not calculated in the throughflow analysis and performance maps of throughflow and CFD analysis show differences. Throat calculation is introduced in blade profiling mode but not applied in the throughflow analysis.

5.2.Optimization of Axial Compressor Stage

One stage axial compressor design conditions and geometry information are given in Table 5.4 and 5.5.

Table 5.4. Design conditions for single stage axial compressor

Inlet Po	Pa	101325.00
Inlet To	Kelvin	288.00
Mass Flow Rate	kg/s	6.63
Rotational Speed	RPM	26000.00
Total to Total Pressure Ratio		1.50

Table 5.5. Geometry information for single stage axial compressor

	Rotor			Stator		
	Hub	Mean	Tip	Hub	Mean	Tip
Metal Angle @ Inlet (°)	38.66	45.72	51.36	33.71	36.31	37.34
Metal Angle @ Outlet (°)	19.00	30.00	38.00	-5.00	-5.00	-5.00
Solidity	1.42	1.21	1.11	1.20	0.94	0.75
Aspect Ratio	2.08	1.69	1.69	1.96	2.07	2.19
Chord (mm)	22.00	27.00	27.00	19.00	18.00	17.00
Radius @ Inlet (mm)	81.11	103.97	126.82	87.74	106.39	125.04
Radius @ Outlet (mm)	85.58	105.61	125.63	91.30	107.64	123.99
Blade Type	DCA	DCA	DCA	DCA	DCA	DCA

Rotor is parametrically modeled in UG CAD software. Suction side and pressure side are fitted with a spline that has five control points. Two of the control points that are on leading and trailing edges are kept unchanged. Remaining control points are changed in optimization process. Figure 5.36 give the parametric model of rotor at 75% spanwise location.

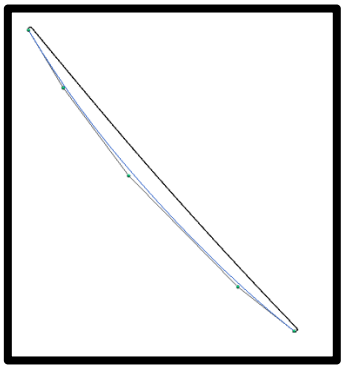

Figure 5.36. Parametric model of rotor at 75% spanwise location

After parameric modelling, by randomly changing the spline control points a database is generated. Artificial Neural Network is used to correlate the coordinates of spline control points with isentropic efficiency calculated by 3-D CFD computation. After Artificial Neural Network training with the initial database, Genetic Algorithm is used to find the spline control point combination that results with maximum efficiency. There exist 40 generations in each Genetic

Algorithm-Artificial Neural Network loop. At each generation number of eliminated chromosome pairs change from 4 to 10. Genetic Algorithm use real numbers and at mutation part selected pairs are changed between 1% - 40%. Trained Artificial Neural Network is used as a response surface to evaluate the fitness of a spline control point combination.

Rotor and stator are cut into equally spaced five sections. Rotor is optimized first and stator is optimized with the previously optimized rotor in front. Optimization of rotor is done in three steps.

At the first step two sections which are the tip section and 75% spanwise section are optimized first. At the first step with three spline control points at each profile surface Artificial Neural Network has 12 inputs at the input layer. At the second step optimized profiles at tip section and 75% spanwise location are fixed and 50% spanwise location is optimized. At the second step with three spline control points at each profile surface Artificial Neural Network has 6 inputs at the input layer. At the third step previously optimized three sections are fixed. Hub section and 25% spanwise section are optimized. At the third step with three spline control points at each profile surface Artificial Neural Network has 12 inputs at the input layer. Optimization of stator is done in single pass. At each step initial database for the Artificial Neural Network is generated by 5-10 CFD analysis. Optimization procedure is given in Figure 5.37.

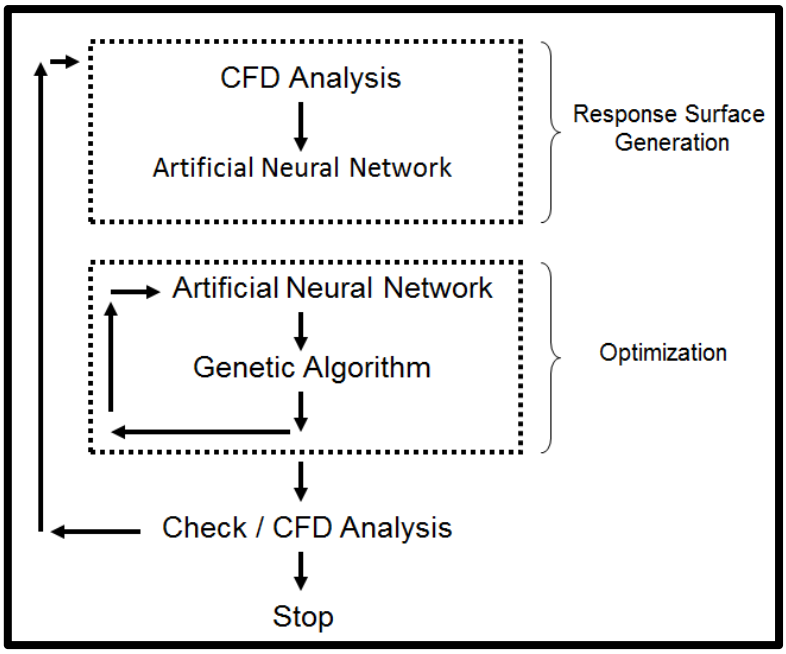

Figure 5.37. Optimization procedure

Optimization history for the rotor is given in Figure 5.38. Initial and final geometries are given in Figure 5.40 and Figure 5.41 for 50% and 75% spanwise locations. Full lines correspond to initial profile and dashed lines correspond to final profile.

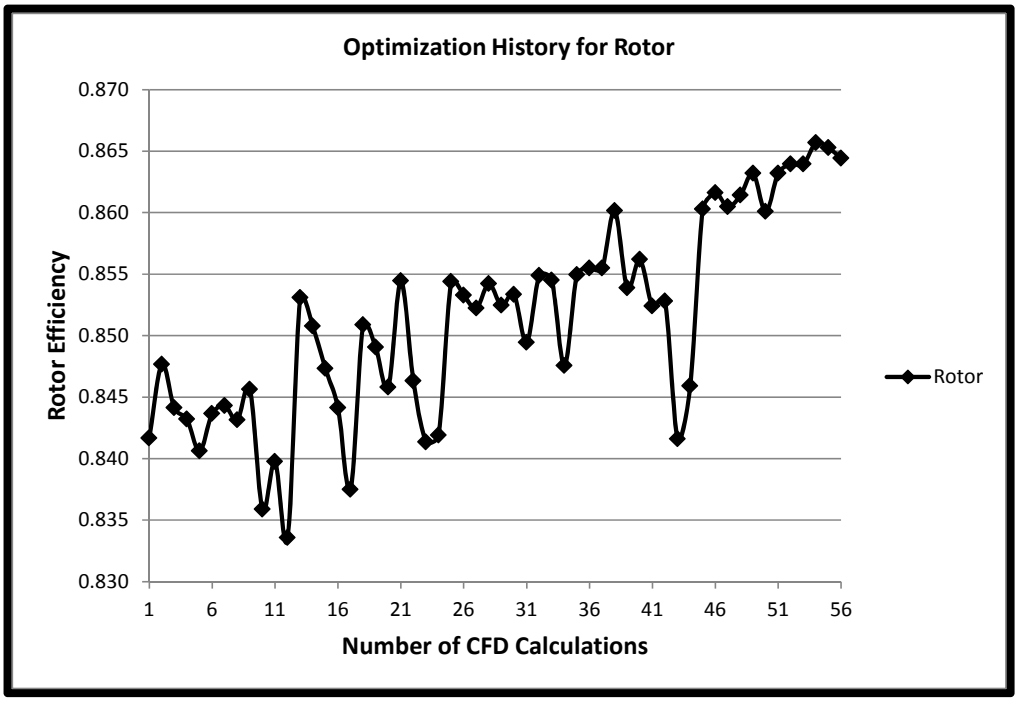

Figure 5.38. Optimization history for the rotor

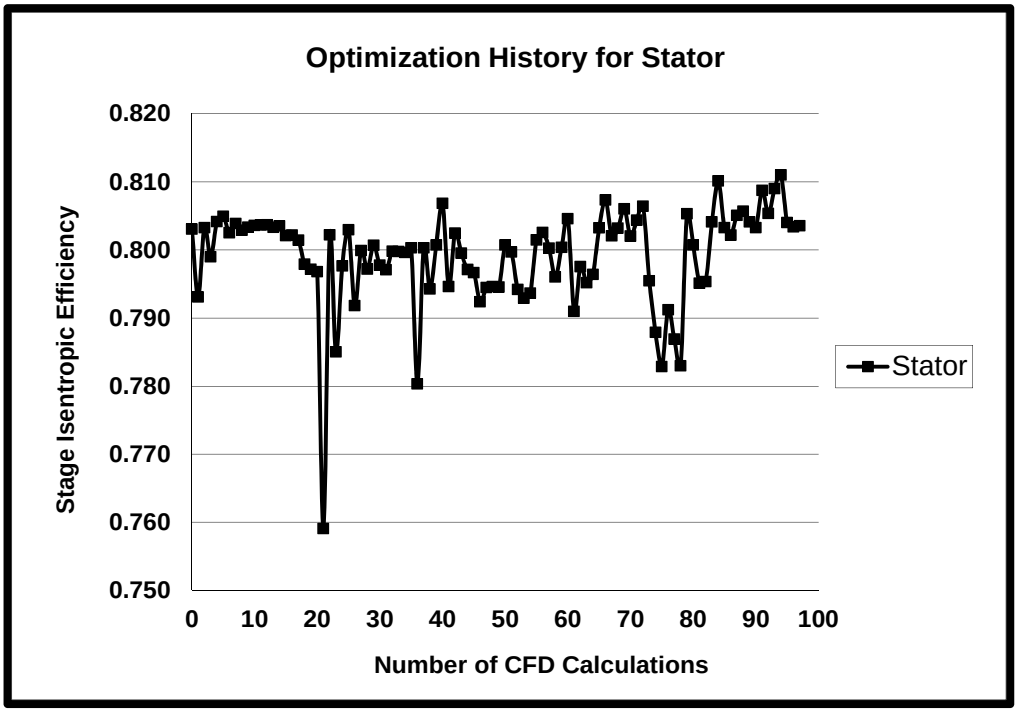

Figure 5.39. Optimization history for the stator

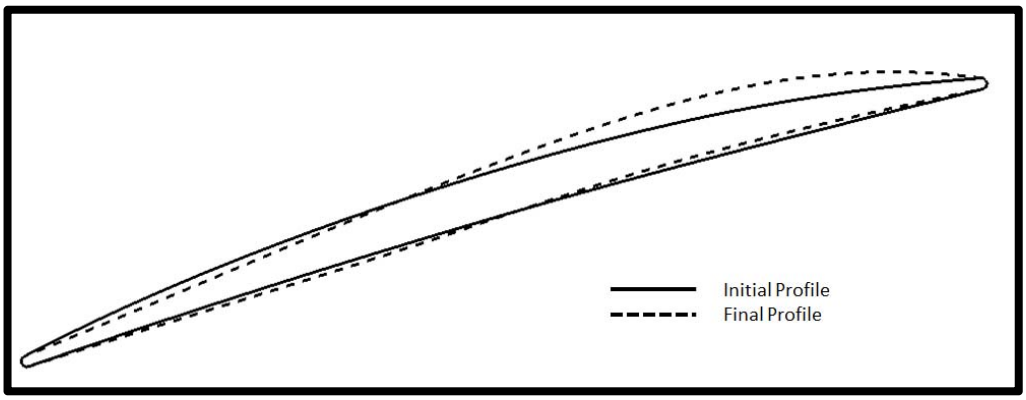

Figure 5.40. Initial and final profiles at 50% spanwise location

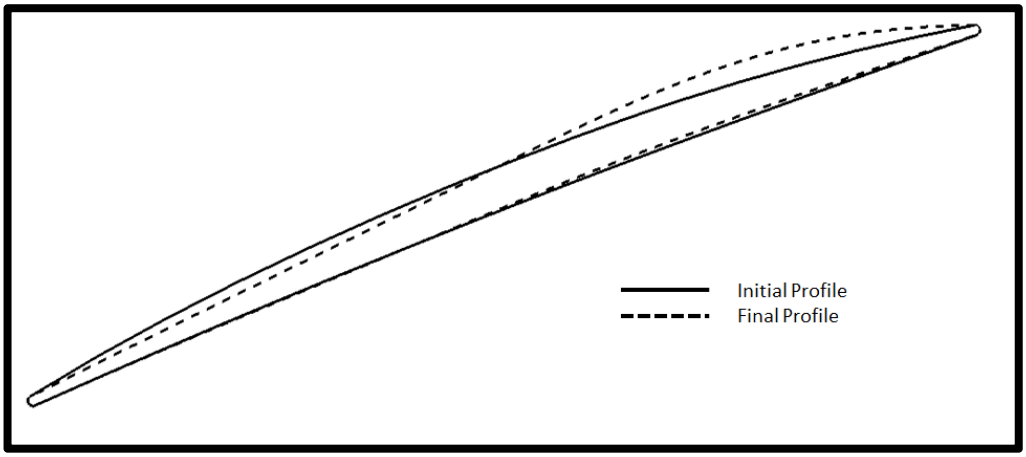

Figure 5.41. Initial and final profiles at 75% spanwise location

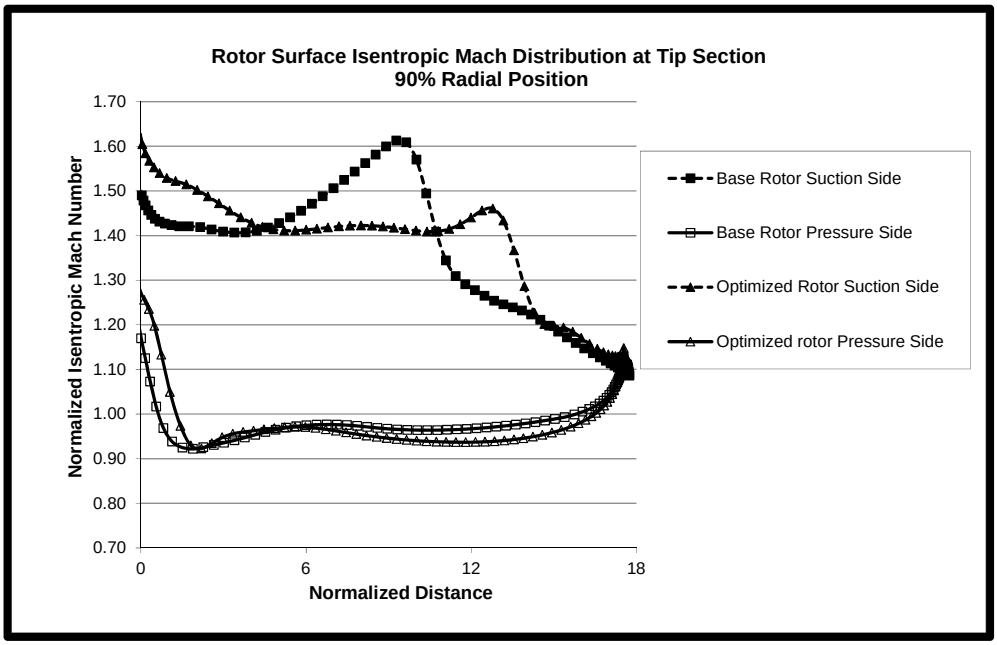

Figure 5.42. Rotor surface isentropic mach distribution at 90% span

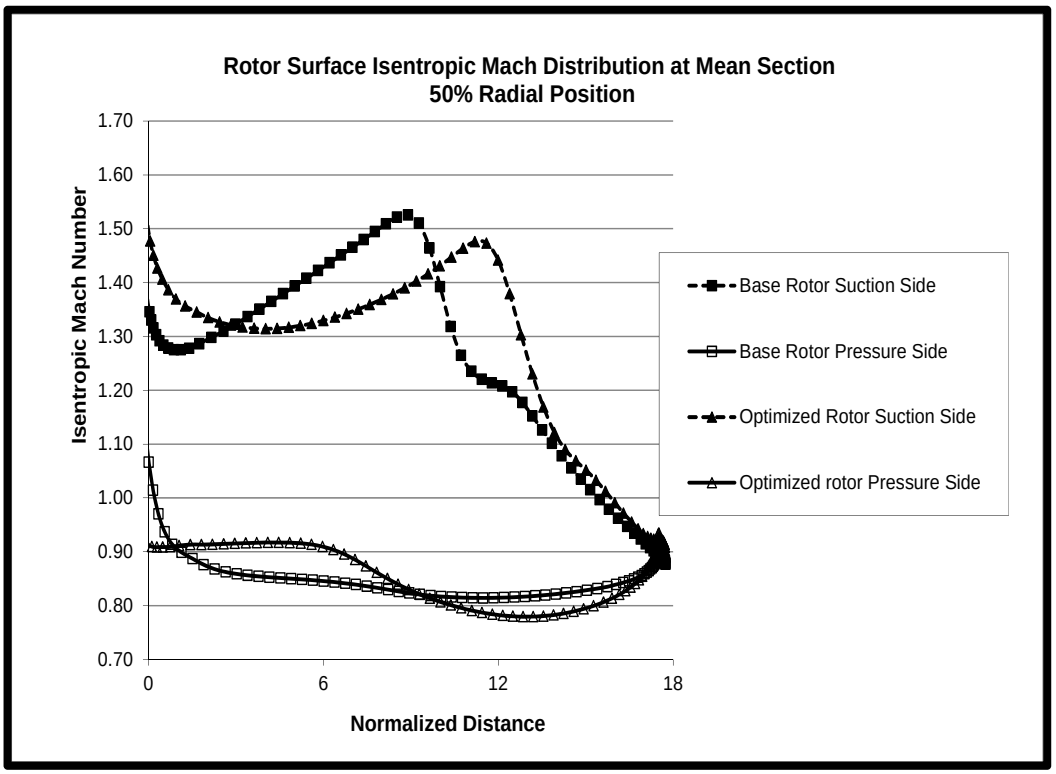

Figure 5.43. Rotor surface isentropic mach distribution at 50% span

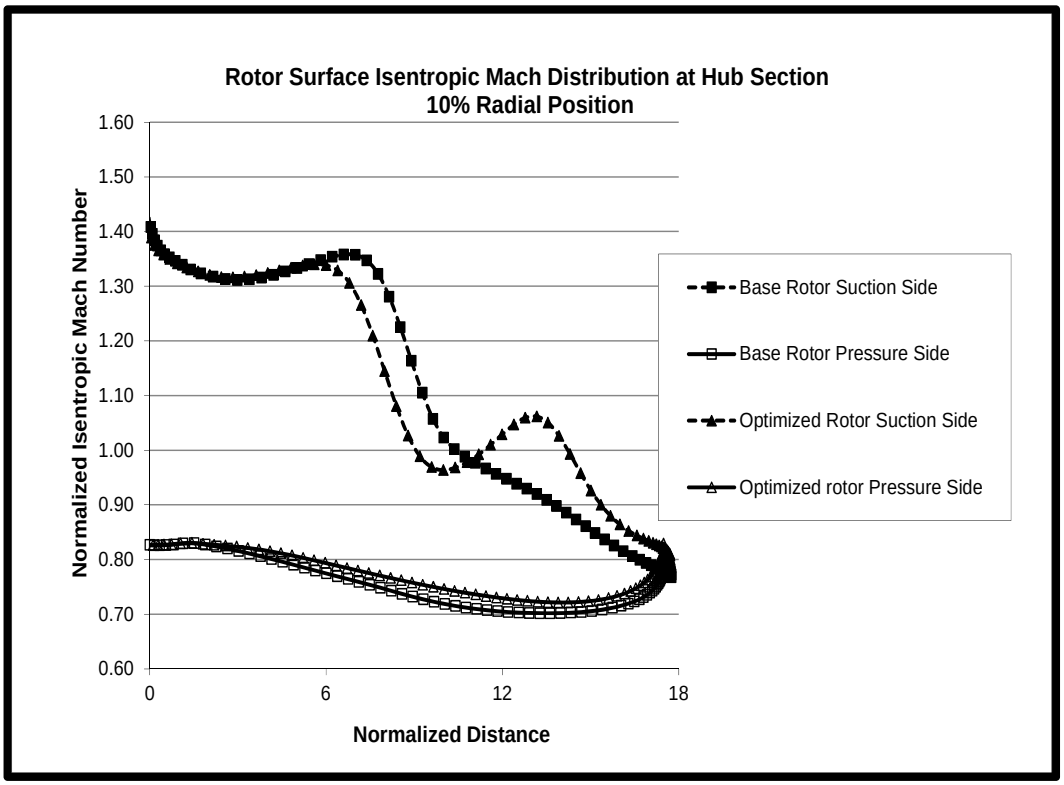

Figure 5.44. Rotor surface isentropic mach distribution at 10% span

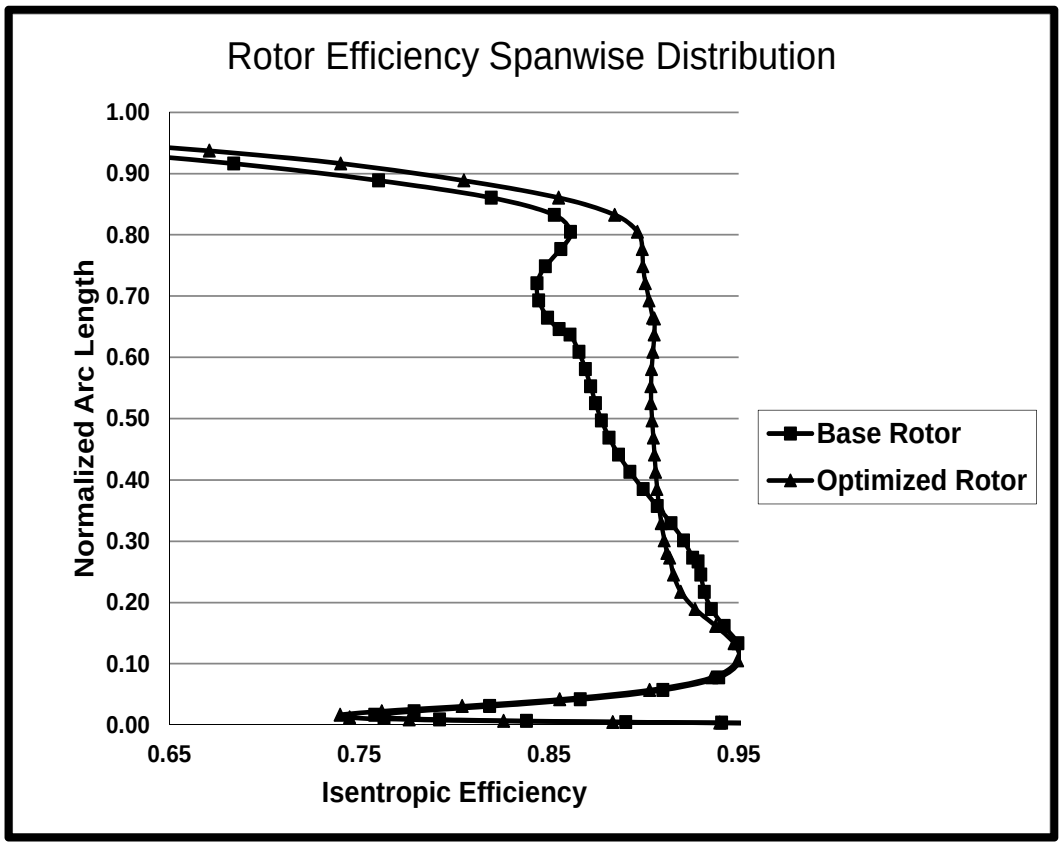

Figure 5.45. Rotor efficiency distribution for baseline and optimized geoemtries

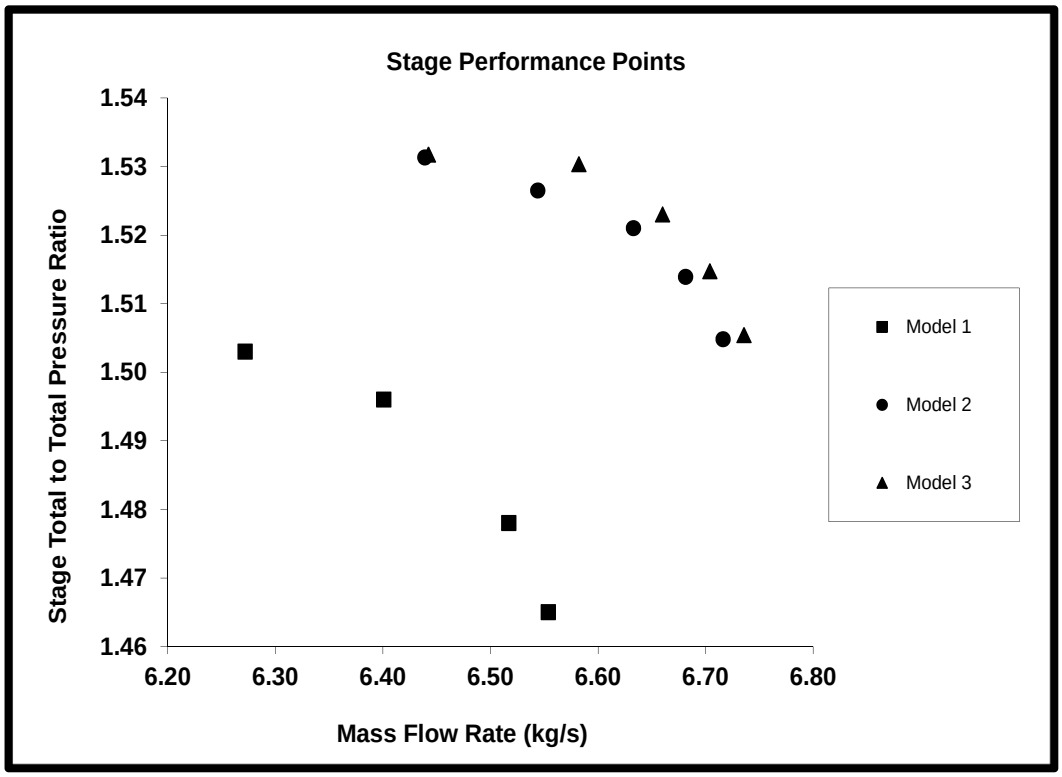

Figure 5.46. Stage performance points mass flow rate vs pressure ratio

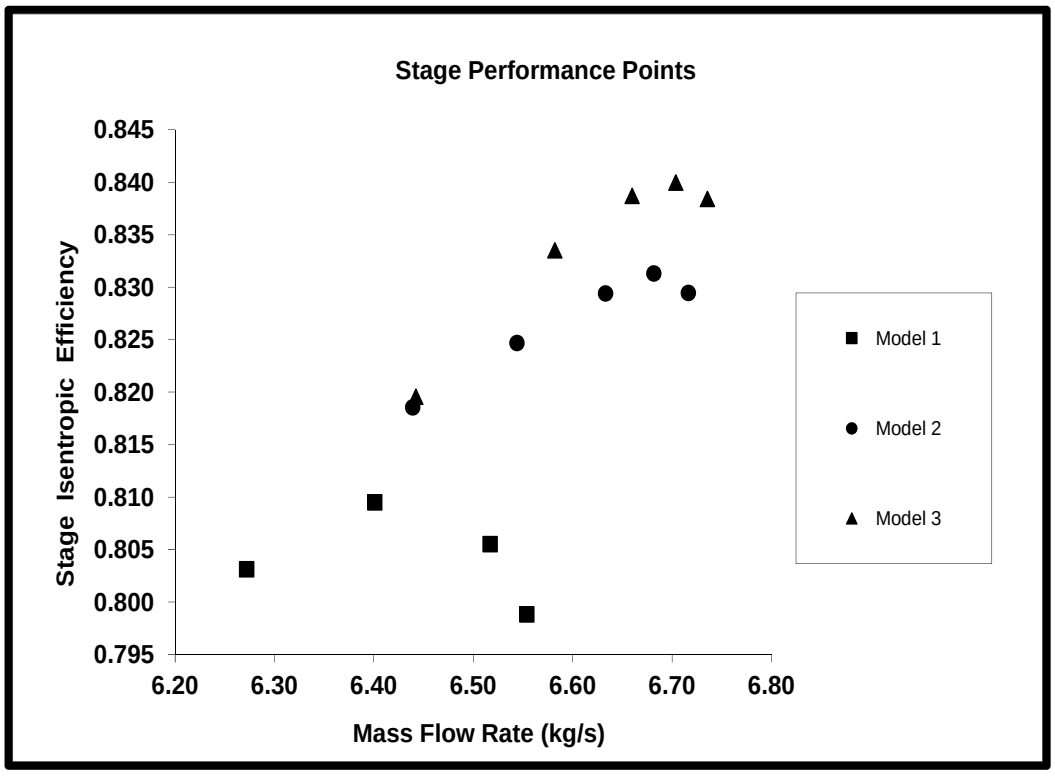

Figure 5.47. Stage performance points mass flow rate vs efficiency

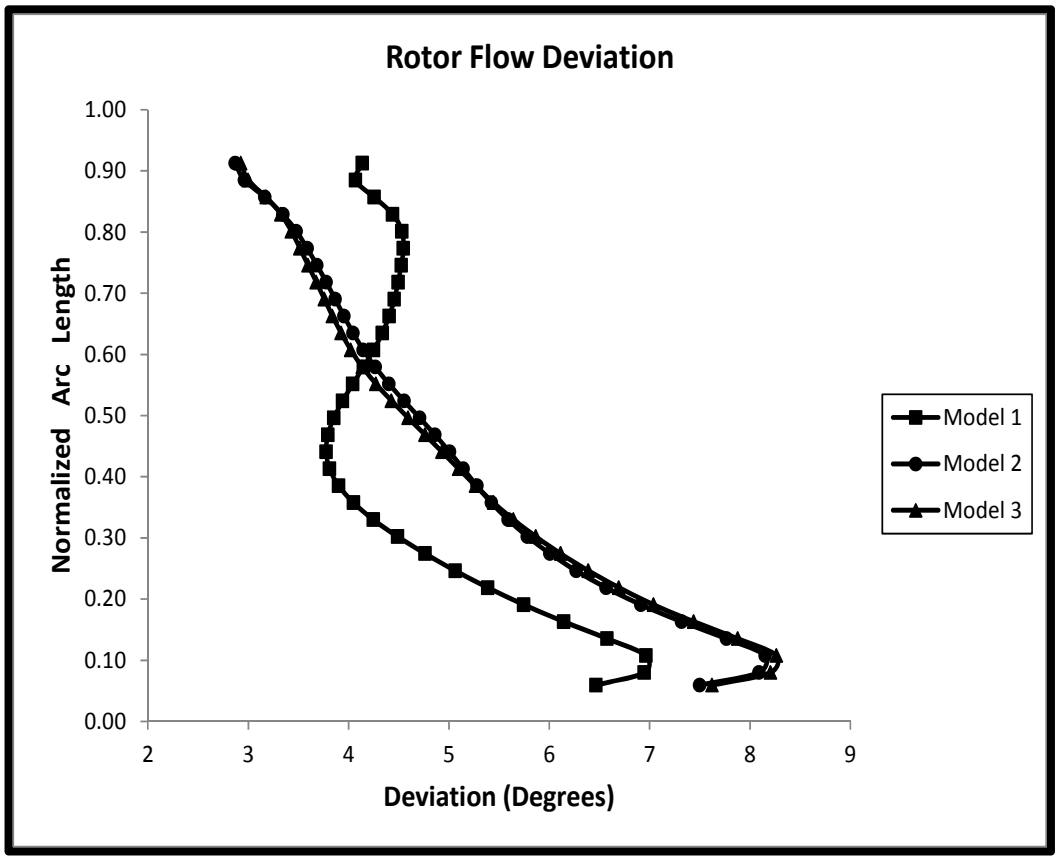

Figure 5.48. Rotor flow deviation for baseline and optimized geometries

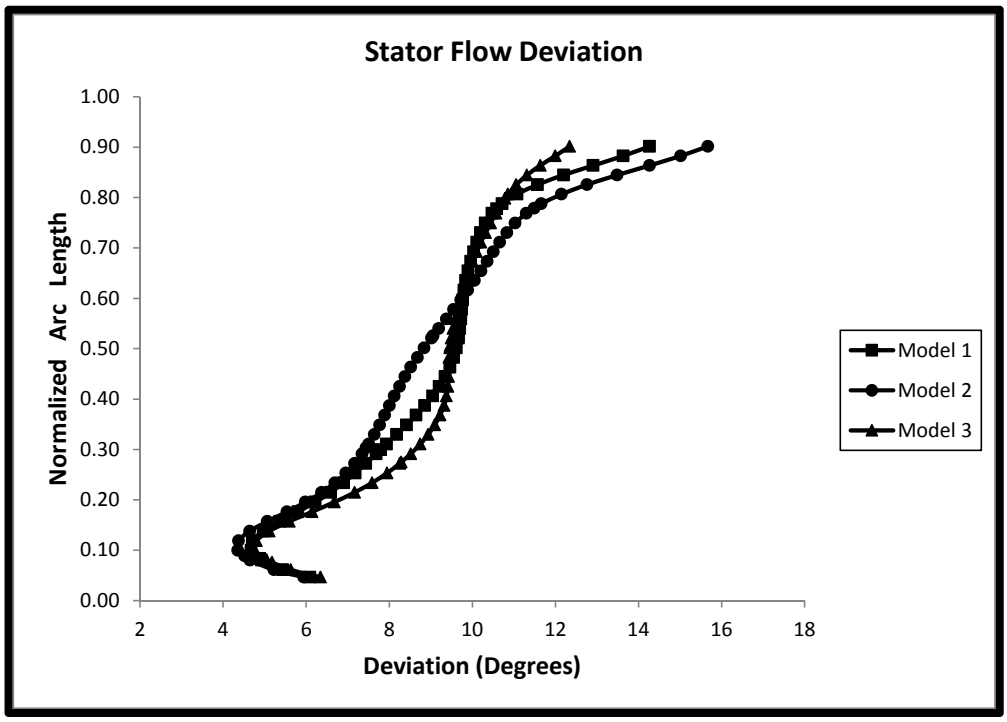

Figure 5.49. Stator flow deviation for baseline and optimized geometries

Increase in efficiency can be related to decrease in peak Mach number on suction surface in blade to blade plane from hub to tip. Deviation values seem to be not effected from the optimization. Also mass flow capacity is increased during optimization process. Since optimization is done in single objective manner, only increase in isentropic efficiency is taken into account.

Effectiveness of the Artificial Neural Network is investigated by a process capability analysis. After the rotor optimization work finished two Neural Networks are trained until a predefined coefficient of determination (R-sq) value is obtained. Neural Networks in the effectiveness study have three hidden layers each containing 8-12-8 neurons respectively. Learning rate is fixed to 0.1 for the effectiveness study. Predictions of two Neural Networks which have two different R-sq values from training are compared and analysed with commercial statistical software Minitab 16. With the distribution of actual and predicted values, process capability charts of two neural networks are obtained. Long term and short term process capabilities are compared in terms of C_{pk} and P_{pk} values. According to Jim Parnelle [30] " C_{pk} tells you what the process is capable of doing in future, assuming it remains in a state of statistical control. P_{pk} tells you how the process has performed in the past". Process capability charts of Artifical

Neural Networks having R-sq 0.8 and R-sq 0.9 are given in Figure 5.50 and Figure 5.51.

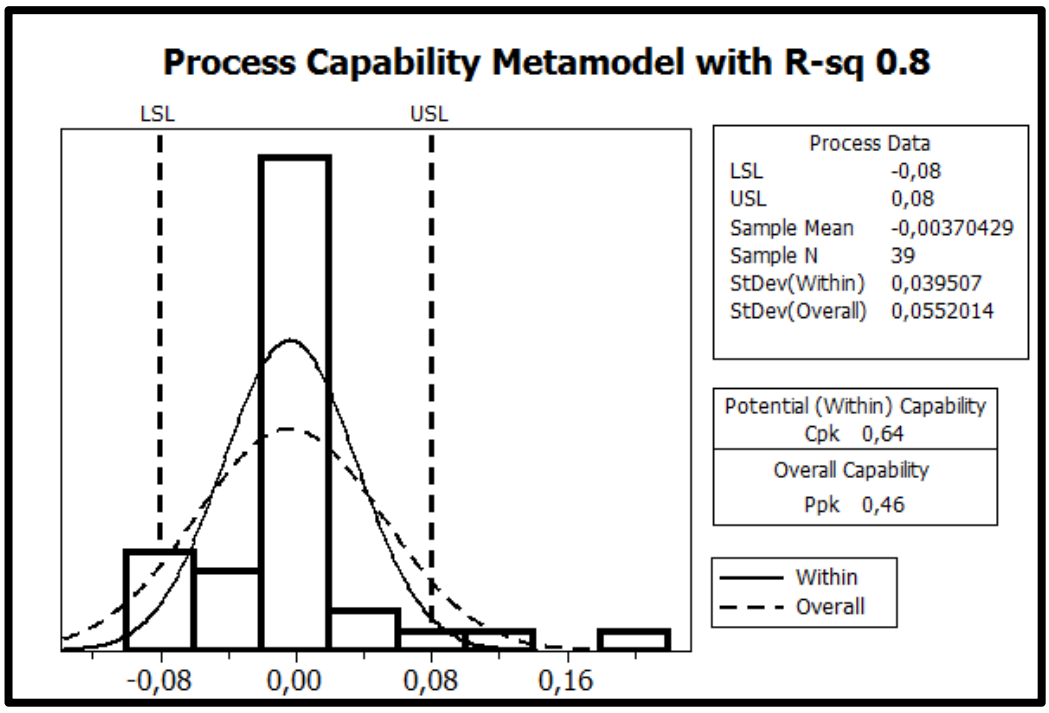

Figure 5.50. Process capability chart of ANN predictions with R-sq 0.8

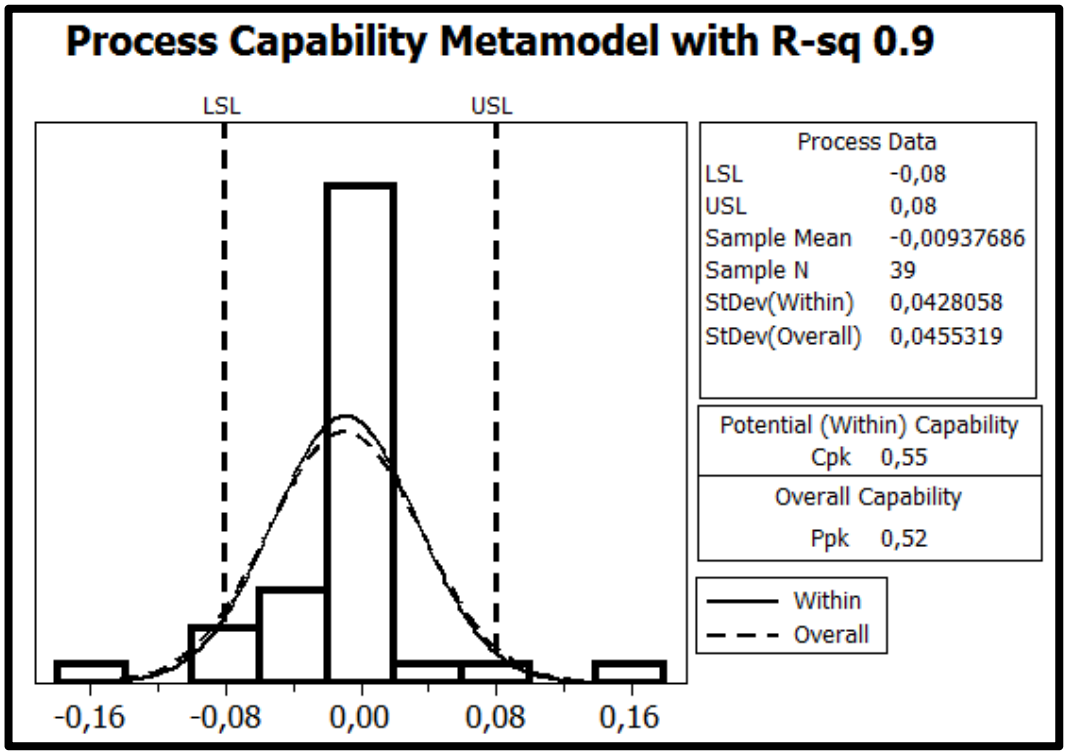

Figure 5.51. Process capability chart of ANN predictions with R-sq 0.9

When two metamodels with differing R-sq values in their trainng processes are analyzed with the same upper (USL) and lower (LSL) specification limits C_{pk} and P_{pk} values do not show large difference. For a metamodel there exist two important things. Ability of generalization is the first neccessity to have a continuous increase in the rotor optimization history as in the Figure 5.38. Second thing is the ability of representing the real to decrease number of iteration of the whole optimization process.

CFD can also be used in fitness evaluation of Genetic Algorithm rather than Artificial Neural Network. Using CFD in fitness evaluation may be helpful since real values will be considered rather than estimation of real values. Two disadvantages will appear when using CFD in fitness evaluation. Computation time is the first disadvantage. CFD analysis will take time in Genetic Algorithm generation loops, while a trained Neural Network produces its output in milliseconds. Local minimum is the second disadvantage. Number of unnecessary CFD will be carried out for the inputs that generate the same output, although mutation is done in genetic algorithm to avoid falling into local minima. Using ANN will accelerate the generation loops dramatically and the risk for local minimum will be lowered.

Overtraining and lack of fit are disadvantages of Artificial Neural Network. An over trained Neural Network will summarize the training data and will loose generalization capability. Artificial Neural Network with lower generalization capability will result in inappropriate predictions that will reverse the direction of optimization. There is a possibility that Artificial Neural Network can not handle the training datasets when number of inputs and training database for Artficial Neural Network get larger. This will result in lack of fit and generalization capability of the metamodel will be lowered. Also to stop ANN trainings, selection criteria for R-sq value will be unclear because it will be difficult to find the right location or acceptable location where generalization capability or representation capability is optimum.

6. CONCLUSION

In this part results and conclusions are summarized in the thesis study. Lessons learnt, significance of results and future recommendations are discussed.

Purpose of the thesis study was developing design, analysis and optimization tools for flow field investigation in axial compressor. Meridional design methodology is based on simple isentropic radial equilibrium. Meridional analysis is based on non isentropic radial euilibrium supported by loss and deviation correlations available in open literature. 3-D CFD analysis is based on Reynolds Averaged Navier Stokes computations. Optimization is based on Artificial Neural Network coupled Genetic Algorithm.

Success in meridional analysis is based on prediction of losses and deviations across blade rows. According to the results integral compressor performance is predicted well except meridional velocities as well as incidence angles. Differences for the meridional velocities and incidence angles arise from primarily radial equilibrium solution and secondarily from loss, deviation predictions. For this reason throughflow analysis of a multistage axial compressor that has more than two stages will have serious problems in terms of meridional velocities with the method used in the thesis. Added scaling factors from hub to tip may reduce the effect of problems arising from loss and deviation predicitons. For future work improvements in radial equilibrium solution such as introducing streamline effects may be done.

Optimization is carried in a single objective manner. Only target is achieving maximum isentropic efficiency for the axial compressor stage. Efficiency increase is obtained about 3 %. With the increase in efficiency mass flow rate is also increased by 3 %. Reduction in shock Mach number is more effective on efficiency than other flow or cascade parameters, so only by closing the bade angles after optimization original mass flow rate value will be reobtained. Rather than optimizing the compressor stage one by one, introducing multi objective optimization in future will be more suitable and faster. With that case while optimizing the stage for increasing efficiency other performance parameters such as mass flow rate can also be controlled.

REFERENCES

[1] Saravanamuttoo, W., Rogers, G., Cohen, H., *Gas Turbine Theory Fifth Edition*. Harlow, Pearson Prentice Hall, 2001.

[2] Aungier, R., *Axial Flow Compressors, A Strategy for Aerodynamic Design and Analysis*. New York, ASME Press, 2003.

[3] Johnsen, I., Bullock, R., NASA SP-36 Aerodynamic Design of Axial Flow Compressors, Washington D.C. , NASA, 1965.

[4] Cetin, M., Ücer, A., Hirsch, C., Serovy, G., AGARD AR-745 Application of Modified Loss and Deviation Correlations to Transonic Axial Compressors, Neuilly sur Seine, AGARD NATO, 1987.

[5] Pachidis, V., Gas Turbine Advanced Performance Simulation, Phd. Thesis, Cranfield University, 2006.

[6] Schobeiri, M., Advanced Compressor Loss Correlations Part 1: Theoretical Aspects, International Journal of Turbomachinery Vol. 3 No.3 pp. 163-177, 1997.

[7] Cumpsty, N., *Compressor Aerodynamics*. Florida, Kreiger, 2004.

[8] Sonntag, R., Borgnakke, C., Wylen, G., *Fundamentals of Thermodynamics Sixth Edition*. USA, John Wiley & Sons, 2003.

[9] Brown, R., *Compressors Selection and Sizing Second Edition*. USA, Gulf Professional Publishing, 1997.

[10] Principles of Jet Engine Operation (Online) Available: www.leitemlane.com/ jetoperation.htm, August 16, 2013.

[11] Centrifugal Compressor Test Rig Specifications (Online) Available: www. dlr.de August 16, 2013.

[12] Boyce, M., Axial Flow Compressors (Online) Available: http://www.netl.doe.gov/technologies/coalpower/turbines/ refshelf/handbook /2.0.pdf August 16, 2013.

[13] Leboeuf, F., RTO-EN-1 AC/323 AVT TP/1 Integrated Multidisciplinary Design of High Pressure Multistage Compressor Systems, Neuilly sur Seine, NATO, 1998.

[14] Attia, M., Schobeiri, M., A New Method for the Prediction of Compressor Performance Maps Using One-Dimensional Row-by-Row Analysis, International GasTurbine and Aeroengine Congress, 95-GT-434, 1995.

[15] Lieblein, S., NACA RM-E53L22 Review of High Performance Axial Flow Compressor Blade Element Theory, Washington, NACA, 1954.

[16] Hirsch, C., Denton, J., AGARD AR-175 Throughflow Calculations in Axial Flow Turbomachines, Neuilly sur Seine, AGARD NATO, 1981.

[17] Wu, C., NACA TN-2604 A General Theory of Three Dimensional Flow in Subsonic and Supersonic Turbomachines of Axial, Radial an Mixed Flow Types, Washington, NACA, 1952.

[18] Verstraete, T., Introduction to Optimization Methods and Tools for Multidisciplinary Design in Turbomachinery Workshop, ASME Turbo Expo, 2011.

[19] Thevenin, D., Janiga, G., *Optimization and Computational Fluid Dynamics*. Germany, Springer, 2008.

[20] Oyama, A., Liou, M., Obayashi, S., Transonic Axial Flow Blade Shape Optimization Using Evolutionary Algorithm And three Dimensional Navier Stokes Solver, AIAA 2002-5642, 2002.

[21] Song, P., Sun, J., Wang, K.., He, Z., Development of an Optimization Design Method for Turbomachinery by Incorporating the Cooperative Coevolution Genetic Algorithm and Adaptive approximate Model, Asme Turbo Expo GT2011-45411, 2011.

[22] Lian, Y., Liou, M., Aerostructural Optimization of a Transonic Compressor Rotor, Journal of Propulsion and Power Vol. 22 No. 4, 2006.

[23] Meier, R., Grosse, L., Joos, F., The Use of ANN for Turbo Engine Applications, European Symposium on Artificial Neural Networks, 2009

[24] Howel , A., RM-2095, The Present Basis of Axial Compressor Design Part 1 Cascade Theory. Aeronautical Research Council, 1942.

[25] Chapra, S., Canale, R., *Numerical Methods for Engineers Sixth Edition*. McGraw-Hill, 2009.

[26] Aksel, H., Eralp, C., *Gas Dynamics*. Ankara, METU , 1992.

[27] Genetic Algorithms and Their Applications (Online)
Available:http://www.informatics.indiana.edu/fil/CAS/PPT/Davis/
August 16, 2013.

[28] Introduction to Neural Networks CMSC475/675 (Online)
Available:http://www.csee.umbc.edu/~ypeng/F09NN/NN-lecture-notes.htm October 29, 2010.

[29] MacLeod, C., An Introduction to Practical Neural Networks and Genetic Algorithms For Engineers and Scientists, (Online) Available:
http://www4.rgu.ac.uk/eng/compint/page.cfm?pge=28907
October 29, 2010

[30] Process Capability and Process Performance (Online) Available:
http://www.isixsigma.com/tools-templates /capability-indices-process capability/ process- capability-cp-cpk-and-process-performance-pp-ppk-what-difference/ , April 10, 2013

[31] Swan, W., A Practical Method of Predicting Transonic Compressor Performance, Trans. Journal of Engineering and Power Vol. 83 July pp.322-330, 1961.

[32] Barbosa, J., A Streamline Curvature Computational Program for Axial Compressor Performance Prediction. PhD Thesis, Vol. 1, School of Mechanical Engineering, Cranfield Institute of Technology, 1987.

[33] Schwenk, F., Lewis, G., Hartman, M., NACA RM E57A30 A Preliminary Analysis of the Magnitude of Shock Losses in Transonic Compressors, 1957.

[34] Creveling, H., Carmody, R., NASA CR-54532 Axial Flow Compressor Design Computer Programs Incorporating Full Radial Equilibrium, Ohio, NASA, 1968.